

**Development of Nanobodies to Image
Synaptic Proteins in Super-Resolution Microscopy**

Dissertation

in partial fulfilment of the requirements for the degree

Doctor rerum naturalium

at the Georg-August University Göttingen

within in the International Max Planck School for Molecular Biology
of the Göttingen Graduate School for Neurosciences,
Biophysics and Molecular Biosciences

submitted by

Manuel Maidorn

from Gronau (Leine), Germany

Göttingen, September 2017

Examination Board

Thesis Committee and Examination Board:

Prof. Dr. Silvio Rizzoli (first referee)
Department of Neuro- and Sensory Physiology
University Medical Center Göttingen
Göttingen, Germany

Prof. Dr. Peter Rehling (second referee)
Department of Cellular Biochemistry
University Medical Center Göttingen
Göttingen, Germany

Prof. Dr. Mikael Simons
Institute of Neuronal Cell Biology
German Center for Neurodegenerative Diseases / Technical University Munich
Munich, Germany

Extended Examination Board:

Prof. Dr. Henning Urlaub
Bioanalytical Mass Spectrometry
Max Planck Institute for Biophysical Chemistry
Göttingen, Germany

Prof. Dr. Jörg Enderlein
Institute for Biophysics
Georg-August-University Göttingen
Göttingen, Germany

Prof. Dr. Markus Bohnsack
Institute for Molecular Biology
University Medical Center Göttingen
Göttingen, Germany

Every day for us something new
Open mind for a different view
And nothing else matters.



Affidavit

I hereby declare that I prepared this dissertation entitled '**Development of Nanobodies to Image Synaptic Proteins in Super-Resolution Microscopy**' independently and with no other aid or sources than quoted.

Göttingen, September 2017

(Manuel Maidorn)

Für Margarete und Manfred

Table of Contents

Examination Board	III
Affidavit	VII
Acknowledgement	XIV
List of Publications	XVI
List of Figures.....	XVII
List of Tables.....	XIX
List of Equations	XX
List of Abbreviations	XXI
Abstract.....	1
Zusammenfassung (German Abstract).....	2
1. Introduction.....	3
1.1 Basic Concepts of Light Microscopy.....	3
1.2 Super-Resolution Microscopy Techniques.....	5
1.2.1 STED-Microscopy	5
1.2.2 STORM / PALM.....	7
1.2.3 Other Approaches for Sub-Diffraction Imaging.....	7
1.3 Labelling Tools used in Fluorescence Microscopy	9
1.3.1 Detection of Proteins via Recombinant Tags.....	9
1.3.2 Affinity-Based Detection.....	10
1.4 Affinity Probes in Microscopy	12
1.4.1 Antibodies.....	12
1.4.2 Small Probes.....	13
1.4.3 <i>In vitro</i> Selection Techniques.....	17
1.4.4 Nanobodies.....	18
1.5 Comparison of Nanobodies to Conventional Probes.....	19
1.6 Imaging Approaches to Study the Synaptic Architecture	23
1.7 Aims of the Project.....	27

2.	Material and Methods	28
2.1	Materials and Reagents	28
2.1.1	General Chemicals	28
2.1.2	Buffers, Solutions and Media.....	30
2.1.3	Molecular Kits	34
2.1.4	Antibodies.....	34
2.1.5	Purified Proteins	35
2.1.6	Consumables.....	36
2.1.7	Instrumentation / Equipment.....	37
2.1.8	Software.....	39
2.2	Methods and Protocols.....	40
2.2.1	Molecular Cloning / Gene Constructs.....	40
2.2.2	Glycerol Stocks.....	44
2.2.3	Bacterial Protein Expression and Purification.....	45
2.2.4	SDS PAGE.....	47
2.2.5	Preparation of Competent Bacteria.....	47
2.2.6	Cell-Line Culture and Transfection.....	49
2.2.7	Immunostainings	50
2.2.8	Fluorescence Imaging	50
2.2.9	Protein Purification from Mammalian Cell Lines.....	52
2.2.10	Primary Neuronal Culture.....	52
2.2.11	Brain Slice Preparation.....	53
2.2.12	Tissue Isolation	53
2.2.13	Western Blotting.....	54
2.2.14	Animal Immunization.....	54
2.2.15	Nanobody Library Construction.....	55
2.2.16	Phage Display.....	60
2.2.17	Validation and Characterization of Nanobody Candidates.....	64
2.2.18	Labelling of Nanobodies	65
2.2.19	Affinity Measurements	69
2.2.20	Image Analysis and Evaluation	69
2.2.21	Molecular Modelling.....	69

3. Results	70
3.1 Establishing the Workflow for Protein Production.....	71
3.2 Creating the Nanobody Libraries for Phage Display.....	72
3.3 Selection of Nanobodies from Phage Display Libraries.....	76
3.3.1 Screening for Nanobodies via Phage Display.....	76
3.3.2 Establishing a Robust Validation Protocol.....	79
3.3.3 Optimizing the Selection Procedure.....	81
3.4 Final Nanobody Candidates.....	83
3.4.1 Qualitative Selection for Final Candidates.....	83
3.4.2 Conjugation of Nanobodies to Functionalized Fluorophores.....	84
3.4.3 Affinity Determination of the Nanobodies S25-Nb10 and stx-Nb6.....	86
3.4.4 Specificity Analysis of S25-Nb10 and stx-Nb6.....	87
3.4.5 Epitope Mapping.....	91
3.5 Comparison of Novel Nanobodies to Conventional Probes in IF.....	92
3.5.1 Test for Epitope Competition.....	92
3.5.2 Comparative Staining in Cell Lines.....	93
3.5.3 Penetration into Tissue Sections.....	95
3.5.4 Staining of Endogenous Antigens in PC-12 Cells.....	97
3.5.5 Staining of Endogenous Antigens in Primary Cultures Neurons.....	98
3.5.6 Imaging SNAP-25 and Syntaxin 1A in Dual Color STED Microscopy.....	102
4. Discussion	103
4.1 Library Generation.....	104
4.2 Selection Procedure by Phage Display.....	106
4.3 Developing a Robust Validation Protocol.....	109
4.4 Characterization of S25-Nb10 and stx-Nb6.....	111
4.5 Labeling of Nanobodies.....	115
4.6 Comparison of Nanobodies to Classical Affinity Probes.....	117
4.7 Organization of Synaptic Proteins Revealed by Nanobodies.....	122
4.8 Future Applications for Selected Nanobodies.....	124
4.9 Summary and Conclusion.....	126
5. References	127
6. Curriculum Vitae	140

Acknowledgement

After conducting this project for several years, I owe deep gratitude to quite a few people for supporting me throughout this whole time.

First of all, I would like to thank Professor Silvio Rizzoli for letting me be a member of his lab and investing both ideological and economical capital in my project. I am very grateful for the high level of freedom allowing both my personal and scientific development, while always being available when he is needed. Thank you, Silvio!

Along the same lines I would express my gratitude to my supervisor Dr. Felipe Opazo, who has become a friend rather than a boss throughout the years. I also thank him for his inexhaustible repertoire of advice and new ideas to develop the project together. I literally could not have wished for a better atmosphere in the lab consistently keeping up my motivation enthusiasm.

Thank you, Felipe!

I would also like to thank my colleagues, who supported me in this project. First I thank my direct colleague Shama, who shared both office and lab with me to search for new nanobodies. Moreover, I would also like to thank Eugenio for countless advices, Martin and Sebastian for sharing their neuronal cultures, Hanna for sharing her insights into single molecule microscopy and Dagmar for help with the brain slice preparation.

But I would also like to thank all my other colleagues for constantly providing a friendly and productive atmosphere, making work feel like a comfortable place. I also thank the alpaca Johnny for providing his blood and RNA without even being asked.

Last, I would like to give personal thanks to all my friends and family for endless support, believing in me and keeping me up throughout these years. This especially includes my parents Margarete and Manfred, but also my godfather Ewald and godmother Hildegard and all other family members, who always encouraged and believed in me.

I surely would not have come so far without my friends from school, university and beyond. I particularly deeply treasure my friends of the Sailing Crew, with whom I shared half of my life by now, including countless unforgettable moments.

You all know what you mean to me and I am incredible grateful to have you by my side. Most of all, this holds true for my big sister in spirit, who made my life richer and brighter every single day by her omnipresent care.

List of Publications

Mikhaylova, M., Cloin, B. M. C., Finan, K., van den Berg, R., Teeuw, J., Kijanka, M. M., Sokolowski, M., Katrukha, E. a., **Maidorn, M.**, Opazo, F., et al. (2015) Resolving bundled microtubules using anti-tubulin nanobodies. *Nat. Commun.*, **6**, 7933.

Maidorn, M., Rizzoli, S. O. and Opazo, F. (2016) Tools and limitations to study the molecular composition of synapses by fluorescence microscopy. *Biochem. J.* **473**, 3385–3399.

Truckenbrodt, S., **Maidorn, M.**, Crzan, D., Wildhagen, H., Kabatas, S. and Rizzoli, S. O. (2017) X10 Expansion Microscopy Enables 25 nm Resolution on Conventional Microscopes. *bioRxiv*.

List of Figures

Figure 1: Schematic illustration of the STED-principle.....	6
Figure 2: Affinity probes derived from immunoglobulin scaffolds	14
Figure 3: Examples of small affinity probes for specific target detection.....	16
Figure 4: Smaller labels allow better resolution of microtubules.....	20
Figure 5: Schematic comparison of antigen detection by antibodies (top) or nanobodies (bottom) ..	22
Figure 6: Electron micrograph and models describing synaptic organization	26
Figure 7: Main vectors for bacterial and mammalian expression systems used in the project	42
Figure 8: Schematic and cartoon model of recombinant antigens used for immunization	55
Figure 9: Vectors generated and used to create phage display libraries.....	58
Figure 10: Schematic representation of the phage display procedure.....	63
Figure 11: Different strategies for labeling nanobodies with fluorophores	68
Figure 12: Compilation of different protein purification strategies.....	72
Figure 13: Extraction of nanobody DNA sequences from alpaca IgG antibodies.	75
Figure 14: Titer of amplified phages during subsequent panning rounds.	78
Figure 15: Sequence alignment of selected nanobody candidates	78
Figure 16: Flow-scheme for stepwise validation procedure of nanobody candidates	80
Figure 17: Validation steps of final candidates used for further experiments	84
Figure 18: Exemplary HPCL run to remove excess of unreacted dye after nanobody labeling.....	85
Figure 19: Affinity analysis of S25-Nb10 and stx-Nb6 by MST	86
Figure 20: Specificity analysis of S25-Nb10 and stx-Nb6 by Western blotting	88
Figure 21: Analysis of cross-reactivity to alternative SNAP and syntaxin variants	89
Figure 22: Specificity analysis of S25-Nb10 and stx-Nb6 by IF microscopy	90
Figure 23: Mapping the epitope of S25-Nb10 and stx-Nb6	91
Figure 24: Dot blot analysis to investigate epitope competition of antibodies and nanobodies.....	93
Figure 25: Binding of nanobodies to COS-7 cells overexpressing the target antigen fused to EGFP ...	94

Figure 26: Tissue penetration of nanobodies and antibodies in thin sections of rat brains.....	96
Figure 27: Staining the endogenous levels of SNAP-25 and syntaxin 1A in PC-12 cells.....	98
Figure 28: Comparative staining of primary cultured neurons using antibodies or nanobodies	100
Figure 29: Synaptic distribution of SNAP-25 and syntaxin 1A.....	101
Figure 30: Dual channel STED microscopy of primary cultured neurons using nanobodies	102
Figure 31: Phylogenetic alignment of the SNAP and syntaxin protein family	114
Figure 32: Schematic illustration of antibody and nanobody binding to a target antigen	119

List of Tables

Table 1: Characteristics of selected affinity probes commonly used in molecular biology.....	16
Table 2: Specific chemicals and commercial buffers used in the project	28
Table 3: Buffers and solutions.....	30
Table 4: Liquid and solid media used for bacterial cultures	32
Table 5: Media for mammalian cell culture	33
Table 6: Commercial kits for molecular biology used in the project	34
Table 7: Primary antibodies used in IF staining and for comparative studies	34
Table 8: Fluorescently labeled secondary antibodies used to detect primary antibodies	35
Table 9: Specific consumables and equipment used in the project	36
Table 10: Major instrumentation and laboratory equipment used during the project.....	37
Table 11: Software for operation of devices and data analysis.....	39
Table 12: Overview of major backbone plasmids used in the project.....	41
Table 13: Typical PCR protocol used for DNA amplification	43
Table 14: Compilation of methods and column types used for protein purification	46
Table 15: Recipe for casting denaturing SDS-PAGE gels	47
Table 16: Overview of competent <i>Escherichia coli</i> bacteria used in the project.....	49
Table 17: Primers used for generating nanobody library by restriction cloning	56
Table 18: Overview of primers used for the generation of nanobody libraries by Gibson assembly ..	58
Table 19: Nested PCR steps for cDNA amplification to clone into Gibson library	59
Table 20: Selection of fluorophores used for conjugation to affinity molecules.....	66
Table 21: Overview on different libraries created for nanobody selection by phage display	74
Table 22: Compilation of different nanobody families identified via phage display	82

List of Equations

Equation 1: Formula to determine the Numerical Aperture (NA)	4
Equation 2: Formula by Ernst Abbe to determine the attainable planar resolution	4
Equation 3: Formula by Stefan Hell to determine the attainable resolution in STED microscopy	6
Equation 4: Formula for estimation of colony forming units (cfu)	49
Equation 5: Formula to determine the phage titer after precipitation of phage particles	61
Equation 6: Formula to determine the degree of labeling (DOL)	67

List of Abbreviations

×g	-	times gravity
°C	-	degrees Celsius
A	-	Ampere
aa	-	amino acids
APD	-	avalanche-photodiode
bp	-	base pairs
BSA	-	bovine serum albumin
cDNA	-	complementary deoxyribonucleic acid
CDR	-	complementary determining region
cfu	-	colony forming units
CMV	-	cytomegalovirus
C-terminus	-	carboxyl-terminus
Da	-	Dalton (1.66×10^{-24} grams)
ddH ₂ O	-	double distilled water
DL	-	degree of labeling
DMEM	-	Dulbecco's Modified Eagle's Medium
DNA	-	deoxyribonucleic acid
DOL	-	degree of labeling
<i>E. coli</i>	-	<i>Escherichia coli</i>
EDTA	-	ethylenediaminetetraacetic acid
EGFP	-	enhanced green fluorescent protein
ELISA	-	enzyme-linked immunosorbent assay
EM	-	electron microscopy
ER	-	endoplasmatic reticulum
F	-	farad
FCS	-	fetal calf serum
FWHM	-	full width at half maximum
g	-	gram
GFP	-	green fluorescent protein
h	-	hour
HBSS	-	Hank's Balanced Salt Solution
HEPES	-	2-[4-(2-hydroxyethyl)piperazin-1-yl]ethanesulfonic acid
HRP	-	horseradish peroxidase
HS	-	horse serum
Hz	-	Hertz
IF	-	immunofluorescence
IgG	-	immunoglobulin gamma
IPTG	-	isopropyl β-D-1-thiogalactopyranoside
K _D	-	dissociation constant
l	-	liter
LB	-	Lysogeny Broth
M	-	molar
MEM	-	Minimal Essential Media

MHC	-	major histocompatibility complex
MOI	-	multiplicity of infection
MST	-	microscale thermophoresis
MW	-	molecular weight
NA	-	numerical aperture
NHS	-	N-hydroxysuccinimide
NMR	-	nuclear magnetic resonance
N-terminus	-	amino-terminus
OD ₆₀₀	-	optical density measured at 600 nm
PAGE	-	polyacrylamide gel electrophoresis
PALM	-	Photoactivated Localization Microscopy
PCR	-	polymerase chain reaction
PEG	-	polyethylene glycol
PFA	-	paraformaldehyde
PLL	-	poly-L-lysine
PMSF	-	phenylmethane sulfonyl fluoride
POI	-	protein of interest
PSF	-	point spread function
RNA	-	ribonucleic acid
ROI	-	region of interest
rpm	-	revolutions per minute
scFv	-	single chain variable fragment
SDS	-	sodium dodecyl sulfate
sec	-	seconds
SEM	-	standard error of the mean
SNAP-25	-	synaptosomal-associated protein 25
SNARE	-	soluble N-ethylmaleimide-sensitive fusion protein-attachment receptor
SOC	-	Super Optimal Broth with Catabolite repression
SPR	-	surface plasmon resonance
STED	-	Stimulated Emission-Depletion
STORM	-	Stochastic Optical Reconstruction Microscopy
TB	-	Terrific Broth
TCEP	-	tris(2-carboxyethyl)phosphine
TEMED	-	tetramethylethylenediamine
TM	-	transmembrane
tst	-	twin Strep-Tag®
V	-	Volt
v/v	-	volume per volume
VAMP2	-	vesicle-associated protein 2
w/v	-	weight per volume
YT	-	Yeast Tryptone
Ω	-	ohm

Abstract

In the recent decades, super-resolution microscopy substantially contributed to the investigation of subcellular structures. A prominent example is the molecular organization of the synapse which is known to be vital for neuronal signal transmission. Synapses contain a plethora of different proteins which interact in fine-tuned mechanisms on molecular level to provide synaptic function. The observation of those proteins at nanoscale resolution thus provides important information on synaptic mechanisms.

To identify different synaptic proteins they need to be marked with a label, which can be used for detection in microscopy. Commonly, antibodies are used in immunofluorescence microscopy to specifically detect target antigens. However in recent studies, antibodies have been shown to exhibit several drawbacks in super-resolution imaging, primarily imposed by their comparable large size and divalent nature.

In contrast, small probes such as nanobodies gain increasing interest in the field of molecular imaging as they bypass several drawbacks of antibodies. Nanobodies are single-domain binders derived from an antibody subtype devoid of the light chain. They show high thermodynamic stability and can be produced in scalable amounts using bacterial expression systems.

In this project, I selected and characterized two novel nanobodies binding with high affinity and specificity two neuronal SNARE proteins, SNAP-25 and syntaxin 1A. The nanobodies were subsequently used in immunofluorescence microscopy to investigate the organization of these proteins in super-resolution.

I found that the obtained fluorescence image using nanobodies significantly differs from the stainings observed if primary and secondary antibodies are used. Furthermore, the obtained nanobodies show several advantages over conventional antibodies including increased tissue penetration, detection of more epitopes and the absence of artificial clustering effects.

Taking together the findings, I conclude that nanobodies are versatile tools for super-resolution microscopy to study small but complex biological structures such as synapses. The small size and biochemical properties of nanobodies direct the fluorophore in direct proximity to the antigen. This eventually also increases the attainable resolution and thus to the amount of detail observed in microscopy.

Zusammenfassung (German Abstract)

Die Entwicklung von hochauflösender Fluoreszenzmikroskopie hat in den vergangenen Jahrzehnten substanziell zur Erforschung subzellulärer Strukturen beigetragen. Als ein bekanntes Beispiel kann hier die molekulare Organisation der neuronalen Synapse angeführt werden, deren Integrität für die neuronale Reizweiterleitung unerlässlich ist. Synapsen enthalten eine Vielzahl unterschiedlicher Proteine, die auf molekularer Ebene in fein abgestimmten Mechanismen interagieren, um die synaptische Funktion zu gewährleisten. Die hochauflösende Untersuchung solcher Proteine im Nanometer-Bereich kann daher wertvolle Informationen über synaptische Mechanismen liefern.

Es ist dabei unerlässlich, jene synaptischen Proteine mit einer Markierung zu versehen, um sie in mikroskopische Studien zu identifizieren. Üblicherweise werden hierzu Antikörper genutzt um mittels Immunfluoreszenzmikroskopie gezielt zelluläre Antigene zu untersuchen. In jüngsten Studien wurde jedoch gezeigt, dass einige Eigenschaften von Antikörpern von Nachteil für die hochauflösende Fluoreszenzmikroskopie sind. Hierzu zählen unter anderem ihre vergleichsweise große räumliche Ausdehnung und das zweiwertige Binden ihrer Antigene.

Einen Gegensatz hierzu bilden minimale Sonden, wie beispielweise Nanokörper, da sie nicht die genannten Nachteile von Antikörpern aufweisen. Nanokörper stellen Einzeldomänenfragmente dar, die aus einem speziellen Antikörper-Subtyp ohne leichte Ketten isoliert wurden. Sie zeichnen sich insbesondere durch hohe thermodynamische Stabilität aus und können in skalierbaren Mengen aus bakteriellen Expressionssystemen isoliert werden.

Im Rahmen dieses Projektes wurden zwei neue Nanokörper beschrieben, die spezifisch und mit hoher Affinität an die beiden synaptischen SNARE Proteine SNAP-25 und syntaxin 1A binden. Die Nanokörper wurden anschließend genutzt, um diese Proteine mittels hochauflösender Fluoreszenzmikroskopie zu untersuchen.

Es zeigte sich, dass die mikroskopische Beobachtung mittels Nanokörpern signifikant von jenen abweicht, die mittels primären und sekundären Antikörpern gemacht wurden. Des Weiteren weisen die Nanokörper mehrere Vorteile gegenüber konventionellen Antikörpern auf. Hierzu zählen beispielweise eine erhöhte Gewebepenetration, eine erhöhte Dichte von detektierten Antigenen und die Vermeidung artifizieller Clusterbildung.

Zusammenfassend lässt sich schlussfolgern, dass Nanokörper vielseitige Werkzeuge sind, um mittels mikroskopischer Methoden kleine and komplexe biologische Strukturen, wie beispielsweise Synapsen, zu untersuchen. Nanokörper tragen daher durch die erhöhte Präzision in abbildenden Verfahren schlussendlich auch zu einer Verbesserung der Auflösung bei.

1. Introduction

1.1 Basic Concepts of Light Microscopy

Visualization of cellular processes using different microscopy techniques has been a central element of biology throughout the previous centuries. By microscopic observation of both biological structures and dynamic molecular interactions, researchers are able to gain detailed information on cellular and subcellular organization. Furthermore, live-imaging experiments allow to monitor cellular processes and to reveal fundamental principles of cellular biology.

When using any kind of microscopy technique, the maximum achievable resolution is an important parameter. Resolution in microscopy is defined as the minimum distance at, which two objects are still detectable as two individual entities. Hence in biology, a better resolution enables a more detailed visualization of molecular organization and consequently allows for a better understanding of the biological processes.

In 1957, confocal microscopy was introduced, which is based on point illumination of the specimen [1]. An adjustable pinhole is used to prevent the unfocused light from reaching the detector thus increasing the axial resolution. The sample is scanned pixel by pixel to reconstruct the image digitally.

In fluorescence light microscopy, molecular targets or cellular compartments need to be tagged with fluorescent molecules, i.e. molecules emitting fluorescence at a defined spectrum of the visible light. This allows parallel visualization of multiple targets by spectral separation of the fluorophores as individual excitation and detection channels are used for independent detection of the individual channels. To obtain a sharp image, the background in each detection channel needs to be kept to a minimum.

The emitted signal distribution of a single fluorophore can be described by the point spread function (PSF). It mathematically shows how the fluorescent signal generates the image composed of single emitters. For this reason, the PSF is also used to determine the optical resolution of the microscopy setup. The width of the PSF at its half maximum (full width at half maximum, FWHM) is commonly referred to as the attainable resolution for the microscopy setup. However, the maximum resolution of optical microscopy setups was found to be limited due to the physical properties of the light used for illumination.

In 1873, Ernst Abbe postulated a limit for the maximum attainable resolution of optical microscopy setups [2]. He defined the numerical aperture (NA) as a dimensionless constant for a microscopy setup as shown in Equation 1. The NA is proportional to the sine of the half-angle θ under which the excitation light exits and enters the objective and to the refractory index n between the objective and the specimen [3].

$$NA = n \sin \theta$$

Equation 1: Formula to determine the Numerical Aperture (NA). The refractory index n depends on the immersion medium between the specimen and the objective. θ represents the half-angle under which the light exits and enters the objective.

For technical reasons, the maximum value for the half-angle θ is limited to around 70° whereas n depends on the kind of refractory medium used. By using specific immersion oils, the refraction index can be increased to $n=1.52$ which results in a maximum NA of 1.45 for oil immersion objectives typically used in optic microscopy [4].

Abbe demonstrated that the resolution of optical microscopy correlates with the NA as well as with the wavelength of the light used for illumination of the specimen as shown in Equation 2. As NA is a fixed value given by the technicality, the attainable resolution of the setup therefore ultimately depends solely on the wavelength of the light. If the visible spectrum of light (roughly ranging between 400 and 700 nm) is used for illumination, practically a maximum resolution Δx of around 200 nm can be achieved, depending on the wavelength used.

$$\Delta x = \frac{\lambda}{2 NA}$$

Equation 2: Formula by Ernst Abbe to determine the attainable planar resolution. The minimum distance between two points to be resolved as two different entities (Δx) is given by the wavelength of the illumination light λ divided by 2 times the NA defined above.

This phenomenon is referred to as diffraction limit and defined the maximum resolution (i.e. ~ 200 nm) of optical microscopy setups for more than a century. However, a few decades ago this paradigm was shifted by the introduction of microscopy techniques bypassing the diffraction limit and thus termed super-resolution microscopy.

1.2 Super-Resolution Microscopy Techniques

Several methods have been described to overcome the diffraction barrier to increase the resolution and as a consequence the amount of detail observed in a specimen.

The concept of Structured Illumination Microscopy (SIM) was introduced already in 1963 and since has been used to image biological samples below the diffraction limit introduced by Abbe [5,6]. Technically, the illumination of the specimen with a defined pattern causes interference, which contains additional structural information [5]. This information can mathematically be extracted from the SIM image using Fourier-transformation to construct a super-resolution image. Modern SIM setups are capable of modulating the illumination pattern in space doubling the attainable resolution in all the dimensions [5].

Alternatively, super-resolution can be achieved by modulation of the fluorescent signal. Stimulated Emission-Depletion (STED) microscopy uses a depletion laser to “quench” the fluorescence in a defined area. Pointillistic methods such as photoactivated localization microscopy (PALM) or stochastic optical reconstruction microscopy (STORM) are based on the localization of single fluorophores.

More recent approaches combine different imaging techniques to further improve the attainable resolution and achieve nanometer precision. Due to the constant improvements of optical super-resolution microscopy techniques, the attainable resolution in biology virtually approaches the dimension of molecular assemblies [7].

1.2.1 STED-Microscopy

In 1994, Stefan Hell and coworkers published a method termed STED microscopy to increase the resolution of light microscopy setups below the diffraction limit [8]. Technically this is achieved by superimposing the excitation beam with a donut-like shaped depletion beam. The alignment of the excitation and depletion beams effectively results in a fluorescent spot with a smaller PSF compared to diffraction-limited spots. The donut-shaped depletion beam only allows fluorescent photons to be detected in the center where the depletion beam has an intensity of zero. This reduces the size of the PSF, which in turn allows objects in closer proximity to be separated [8,9]. A schematic view of the STED principle is shown in Figure 1.

Mathematically this effect can be described adding an additional term into Abbe’s formula describing the effect of the depletion laser as depicted in Equation 3. By using high-energy depletion lasers the PSF can theoretically approach infinitesimal values setting no limit to the resolution [10]. However, as the resolution Δx scales only with the square root of the depletion laser power (see Equation 3), the limit is given by the laser intensity, which can be damaging biological samples at too high intensities.

$$\Delta x = \frac{\lambda}{2 NA \sqrt{1 + \frac{I}{I_{sat}}}}$$

Equation 3: Formula by Stefan Hell to determine the attainable resolution in STED microscopy. Abbe's formula was complemented with a term describing the STED effect where I describes the intensity of the depletion laser and I_{sat} represents a characteristic saturation intensity of each fluorophore. As a consequence, increasing values for I reduce the term Δx , which deduces a gain in resolution [11].

Only after several years, the STED technology was successfully implemented into biology. Only in 2006, individual synaptic vesicles with an approximate diameter of 40 nm were for the first time resolved under a fluorescent microscope [11]. In subsequent years the spatial resolution of STED microscopes was improved even further after introduction of technical innovations such as time-gated depletion [12,13]. Modern STED setups are capable of achieving resolution of less than 20 nm in multiple detection channels simultaneously [14]. Notably, the application of super-resolution microscopy increasingly requires optimization and adjustment of sample preparation to exploit the full potential of this rapid progressing technology.

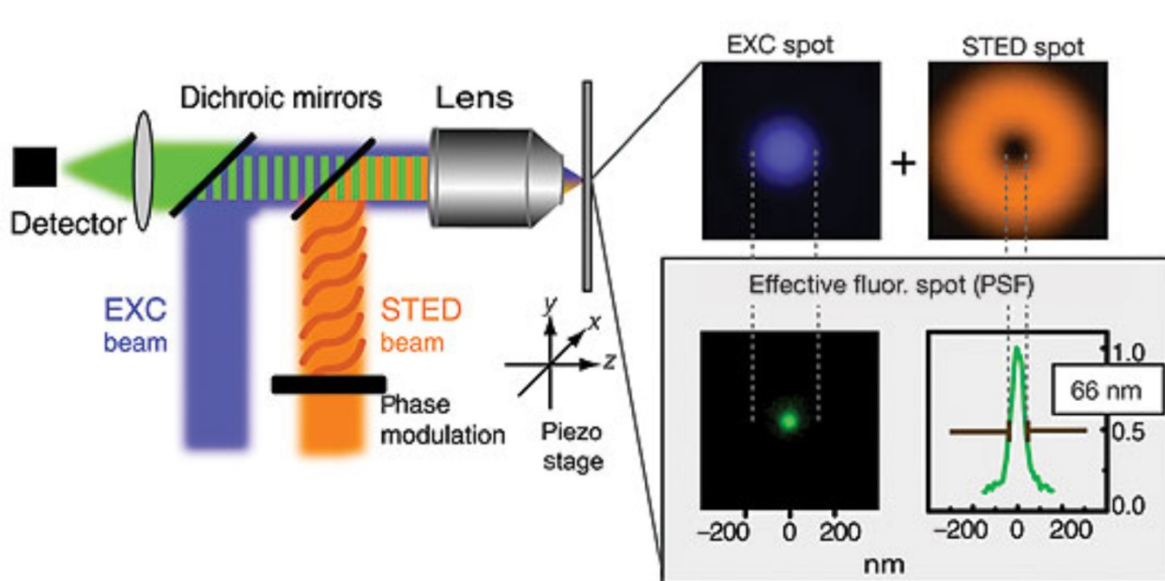


Figure 1: Schematic illustration of the STED-principle. A donut-shaped laser beam (orange) is used to partially deplete the emitted fluorescence created by the excitation beam (blue). That results in a sub-diffraction fluorescence signal (green) increasing the resolution of the microscope. Analyzing the PSF in the effective fluorescent spot the actual resolution can be measured by determining the FWHM, in this case 66 nm (bottom right panel). Modified from Willig *et al.*, Nature, 2006

1.2.2 STORM / PALM

In addition to STED microscopy, also other super-resolution technologies such as STORM and PALM have been developed to overcome the diffraction limit defined by Abbe depicted in Equation 2 [15,16]. Those methods are based on repeated stochastic emission of fluorophores, followed by reconstruction of the image *in silico*. In each image only a small subset of fluorophores is in an 'on'-state emitting fluorescence whereas the majority of fluorophores resides in an 'off'-state. The density of fluorophores plays an important role as the method relies on the separation of individual fluorophores with diffraction-limited microscopy. By using a common epifluorescence microscopy setup, several thousand images are recorded, which capture a differential set of fluorophores in the 'on'-state. Commonly specific dyes are used for this method, which are designed for fast switches between a fluorescent and a dark state [17].

A Gaussian fit is used to map the fluorescence signals determining the actual position of each fluorophore by mathematic reconstruction. The distance between two emitting molecules has to be higher than the diffraction limit of 200 nm to allow spatial separation and filtering of the fluorescent signals. Hence the attainable resolution depends on the density of fluorophores and the precision of localization. The latter correlates with the square root of the number of detected photons and can be increased by recording a higher number of images if the fluorophores withstand the long imaging protocol [18]. This way in biological samples, a resolution of a few nanometers can be obtained in [9].

1.2.3 Other Approaches for Sub-Diffraction Imaging

Apart from light microscopy also other microscopy techniques exist which provide similar or yet even higher resolution. Electron microscopy (EM) and scanning probe microscopy were used long before the invention of fluorescence super-resolution methods to investigate molecular organization down to atomic detail by measuring biophysical interactions [19,20]. Notably, these techniques require harsh and sophisticated treatments of the sample and thus require rather inflexible staining protocol, which may limit their application in biology. For instance unlike in IF microscopy, live-cell imaging cannot be performed in EM due to the strong fixation required.

Conventional EM experiments use strong fixatives such as glutaraldehyde to preserve the ultrastructure of the sample and osmium tetroxide to increase the contrast of the image. This way of fixation has been reported to impair the detection of target molecules due to interference with the molecular organization in the sample [21,22].

The problem imposed by fixation with glutaraldehyde has been addressed by cryofixation freezing the sample within milliseconds and thus preserving its ultrastructure [23,24]. Recent correlative imaging techniques combine EM with light microscopy to detect multiple targets while maintaining the high spatial resolution of EM [25,26].

Another recent concept of super-resolution microscopy combines the advantages of STED and STORM. The fluorophore is excited with a local intensity minimum of light which reduced the number of photons required for signal localization [27]. With this approach termed MinFlux (deviated from 'minimal emission fluxes'), samples can be imaged with ~1 nanometer precision [27].

In addition to correlated microscopy approaches, STED microscopy has also been combined with mass spectrometry to reveal the biochemical composition of the sample [28,29]. An atomic map of the sample is generated by nano-secondary-ion mass spectrometry (nanoSIMS) also identifying different isotopes. The secondary ion beam is generated by focusing a primary ion beam (typically cesium ions) on the sample to break atomic bonds and sputter away individual atoms. That beam is subsequently analyzed by mass spectrometry, using either time-of-flight measurement or magnetic detectors. The individual atoms in the beam are identified and their determined localization is used to construct an image of the sample [30]. However, the lateral resolution of this technology in biological samples (100-200 nm) is lower than resolution obtained in super-resolution techniques [30]. Hence, a correlated approach combining nanoSIMS and STED microscopy is used to obtain information on localization and molecular identity of multiple targets [28,30]

Recently, also another technology was developed to achieve super-resolution bypassing the necessity of expensive microscopic setups. Instead of optically magnifying the specimen, the sample is submitted to an expansion process, thus terming the technology expansion microscopy [31]. Briefly, the fluorophores of the affinity probes are covalently linked to a polymer network after conventional immunostaining [32]. After digestion of the sample, this network is physically expanded enhancing the resolution by separating individual fluorophores in space. After that, the sample can be imaged using a standard confocal microscope achieving super-resolution due to the expansion process. Expansion factors of up to 10-fold on a routine basis of even 20-fold if using more complex protocols have been reported, generating a resolution of 25 nm [33,34].

Taken together, fluorescence microscopy techniques and particular super-resolution approaches are important methods to investigate biological samples. Yet to detect specific target molecules such as proteins in microscopy, they need to be specifically marked for visualization.

1.3 Labelling Tools used in Fluorescence Microscopy

Proteins are known to play a major part in maintaining cellular integrity, including processes such as catalytic activity, molecular transport, signaling cascades, metabolism and cell adhesion. Consequently various proteins of interest (POI) are in the focus of many researches employing fluorescence microscopy. Most proteins are not able to emit a fluorescent signal by themselves and thus need to be marked with a label to study their localization and organization in a cellular context. Most commonly either a recombinant protein tag or an organic dye molecule coupled to a specific affinity probe is used to introduce fluorescence.

1.3.1 Detection of Proteins via Recombinant Tags

On DNA level different variants of the (enhanced) green fluorescent protein (GFP/EGFP) or other fluorescent proteins can be added as a recombinant fusion tag to the POI [35]. This way the POI can be observed or followed under a fluorescence microscope to study its cellular localizations. Today, after 23 years that the GFP was presented to the scientific community, thousands of laboratories around the world use it together with several dozens of modified fluorescent proteins that cover the whole visual spectrum.

As an alternative to already fluorescent proteins, also other recombinant tags such as the HALO, CLIP or SNAP-tag can be fused to the POI. These engineered enzymes acquired their fluorescence by adding a modified fluorophore that it can be recognized as the substrate for these enzymes, whereas the enzyme activity results in the covalent binding of the fluorophore to itself. Today, several modified fluorophores, both cell-permeable and cell-impermeable, as well as and different colors allow these system to be very flexible to follow fusion proteins in living cells with different colors [36].

To introduce such modified protein constructs into cells, transient or stable transfection is required, which is commonly associated with overexpression of the fusion protein. This may result in mislocalization of the protein induced by the recombinant tag or impair the actual function and interactions of the POI [37]. Additionally, if the cell-type used for the transfection also expresses the POI endogenously, this protein will not be fluorescent and thus not be detected under a fluorescent microscope, which might exacerbate the conclusions.

Recent gene technologies can overcome these limitations by using molecular toolkits to directly edit the cellular genome. Specific genes can for instance be modified using the clustered regularly interspaced short palindromic repeats (CRISPR)/ CRISPR-associated 9 (Cas9) - system in cell cultures [38]. Due to direct modification of the endogenous protein, artifacts caused by overexpression can be omitted.

In conclusion, the addition of recombinant tags to the POI is a straight forward approach and requires relatively little effort to study protein organization in fluorescence microscopy. The CRISPR/Cas9-system is very promising to reduce overexpression of the target protein, however it is still in development and few labs worldwide are using it routinely. Fusion chimeras expressed at endogenous levels with this technology might create transport, activation or localization problems. Moreover, genome editing or overexpression of protein fusion constructs so far cannot be applied on human pathology samples or biopsies. Therefore, many applications and scientists still rely in affinity probes as an alternative detection method.

1.3.2 Affinity-Based Detection

The interaction and affinity of proteins is an alternative way to visualize the target POI, which can be used for indirect labeling based on detection with specific affinity probes.

For instance the specific binding of natural toxins to cellular proteins can be exploited for molecular marking. The cholera and pertussis toxins interfere with cellular signaling by binding to specific domains of G-protein coupled receptors. This interaction can be used to employ fluorescently labeled toxins *in vitro* for binding assays using fluorescence microscopy [39].

Another prominent example is the fungus toxin phalloidin, which binds and stabilizes filamentous actin molecules [40]. Fluorescently labeled derivatives of phalloidin are widely used in fluorescence microscopy to visualize intracellular actin filaments [40].

The specific binding between molecules is not limited to the detection of protein-protein interactions, but can also be used to detect lipids or even ion concentrations.

The pleckstrin homology domain binds to phosphatidylinositol in various cellular signaling pathways mediating signal transduction [41]. Fluorescently labeled pleckstrin homology domains have been used to monitor the intercellular pools of different phosphoinositide pools in microscopy [42].

Yet the number of known natural ligands binding strongly to specific proteins is limited, hence only a minor subset of POI can be studied by this method. Therefore antibodies, evolved to detect a plethora of different targets, are commonly raised to specifically bind target antigens for indirect detection in microscopy.

Upon immunization with a target antigen, animals present peptides of the antigen on their major histocompatibility complexes (MHC), which generates an immune response [43]. Due to genetic recombination and somatic hypermutation antibodies are created binding to the antigen. These molecules can be purified and subsequently used for the specific detection of POI in biological samples.

The implementation of antibodies into fluorescence microscopy constituted the concept of immunofluorescence (IF) microscopy, which is up to now a common technique used in many laboratories. Commonly, the immunoglobulin gamma (IgG) antibodies used for IF are raised by animal immunization. When extracted from the serum and selected to bind a specific antigen, usually a plethora of IgG molecules is obtained that bind different epitopes of the same antigen. Such preparations are thus referred to as affinity-purified polyclonal antibodies.

In contrast, monoclonal antibodies are typically produced by single B-cells, producing a defined type of antibody, which were fused with an immortalized cell line. This procedure allows the creation of hybridoma cell lines that are able to be maintained growing while secreting one defined type of IgG molecules [44]. Consequently, monoclonal antibodies bind to their target antigen at one defined epitope, although the exact localization or sequence of the epitope is not always known. In IF microscopy, the POI is conventionally detected indirectly using a two-step antibody detection procedure. Antigen-specific primary antibodies are used to bind the POI and these are subsequently detected by secondary antibodies that carry enzymatic or fluorescent labels.

Secondary antibodies are mostly polyclonal, which results in signal amplification due to the binding of multiple secondary antibodies per primary antibody. This system provides high flexibility as differentially conjugated secondary antibodies can easily be substituted without requiring the use of a different primary antibody.

1.4 Affinity Probes in Microscopy

Due to their capability to detect virtually any cellular target, affinity probes gained a high popularity in molecular imaging approaches. Apart from conventional antibodies, also alternative probes with different biochemical properties have been developed. These alternative affinity probes are typically selected from comprehensive libraries generated from animal immune repertoires or by synthetic design to perform *in vitro* screenings and to identify specific binders to a desired target molecule.

1.4.1 Antibodies

Most immune systems of animals possess different isotypes of immunoglobulins performing different functions. The immunoglobulin gamma (IgG) is the most frequently antibody isotype used for immunostaining methodologies. At the molecular level, IgG molecules are composed of two identical heavy and two identical light chains, which are linked by disulfide bridges (see Figure 2A). Moreover, the heavy chains are also interlinked by two disulfide bridges resulting in a divalent affinity probe with a molecular weight (MW) of around 150 kDa and a spatial extent of approximately 10 nm [43]. The antibody heavy chain is composed of a conserved and a variable part, referred to as C_H1-C_H3 and V_H -domain, respectively (see Figure 2C). Similarly, the light chain is also composed of a constant (C_L) and a variable (V_L) domain.

The variable domains generally have a rather conserved sequence apart from three complementary determining regions (CDRs) on each chain. These regions are highly variable in amino acid composition and ultimately define the binding properties of the IgG molecule.

In the animal immune system, those CDR loops are assembled by somatic recombination and hypermutation upon immune cell maturation, creating a highly specific affinity molecule. Although the constant part of the IgG molecule (F_c) is not involved in antigen recognition, it participates in the mediation of the immune response in the animal. For stainings in IF microscopy, typically full IgG molecules are used. However, some features of full IgG molecules such as their bivalent binding, polyclonal nature and their large size can affect the accuracy of biological stainings [45,46].

1.4.2 Small Probes

As an alternative to full antibodies, smaller probes exist that can be used for specific target detection. One possibility is to engineer conventional antibodies by removing the domains not involved in epitope detection, thus reducing the size of the molecule.

Enzymes such as papain or pepsin can be used to cleave off the F_c -domain generating F_{ab} - and $F_{(ab)_2}$ -fragments, respectively as shown in Figure 2C. F_{ab} -fragments are monovalent affinity probes accounting for about one third of the IgG original size [47]. However, the production of antibody fragments is relatively expensive as large quantities of purified IgG molecules are required as a starting material.

Alternatively, both variable domains (V_H and V_L) of the antibody can be expressed as a recombinant protein fused together with an amino acid linker sequence. This procedure has been established already three decades ago, which allowed the generation of monovalent affinity probes termed single-chain variable fragments (scFvs, depicted in Figure 2C), which are commonly produced in bacteria [48]. Due to convenient modification in the expression host, scFvs can be engineered for various applications in molecular imaging approaches [45,46].

Yet, scFvs require a defined molecular conformation to mimic their adjoined localization in IgG antibodies and to acquire functionality. As the two domains of the scFv are naturally not linked but artificially fused, this has been observed to be a challenge in the generation of functional scFvs [49].

In 1993, two new classes of IgG antibodies were discovered in camelids [50]. They were described as IgG2 and IgG3, possessing a long and short hinge region, respectively. But in contrast to the classical IgG1 molecules, those IgG2 and IgG3 antibodies lack their light chains (see Figure 2B) and thus were termed heavy chain antibodies. Due to the absence of the light chains, the variable domains of the heavy chain antibody (V_H H-domain) solely mediate the interaction with the target antigen. Isolated V_H H domains, also-called nanobodies, have been used as a new versatile class of affinity molecules in the last years [51]. In contrast to scFvs, they do not require the introduction of a linker sequence and thus can readily be produced in bacteria without losing their binding specificity.

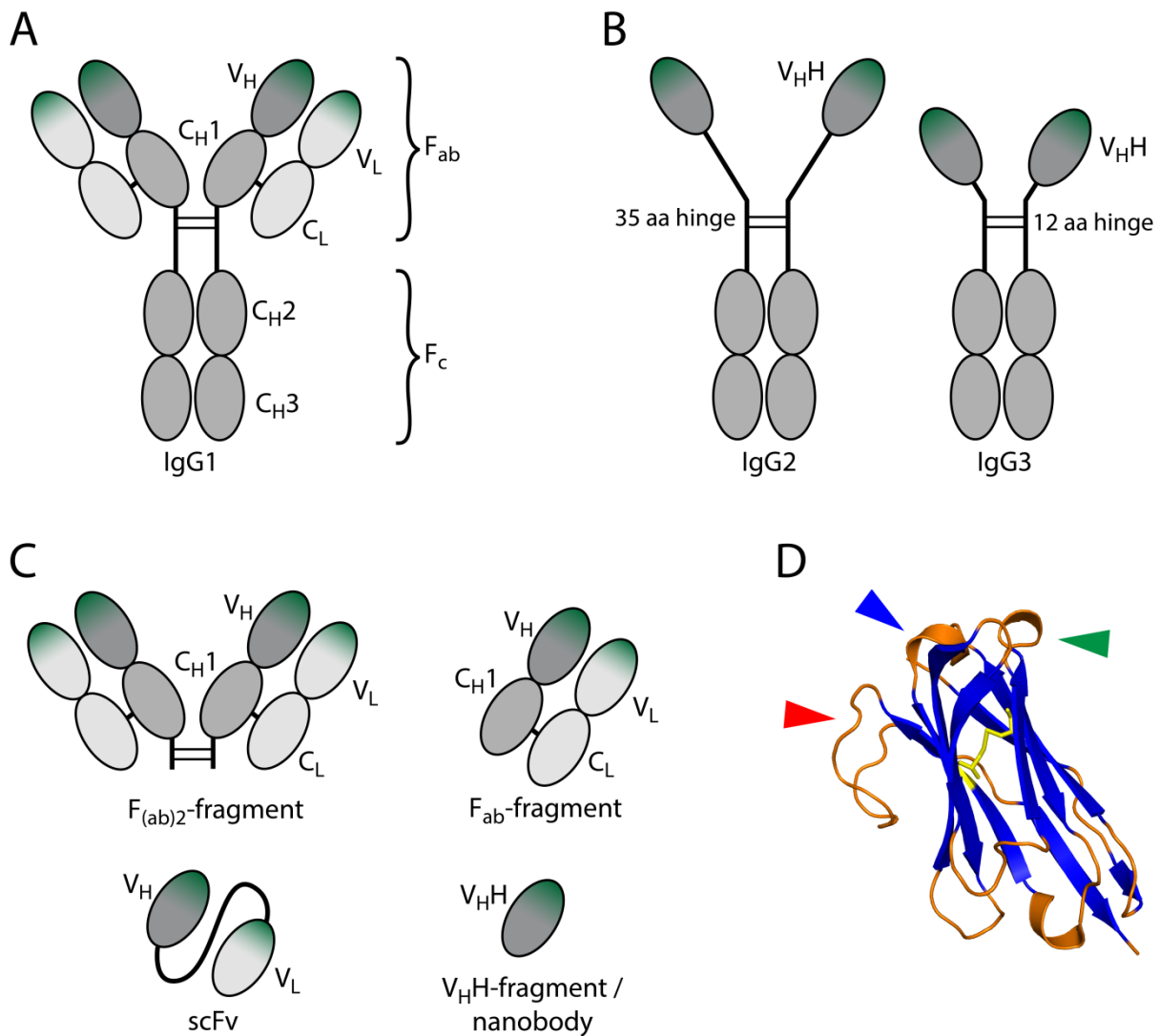


Figure 2: Affinity probes derived from immunoglobulin scaffolds. **A:** Conventional IgG1 antibodies are composed of two heavy and two light chains linked by disulfide bridges. Their constant domains (C_{H1-3} and C_L) primarily serve as a scaffold and mediator for immune response, whereas the variable domains V_H and V_L determine the antigen specificity and form the paratope. **B:** Novel classes of IgG antibodies devoid of the light chains were discovered by Hamers-Casterman *et al.* in 1993 [50]. In contrast to IgG1 antibodies, epitope binding is mediated by the heavy chain only thus terming them heavy chain antibodies. **C:** $F_{(ab)2}$ -fragments, F_{ab} -fragments and single chain variable fragments (scFvs) are obtained by enzymatic cleavage or recombinant expression of the antibody domains. In contrast, V_{HH} -fragments or nanobodies are derived from heavy-chain IgG antibodies and thus consist of a single domain. **D:** Ribbon cartoon model of a nanobody. The rigid scaffold is colored in blue pointing out the intramolecular disulfide bridge colored in yellow. The three CDR regions used for antigen detection are indicated by arrowheads. It can be seen that the CDR3 region (red arrowhead) forms an extended loop increasing interaction surface and allowing penetration into binding pockets. Structural information was obtained from the Protein Data Bank, accession number 1i3v.

Apart from affinity probes based on IgG scaffolds, also other small probes have been developed to be used as specific affinity molecules [52]. Figure 3 and Table 1 illustrate a selection of small probes commonly used in molecular biology. In addition to the probes depicted here, many other classes of probes have been described in the literature [46,52]. Analogous to nanobodies, those small probes are typically composed of a stable backbone scaffold and a variable region, providing affinity to the target antigen. In contrast to conventional antibodies, they often are capable of withstanding extreme pH and temperature conditions due to their compact and stable scaffold [53,54].

The principle of many small probes is based on molecular interactions found in nature. By randomizing a particular region of the probe, a variable region is generated while an overall rigid scaffold structure is maintained. Prominent examples for such probes are affibodies derived from the prokaryotic protein A, which binds to IgG molecules in nature (see Table 1 and Figure 3). Alternatively, the scaffold of affinity probes can be completely designed artificially as in the example of alphabodies [55,56]. Three short alpha-helices align laterally and hereby form the alphabody. The binding specificity is obtained by variable regions in two of the helices as also shown in Figure 3 and Table 1.

In addition to molecules based on protein scaffolds, assemblies of nucleic acids can be also used as affinity probes. Short stretches of DNA or RNA, commonly known as aptamers, were shown to bind a target antigen with high specificity [57,58]. However, the use of aptamers faces several challenges as they are highly negatively charged, rapidly degraded and their scaffold organization may be sensitive to pH and salt concentrations in the medium [57]. Still, the use of aptamers also follows the trend to minimize the size of the affinity probe used to detect specific target proteins.

Table 1: Characteristics of selected affinity probes commonly used in molecular biology. The probes are either derived from full IgG antibodies (blue), alternative protein scaffolds (green) or nucleotide-based scaffolds (orange). The dissociation constant K_D of all listed affinity probes can be found in the nanomolar range comparable to the affinity values obtained for conventional IgG antibodies ($k_D = 10^{-7}$ - 10^{-9} M). aa = amino acids, bp = base pairs MW [kDa] = molecular weight in kilo Dalton. Modified from Maidorn *et al.*, Biochem J, 2016

Name [reference]	Composition	Origin	Sequence length	Ø MW [kDa]	Ø Size	S-S bridges
IgG antibodies [44]	2 Heavy chains & 2 light chains	Immunization / hybridomas	≈1450 aa	≈150	10 nm	≥4
Fab-fragments [45]	Truncated heavy chain + light chain	IgG, cleaved by papain	≈450 aa	≈50	5 nm	≥2
Single chain variable fragments (scFvs) [46]	VH + VL domain of IgG antibody	Recombinant variable IgG domains	≈220 aa	≈25	3 nm	≥1
VHH fragments/ Nanobodies [51]	Variable domain of heavy chain antibody	Camelidae heavy chain IgG subtype	70-110 aa	≈15	2 nm	≤2
Affibody [53]	α-helical structure	<i>Staphylococcus aureus</i> protein A	≈58 aa	≈6	≈2 nm	0
Affitin [59]	Sac7d (DNA-binding protein)	<i>Sulfolobus acidocaldarius</i>	≈66 aa	≈7	≈2 nm	0
Alphabody [55,56]	3 α-helices	Artificial peptides	70-120aa	≈10	3 nm	0
DARPIN [60]	3-5 Ankyrin repeats	Membrane adaptor protein	≈160 aa	≈15-18	2 nm	0
Monobody [61]	7 β-sheets	Human fibronectin	≈90 aa	≈10	2 nm	0
Aptamers [58]	Strands of DNA or RNA	Synthetic sequence	15-60 bp	5-15	3-5 nm	-

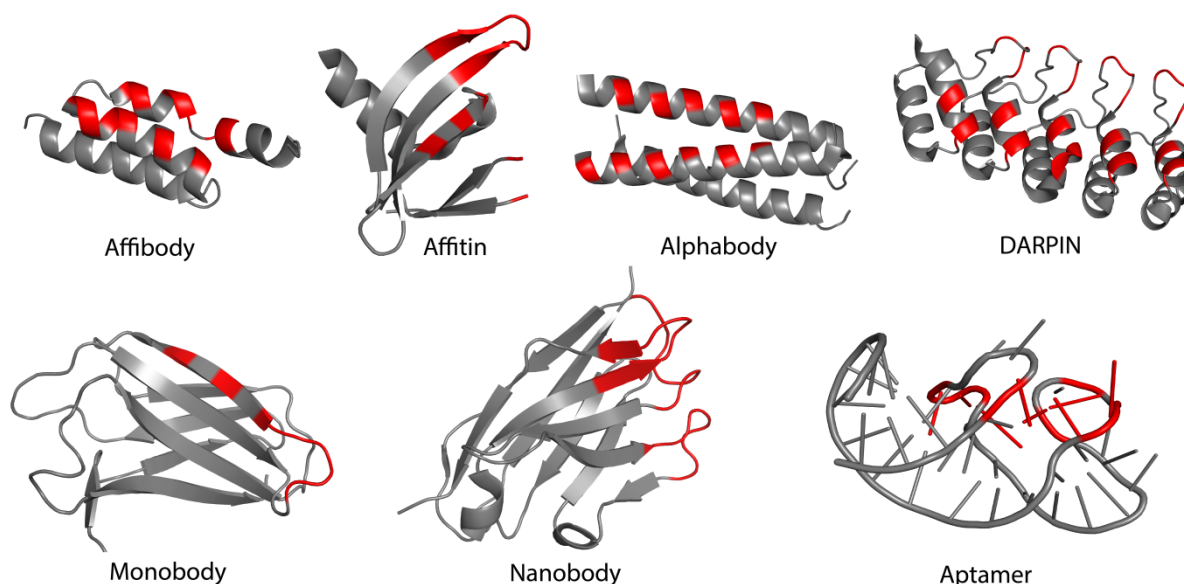


Figure 3: Examples of small affinity probes for specific target detection. Residues typically mediating the interaction to the antigen are colored in red; the constant scaffold of the molecule is shown in grey. An overview on the characteristic of the probes is provided in Table 1. Exemplary sequences were obtained from the Protein Data Bank (affibody: 2KZI; affitin: 4CJ1; alphabody: 4OE8; DARPIN: 4YDW; monobody: 5DC9; nanobody: 3K1K; aptamer: 4R8I). Modified from Maidorn *et al.*, Biochem J, 2016

1.4.3 *In vitro* Selection Techniques

The development of new affinity probes is usually based on screening complex libraries with a shuffled composition of amino acid residues in their variable region (see Figure 3, red color). The candidates, which show affinity to the target antigen, are subsequently identified from typically several million different molecules. Most commonly, the screening procedure is carried out using molecular display techniques such as phage display [62], yeast display [63] or ribosome display [64]. Those techniques link the biochemical properties of the expressed affinity probe to its genotype, allowing the identification of molecules with a defined sequence identity. The libraries used for screening require careful preparations to increase the chance of positive selection due to the presence of a high number of different molecules, commonly referred to as diversity.

Libraries for molecular display can be created in different ways. So-called naïve libraries are created from RNA preparations resembling sequences of variable IgG domains of a non-immunized animal. However, the existing IgG repertoire might not contain any specific binder to the POI, which may result in negative results during the screening procedure [65]. Libraries containing probes derived from IgG scaffolds, such as scFvs or nanobodies, are therefore typically created after immunization of the animal. This results in a pre-selection of affinity probes due to the immune response of the animal facilitating the later screening procedure [66,67].

To introduce a high diversity into the sequence composition of libraries or to modify the conserved scaffold of the probe, the variable regions can alternatively also be created synthetically. This can be used to increase solubility of the molecule or to mimic the scaffold of other species to avoid degradation in live experiments [51,68].

By permuting the arrangement of amino acids, which mediate the binding a plethora of sequence combinations may be created, which may not have been present in the animal. In addition to modulation of the variable regions, also the scaffold of the molecule can be modified to increase its stability. Synthetic libraries of nanobodies have been created, which use an improved molecular scaffold to optimize the solubility and stability of the probe [51]. Those libraries are often used by companies, which offer the service to screen for custom nanobodies while bypassing the laborious time-costly process of immunization and *de novo* library generation [69]. Synthetic libraries have been reported to achieve a diversity of up to 4×10^{10} different sequences, albeit the design of such libraries is an expensive and sophisticated procedure [70,71].

The molecular screening of either library reveals those candidates, which show affinity to the POI. After the screening procedure, the identified probes need to be validated further to test their applicability in experimental procedures. As most molecular display techniques are set up *in vitro*, the selected affinity probes might still cross-react with other proteins present in cells or other

biological samples. Various methods are used to validate the binding of the probe, including enzyme-linked immunosorbent assays (ELISA), affinity chromatography, immunoblotting and IF [67,72–74]. After confirming both affinity and specificity for a defined target protein, the new probes can be implemented in molecular and cell biology approaches.

Although synthetic libraries can achieve a higher diversity of different molecules, immune libraries contain already a larger proportion of specific probes, which were pre-selected by the animal immune system. This facilitates the selection and results in higher number of positive binders after the screening procedure. Nanobodies identified from camelid immune libraries therefore gain increasing attention as molecular tools.

1.4.4 Nanobodies

Although nanobodies are derived from antibodies, the molecular composition of their scaffold typically differs from its V_H counterpart found in IgG1 antibodies.

First, the nanobody scaffold shows an increased solubility compared to V_H -domains of conventional antibodies, as the hydrophobic amino acids usually mediating the interaction with the light chain are replaced by more hydrophilic residues [51].

Second, nanobodies commonly possess a very robust scaffold due to an intramolecular disulfide bridge, which contributes to the structural integrity of the molecule [23, 24]. They retain their function even during or after elongated exposure to high temperatures of up to 90 °C [76]. In addition to this, nanobodies also partially refold after denaturation, highlighting the thermodynamic stability of those molecules [77]. These biochemical properties essentially facilitate the production and handling of nanobodies during experimental applications.

Third, the CDR3 region was found to be more variable in length in comparison to V_H domains, thus increasing the interaction surface and generating a flexible loop for penetration in binding pockets [74]. It has been proposed that the elongated CDR3 loop of IgG2 and IgG3 antibodies constitutes an evolutionary strategy to increase the interaction surface of the affinity molecule with the antigen. This way those IgG types may be able to compensate the absence of a light chain, resulting in affinities of nanobodies comparable to conventional full IgG molecules [78,79].

Interestingly, nanobodies with very short CDR3 loops have been discovered also exhibiting high affinities to their target antigen [80,81].

Due to the gain in length and flexibility of the CDR3 region, nanobodies are even capable of detecting epitopes with a concave structure like enzymatic pockets or ligand binding sites. Such epitopes are typically difficult to access by conventional IgG1 antibodies, which possess a comparable flat paratope [82,83]. The CDR3 loop might as well enclose its target antigen, creating a headlock-like

interaction also involving the nanobody scaffold, which results in high affinities to the target antigen [84].

Figure 2D shows a cartoon model of a nanobody indicating the CDR regions and the intramolecular disulfide bridge. Due to their composition of a single peptide chain, nanobodies can also readily be expressed in bacteria bypassing the need of hybridoma cell lines. The formation of the intramolecular disulfide bridge can be promoted by directing the expression of the nanobody to the periplasmic space, which provides more oxidizing conditions [81,85]. A more recent strategy to increase the efficiency of nanobody production uses bacterial strains, such as SHuffle express® (New England Biolabs), constitutively expressing disulfide bond isomerases in the cytoplasm [86].

The recombinant expression of nanobodies allows modification such as adding molecular tags for purification and site-directed coupling reactions to the molecule. After expression and purification, fluorescent molecules can specifically be coupled to different positions of the expressed protein [87]. Up to now, custom labeled nanobodies have been used in various biological and medical applications including virus neutralization, positron emission tomography and other molecular imaging approaches [88–92].

1.5 Comparison of Nanobodies to Conventional Probes

During the last decades, new affinity probes and particularly nanobodies got increasing attention of many researchers. The small size of nanobodies (around 15 kDa) and their monovalent nature enables high tissue penetration and improved epitope detection even in protein-dense regions [52]. Since nanobodies can readily be produced in bacteria in scalable amounts, the maintenance of hybrid cell lines or animals is obsolete for production of the probe. Nanobodies linked to a fluorescent reporter or to a biochemical tag have already been used in various approaches including molecular imaging [51,80,93,94]. Fusion constructs with GFP can be expressed in cells as so-called intrabodies, which target their antigen *in vivo*. This approach has originally been suggested using full antibodies, which however require a complex expression and assembly process exacerbating the procedure [95]. Although the overexpression of intrabodies is an efficient and well-established procedure, it confines the sensitivity of detection due to high background signal [94]. The removal of background fluorescence thus requires the protein to be localized in specific compartment and the use of advanced image analysis tools to identify the specific signal of intrabody localization [96]. Intrabodies have also been suggested to be a potential tool in medical applications such as gene therapies [93,97].

Nanobodies are generally discussed as efficient therapeutic agents due to their high stability, limited cleavage by cellular proteases and low immunogenicity in humans [98,99]. Recently, nanobodies

targeting medically relevant targets, such as viral proteins [90,100,101] have been reported, preventing the assembly and propagation of the virus. Their additional high tissue penetration and fast clearance from the bloodstream makes nanobodies attractive for selective tumor targeting in cancer therapy [102–104]. So far, several clinical studies using commercial nanobodies for therapy are conducted or have already been completed [69]. In addition to their use in research, nanobodies may therefore also constitute new alternatives of medical treatments in the near future.

In research, nanobodies are already used as an alternative to conventional antibodies. They have been demonstrated to be valuable and versatile tools in molecular imaging and particular in super-resolution microscopy [91,105]. One example is shown in Figure 4 where antibodies or nanobodies are used to stain spatially separated microtubules *in vitro*. In single molecule localization images it was found that directly labeled nanobodies reveal a better separation of individual microtubules than directly modified antibodies [105].

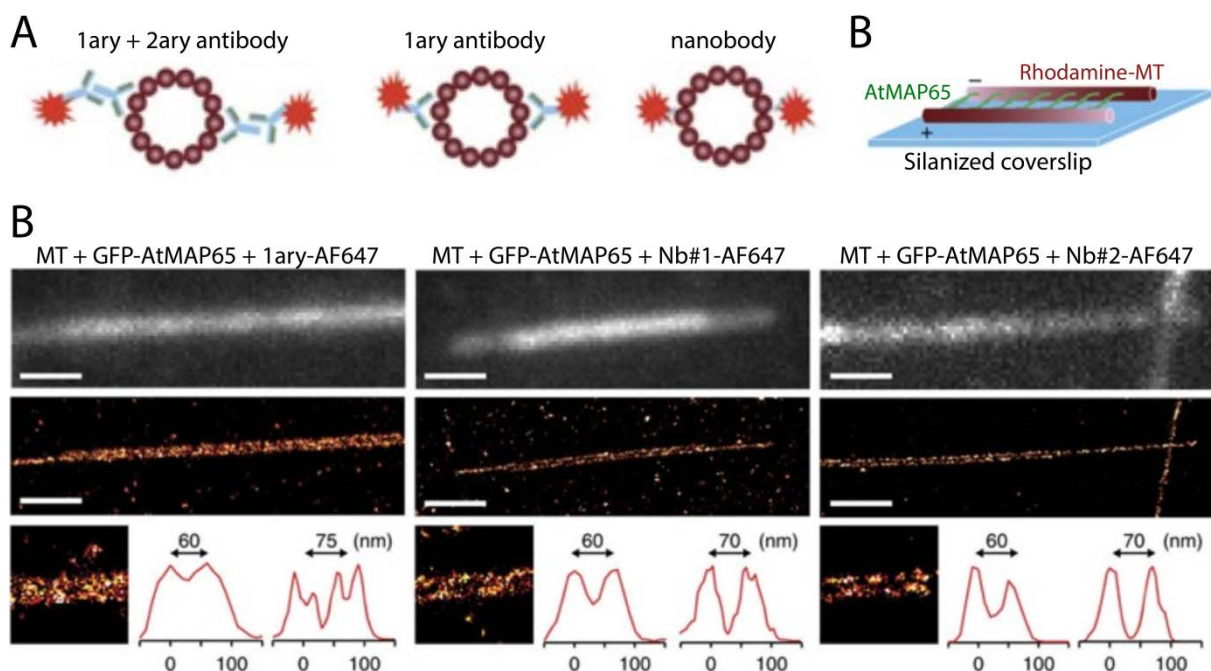


Figure 4: Smaller labels allow better resolution of microtubules. **A:** Illustration of different detection strategies using primary and labeled secondary antibody (1ary + 2ary), a directly labeled primary antibody (1ary) or directly labeled nanobody. **B:** Scheme of the *in vitro* microtubule bundling assay to test the resolving power of different microtubule labelling strategies. Rhodamine-labelled microtubules are assembled into planar bundles with defined spacing formed by the microtubule-bundler GFP-AtMAP65-1. **C:** Conventional (top) and single molecule localization (middle and bottom left) images and representative line scans (bottom right) of *in vitro* microtubule bundles stained with a fluorescently labelled primary anti- α -tubulin antibody (1ary-AF647) or two novel tubulin nanobodies (VHH#1 and VHH#2) conjugated to AF647. As shown in the bottom panel, nanobodies allow better separation of individual microtubules. Scale bar represents 1 μ m.

Modified from Mikhaylova *et al.*, Nat Comm, 2015

Nanobodies show an improved penetration capability into tissues compared to conventional antibodies, which often detect only a subset of their target antigen [72,106]. Also in staining cultured cells in IF microscopy, nanobodies provide several advantages. Unlike antibodies, they are monovalent probes and therefore cannot induce molecular clustering by binding multiple proteins as described in section 1.4. This clustering effect of antibodies is commonly known to create artifacts in immunostaining, which might lead to misinterpretation of the data [58,107,108].

Classical staining protocols for IF microscopy rely on primary and secondary antibodies for detection. This additionally enhances the clustering effect by binding of the secondary antibody as illustrated in Figure 5 [108]. When using different antibody species for a staining, intermolecular cross-reactivity or limited compatibility of secondary antibodies may impose another level of complication [109]. Directly conjugated nanobodies do not require the use of secondary molecules and omit this problem.

It has also been shown in super-resolution that the assembly of an antibody complex delocalizes the fluorescent signal from the antigen, as the fluorophore is typically conjugated to the secondary antibody [91]. Therefore it is required in super-resolution imaging to direct the fluorophore as close to the epitope as possible. Directly conjugated nanobodies can bring the fluorescent moiety as close as 2 nm to the epitope, thus preventing delocalization as shown in Figure 5 [110]. From this effect it has been concluded that conventional antibodies cannot keep up with technical improvements to increase the resolution in microscopy [91,105].

In addition to its displacement, also the intensity of the fluorescent signal depends on the probe used for staining. Commonly used secondary antibodies carry between zero and four fluorophores, primarily due to the random chemistry used in their labeling protocols [111]. Thus, the intensity of the fluorescent signal underlies a stochastic distribution of secondary antibodies detecting and clustering their primary target [111]. Small probes which were coupled to the fluorescent moieties in a controlled stoichiometric ratio in turn can provide a more quantitative detection of the POI [112]. Taking together these arguments, many researchers suggest that monovalent small probes such as nanobodies could provide a valid alternative for antibodies in IF microscopy [92,110,112]. Their good performance even in protein-dense environments makes nanobodies valuable tools to study complex biological structures such as neuronal synapses.

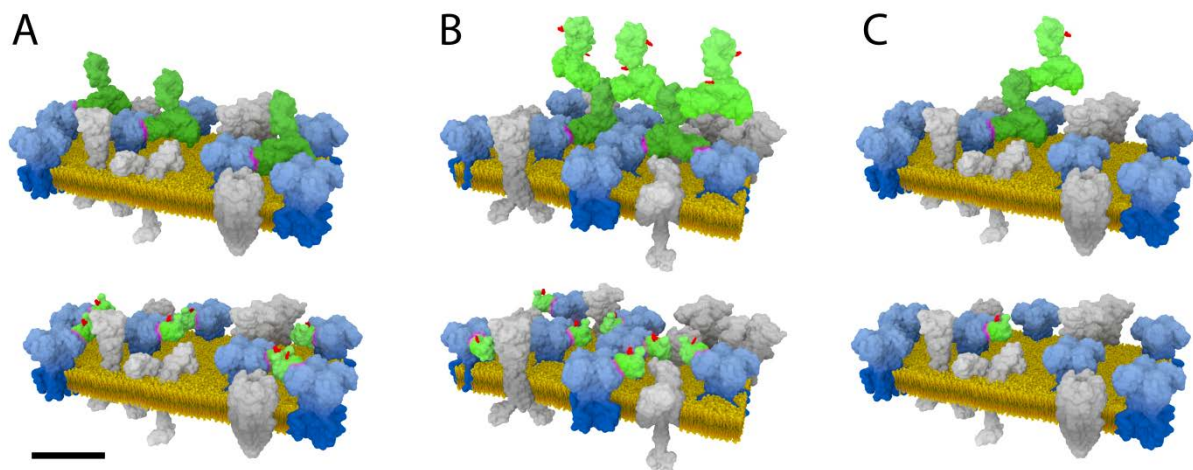


Figure 5: Schematic comparison of antigen detection by antibodies (top) or nanobodies (bottom) on molecular level. A piece of membrane with a fictive arrangement of integral membrane proteins is shown. A potassium ion channel is shown as an example for a membrane residing target antigen. **A:** The size of antibodies (green molecules, top panel) may impair them from detecting the entirety of antigens in a complex biological sample. In contrast, nanobodies (light green molecules, bottom panel) are smaller in size and can even access buried epitopes. **B:** Conventional antibodies might induce cluster formation caused by divalent binding, which can result in staining artifacts (top panel). Monovalent probes such as nanobodies do not show this effect due to stoichiometric binding of their target antigen (bottom panel). **C:** Successive binding of primary and secondary antibody (each 12-15 nm in size, top panel) delocalizes the fluorophore from the actual position of the target antigen. On the other hand, conjugated nanobodies direct the fluorophore in close proximity (around 2 nm [110]) to the antigen and therefore increasing the attainable resolution (bottom panel).

The structures of the proteins used for modelling were obtained from the Protein Data Bank (PDB accession codes: 1HZH, 3OGO, 3KG2, 2BG9, 4PE5, 2VT4, 4PAS, 2RH1, 1EWK, 3LUT, 1EWK, 2E4U, 3KS9, 4OR2 and 5CM4). All elements are displayed in correct relative size scale. The binding interface is highlighted in magenta, and fluorescent molecules conjugated with the affinity probes are colored red. Scale bar represents 10 nm. Modified from Maidorn *et al.*, *Biochem J*, 2016

1.6 Imaging Approaches to Study the Synaptic Architecture

Synapses have already been in the focus of research for more than a century [113]. Due to their key role as central communication platforms between neurons, maintaining synaptic integrity is the basis to ensure the survival of an organism. Hence it has been of major interest to reveal the molecular mechanisms, which underlie synaptic function.

In the past, various microscopy techniques have contributed to reveal the synaptic ultrastructure and understand functional principles of synapses. The first synaptic subcellular structures were already revealed in the 1950s using electron microscopy describing synaptic morphology and anatomy [114,115]. Emerging EM techniques provide a detailed view on synaptic ultrastructure highlighting characteristic structures such as the postsynaptic density and synaptic vesicle pools (see Figure 6) [116,117]. Although modern EM techniques can achieve a spatial resolution as high as 50 pm allowing to visualize molecular complexes [118], it is difficult to follow a particular POI due to different limitations in the methodology. Nevertheless, immuno-EM has been developed to use gold-coupled antibodies to detect specific proteins; yet the affinity probes usually detect only a small fraction of the antigens [119]. A major reason is the harsh sample preparation required to preserve the synaptic ultrastructure for EM. Particularly this includes fixation with high concentrations of glutaraldehyde and treatment with osmium tetroxide as stated in section 1.2.3. This creates a dense proteinaceous network in, which the epitopes might no longer be accessible for antibodies, thus impeding the detection of the target antigen [21,22]. Probes with better tissue penetration might overcome this limitation as they can penetrate also into protein-dense regions.

All in all, EM is still able to reveal major aspects of the synaptic ultrastructure in excellent detail. Yet this technology comes to its limits when multiple target antigens should be observed in parallel or *in vivo* imaging is intended. For this, IF microscopy is the method of choice due to the rather easy sample preparation, spectral separation of individual fluorescent signals and the possibility of *in vivo* imaging of whole brains [120].

Early IF experiments revealed the accumulation of synaptic proteins, which were found to be required for synaptic vesicle fusion. These molecules were termed SNARE proteins, an acronym for soluble N-ethylmaleimide-sensitive fusion protein-attachment receptor [121,122]. These investigations together with anatomic information from EM studies led to the formation of a model describing the regulatory mechanisms of the synapse such as synaptic vesicle fusion [123,124]. Three major SNARE proteins in hippocampal synapses are the vesicle-associated protein 2 (VAMP2 or synaptobrevin), synaptosomal-associated protein 25 (SNAP-25) and syntaxin 1A (see Figure 6B).

Notably, SNARE proteins are not only found in synapses but represent a large family of protein which mediates vesicle fusion in various compartments of the cell. This includes protein trafficking at the Golgi apparatus as well as fusion events at the plasma membrane or involving endosomes [125]. SNARE proteins therefore constitute an important class of molecules in the whole cell, albeit neuronal SNAREs mediating synaptic vesicle fusion have been studied most thoroughly.

The current vision of neurotransmitter release in the nervous system suggests that an action potential arriving to a synapse causes voltage-gated calcium channels to open and let calcium concentration to rise locally [126]. The detection of calcium by synaptotagmin triggers the conformational change in the heteromeric SNARE bundle formed by two alpha helices from SNAP-25 (palmitoylated to the plasma membrane) and one from each synaptobrevin (anchored to the vesicle) and syntaxin 1A (anchored to the plasma membrane). The force resulting from the conformation rearrangement in the helix bundle subsequently mediates the fusion of synaptic vesicles at the active zone of the plasma membrane causing the release of neurotransmitter [126].

For maintaining synaptic integrity and function, the cycling and recycling of synaptic vesicles constitutes a key mechanism. Hence, a detailed understanding of the individual steps in this complex process will allow to describe and modulate overall synaptic activity [124,126,127].

The development of super-resolution techniques such as STED and STORM allowed researchers to investigate synaptic structures on molecular level [128–130]. Small structures such as individual synaptic vesicles cannot be visualized using conventional fluorescence microscopy techniques due to their size of ~40 nm in diameter. Those vesicles were among the first biological structures to be observed by emerging super-resolution techniques, constituting a new benchmark for subcellular investigations on synaptic physiology [11]. In subsequent years, super-resolution microscopy was exploited to map the organization of synaptic proteins [131,132].

As the positioning and composition of proteins is strongly linked to their intracellular role, these studies substantially contribute in understanding the principles of synaptic function [133]. As a consequence, the model on synaptic vesicle cycling and synaptic organization became essentially more elaborate as illustrated in Figure 6C [134,135]. Specifically, SNAP-25 and syntaxin 1A were observed to form clusters all over the plasma membrane, which are regarded as reserve pools for these SNARE proteins [134,135]. In addition different pools of synaptic vesicles have been classified depending on their capability of fusion with the membrane upon stimulation [131,136]. However it should be noted that most experiments indicating the clustering of molecules were conducted using antibodies as affinity probes to detect the POI.

Ultimately the observations on synaptic proteins led to a refinement of models on synaptic function describing the formation of protein microdomain organization and interaction in high detail [126,130,137]. Combining quantitative proteome analysis with imaging, a molecular model of a synaptic vesicle has been created, highlighting the relevance to reveal the stoichiometry of cellular processes [129]. With the help of super-resolution microscopy, this three-dimensional illustration has further been extended in recent years. This resulted in a model mapping the quantitative protein distribution of ~60 proteins in an average hippocampal synapse in molecular detail shown in Figure 6D [128].

A vast majority of the aforementioned studies used specific affinity probes to detect and map the target proteins in the synapse. Both diffraction-limited and super-resolution microscopy rely on the specific detection of endogenous proteins to determine their localization under native conditions. Up to now, conventional antibodies are the most common type of affinity probe used in IF microscopy. As proteins constitute a major fraction of the synapse, the dense congregation of macromolecules is likely to impair the free diffusion of antibodies hampering epitope detection [128]. The clustering effect of antibodies and the signal amplification caused by using polyclonal secondary antibodies additionally exacerbates the quantitative analysis synapses with conventional or advanced microscopy techniques. Taking into account these limitations of antibodies in super-resolution microscopy (see also section 1.5), using alternative small, monovalent and directly conjugated probes is essential to progress further on the molecular study of synaptic physiology using current microscopy. Therefore, nanobodies binding synaptic proteins would be a valuable tool for various investigations on synaptic function.

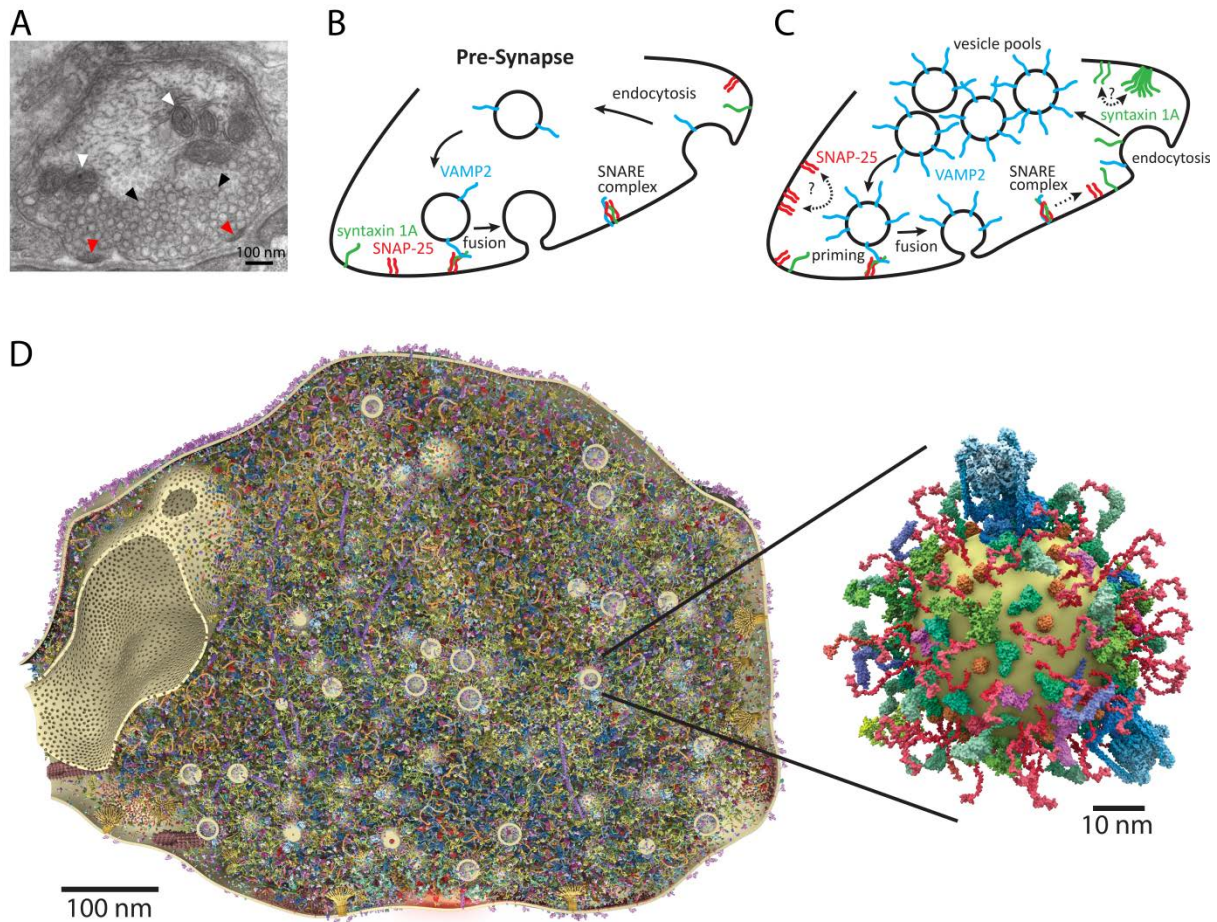


Figure 6: Electron micrograph and models describing synaptic organization. **A:** Electron micrograph depicting the presynaptic ultrastructure. EM clearly shows the distribution of subcellular structures such as mitochondria (white arrowheads) and synaptic vesicles (black arrowheads). The fusion of synaptic vesicles occurs at the active zone (red arrowheads). **B:** A schematic and simplified model describing the synaptic vesicle cycle. SNARE proteins such as VAMP2 on the vesicle (blue) together with SNAP-25 and syntaxin 1A residing on the plasma membrane (red and green, respectively) mediate synaptic vesicle fusion events. The vesicles fuse at the active zone and the vesicle material is subsequently recycled via endocytosis. **C:** Refined model of synaptic vesicle cycling based on super-resolution microscopy data [11]. The SNARE proteins are present in high copy numbers and show cluster formation along the plasma membrane [135]. Different pools of synaptic vesicles have been described showing differential response to stimulation [138,139]. **D:** A 3-dimensional reconstruction of the presynapse considering qualitative and quantitative distribution of the 60 most abundant proteins. The model was generated based on previous data published by Wilhelm *et al.* [128]. Modified from Maidorn *et al.*, Biochem J, 2016

1.7 Aims of the Project

The molecular organization of synapses has so far primarily been analyzed using conventional antibodies. However, these rather large molecules show some limitations when using them in today's super-resolution microscopy, which impair the staining quality and resolution.

Therefore, the aim of this project was to generate nanobodies as alternative affinity probes to investigate the synaptic physiology by super-resolution microscopy. The three major synaptic SNARE proteins VAMP2, SNAP-25 and syntaxin 1A were chosen as antigens for the generation of novel nanobodies. Up to now, no nanobodies against any of these proteins have been reported in the literature. Due to their features beneficial for super-resolution microscopy, such nanobodies would be a very attractive tool to reveal the organization of the synaptic SNARE proteins.

In order to obtain specific nanobodies, it was primarily necessary to establish a standardized protocol for the selection and validation of new affinity probes. In addition to the selection of nanobodies binding the aforementioned SNARE proteins, this protocol ought to become a general procedure for the future selection of nanobodies binding alternative candidates.

2. Material and Methods

2.1 Materials and Reagents

This section lists all commercial equipment specifically used during the project. Information on the manufacturer is given for important chemicals and reagents.

2.1.1 General Chemicals

Generally, all chemicals were purchased from Sigma-Aldrich, St. Louis, MO, USA or VWR, Radnor, PA, USA. The following Table 2 only lists all specific chemicals and commercial buffers used in the project. In subsequent references to individual chemicals, only the chemical abbreviation and company name is given; please refer to Table 2 for further information.

Table 2: Specific chemicals and commercial buffers used in the project

Component	Company	Location
α-select Chemically Competent Cells	Bioline Reagents	London, UK
1-Step™ Ultra TMB-ELISA Substrate Solution	Thermo Fisher Scientific	Waltham, MA, USA
Agarose, peqGOLD	PeqLab	Erlangen, Germany
Albumin	AppliChem	Darmstadt, Germany
Albumin Standard, 2 mg/ml, Pierce™	Thermo Fisher Scientific	Waltham, MA, USA
Ampicillin sodium salt	Sigma-Aldrich	St. Louis, MO, USA
Aprotinin	Sigma-Aldrich	St. Louis, MO, USA
BE Strep-Tactin® Elution Buffer	IBA	Göttingen, Germany
CaCl₂	Merck KGaA	Darmstadt, Germany
cOmplete™ His-Tag purification resin	Sigma-Aldrich	St. Louis, MO, USA
DMSO (anhydrous, 2 ml aliquots)	Thermo Fisher Scientific	Waltham, MA, USA
DNaseI	Sigma-Aldrich	St. Louis, MO, USA
Dulbecco's Modified Eagle's Medium (DMEM)	Lonza	Basel, Switzerland
Dulbecco's Phosphate Buffered Saline (DPBS)	Sigma-Aldrich	St. Louis, MO, USA
Ethidium bromide solution 0.025 %	Carl Roth	Karlsruhe, Germany
FastAP	Thermo Fisher Scientific	Waltham, MA, USA
FastDigest Buffer	Thermo Fisher Scientific	Waltham, MA, USA
FastDigest Restriction enzymes	Thermo Fisher Scientific	Waltham, MA, USA
Fetal calf serum (FCS)	Biochrom	Berlin, Germany
Geneticin, 50 mg/ml	Gibco / Thermo Fisher Scientific	Waltham, MA, USA
Glucose	Merck KGaA	Darmstadt, Germany
Glycerol	VWR	Radnor, PA, USA
Hoechst Solution 20 mM	Thermo Fisher Scientific	Waltham, MA, USA

Horse serum (HS)	Biochrom	Berlin, Germany
Hydroxylamine	Sigma-Aldrich	St. Louis, MO, USA
Hyperphage M13 K07ΔpIII	Progen	Heidelberg, Germany
IPTG	VWR	Radnor, PA, USA
Kanamycin sulfate	Sigma-Aldrich	St. Louis, MO, USA
L-cysteine	Sigma-Aldrich	St. Louis, MO, USA
Leupeptin	Sigma-Aldrich	St. Louis, MO, USA
Lysozyme	Sigma-Aldrich	St. Louis, MO, USA
MagStrep 'type3' XT beads	IBA	Göttingen, Germany
MEM (Minimal Essential Media)	Thermo Fisher Scientific	Waltham, MA, USA
MEM non-essential amino acids, 100x concentrated	Thermo Fisher Scientific	Waltham, MA, USA
Milk powder	Carl Roth	Karlsruhe, Germany
MK13KO7 helper phages	New England Biolabs	Ipswich, MA, USA
Neurobasal-A	Thermo Fisher Scientific	Waltham, MA, USA
Nuclease-free water	Carl Roth	Karlsruhe, Germany
Nucleotide Mix, 100 mM	Thermo Fisher Scientific	Waltham, MA, USA
Papain	Cell Systems	Spich, Germany
PEG-8000	Sigma-Aldrich	St. Louis, MO, USA
Pepstatin A	Sigma-Aldrich	St. Louis, MO, USA
PFA	Sigma-Aldrich	St. Louis, MO, USA
Phusion® High-Fidelity DNA polymerase	New England Biolabs	Ipswich, MA, USA
PMSF	Sigma-Aldrich	St. Louis, MO, USA
Recovery Medium	Lucigen	Middleton, WI, USA
RNAlater®	Sigma-Aldrich	St. Louis, MO, USA
RNaseZAP™	Sigma-Aldrich	St. Louis, MO, USA
Sephadex™ G-25 superfine resin	GE Healthcare	Little Chalfont, UK
Sodium pyruvate	Gibco / Thermo Fisher Scientific	Waltham, MA, USA
Sulphuric acid	Carl Roth	Karlsruhe, Germany
T4 DNA ligase	Thermo Fisher Scientific	Waltham, MA, USA
T4 DNA ligase buffer	Thermo Fisher Scientific	Waltham, MA, USA
TCEP	Sigma-Aldrich	St. Louis, MO, USA
Trypsin (for phage display)	Sigma-Aldrich	St. Louis, MO, USA
Trypsin inhibitor	Sigma-Aldrich	St. Louis, MO, USA
Trypsin/EDTA 170.000 U/l	BioWhittaker/Lonza	Basel, Switzerland
Vectors/plasmids (see also Table 12)	Addgene & Clontech Laboratories	Cambridge, USA Mountain View, California, USA

2.1.2 Buffers, Solutions and Media

The following Table 3 contains all self-prepared buffers and solutions used during the project in alphabetical order. Generally, all buffers were prepared in deionized water obtained from an arium® pro Ultrapure Water System (Sartorius, Göttingen, Germany). The media used for culturing bacteria and mammalian cells are depicted in Table 4 and Table 5, respectively.

Table 3: Buffers and solutions

Buffer / Solution	Composition
A500	50 mM 2-[4-(2-hydroxyethyl)piperazin-1-yl]ethanesulfonic acid (HEPES), pH 8.0 500 mM NaCl 30 mM ultrapure imidazole 5 mM MgCl ₂ 10 % (v/v) glycerol
Anode buffer	200 mM Tris Base, pH 8.8
B500	50 mM HEPES, pH 7.5 500 mM NaCl 500 mM ultrapure imidazole 5 mM MgCl ₂ 5 % (v/v) glycerol
Cathode buffer	100 mM Tris Base, pH 8.3 100 mM Tricine 0.1 % (w/v) sodium dodecyl sulfate (SDS)
Cell lysis buffer	50 mM Tris/HCl, pH 7.5 150 mM NaCl 2 mM ethylenediaminetetraacetic acid (EDTA) 0.5 % (v/v) IgePAL 0.5 % (w/v) Sodium deoxycholate store at 4 °C
Enzyme inactivation solution	DMEM supplemented with 10 % (v/v) FCS (Biochrom) 0.2 mg/ml albumin (AppliChem) 0.2 mg/ml Trypsin inhibitor (Sigma-Aldrich)
Hippocampi digestion solution	DMEM supplemented with 0.5 mg/ml L-cysteine (Sigma-Aldrich) 100 mM CaCl ₂ (Merck) 50 mM EDTA (Merck) 2.5 U/ml papain (Cell Systems)
HS-PBS	500 mM NaCl 4.3 mM Na ₂ HPO ₄ 2.7 mM KCl 1.47 mM KH ₂ PO ₄ adjusted to pH 7.4
M9 salt solution (5x)	450 mM Na ₂ HPO ₄ 110 mM KH ₂ PO ₄ 90 mM NH ₄ Cl 45 mM NaCl
Mowiol solution	100 mM Tris Base, pH 8.5 23 % (v/v) glycerol 9 % (v/v) Mowiol 4-88 (Merck)

PBS	137 mM NaCl 4.3 mM Na ₂ HPO ₄ 2.7 mM KCl 1.47 mM KH ₂ PO ₄ adjusted to pH 7.4
PBS-BSA	PBS supplemented with 3 % (w/v) bovine serum albumin fraction V (AppliChem) and sterile- filtered through 0.22 µm syringe top filter (Sartorius)
PBS-T	PBS supplemented with 0.2 % (v/v) Tween® 20
PBS-T/milk	5 % (w/v) milk powder (Carl Roth) in PBS-T
PBS-Tx	PBS supplemented with 0.1 % (v/v) Triton™-X100 (Sigma-Aldrich)
SDS-PAGE destaining buffer	50 % (v/v) demineralized H ₂ O 40 % (v/v) MeOH 10 % (v/v) glacial acetic acid
SDS-PAGE gel buffer (10x)	3 M Tris/HCl, pH 8.45 0.3 % (w/v) SDS
SDS-PAGE gel staining buffer	1 g Coomassie Brilliant Blue G-250 in SDS-PAGE destaining buffer
SDS-PAGE sample buffer (2x)	100 mM Tris/HCl, pH 6.8 20 % (v/v) glycerol 4 % (w/v) SDS 200 mM DTT 0.02 % (w/v) Coomassie Brilliant Blue R-250
Sortase buffer	50 mM Tris/HCl, pH 7.5 150 mM NaCl 10 mM CaCl ₂
TAE buffer	40 mM Tris-(hydroxymethyl)-aminomethan, pH 8.0 20 mM Acetic acid 1 mM EDTA
TBSC	10 mM Tris/HCl, pH 7.4 137 mM NaCl 1 mM CaCl ₂
TFB1	30 mM potassium acetate 10 mM CaCl ₂ 50 mM MnCl ₂ 100 mM RbCl 15% (w/v) glycerol adjusted to pH 5.8 with acetic acid sterile-filtered (0.22 µm filter)
TFB2	10 mM MOPS 75 mM CaCl ₂ 10 mM RbCl 15% (w/v) glycerol adjusted to pH 6.5 with KOH sterile-filtered (0.22 µm filter)
WB transfer buffer	50 mM Tris/HCl 192 mM glycine 20 % (v/v) MeOH 0.04 % (w/v) SDS

Table 4: Liquid and solid media used for bacterial cultures. All media were autoclaved and cooled to room temperature before use.

Medium	Composition
2-YT (Yeast Tryptone)	16 g tryptone 10 g yeast extract 85 mM NaCl in 1 l H ₂ O
2-YT agar plates	15 g agar in 1 l 2-YT medium
LB (Lysogeny Broth)	10 g tryptone 15 g yeast extract 170 mM NaCl in 1 l H ₂ O
LB agar plates	15 g agar in 1 l LB medium 100 µg/ml ampicillin sodium salt or 50 µg/ml kanamycin sulfate
M9 minimal medium glucose plates	15 g agar in 800 ml H ₂ O 200 ml 5xM9 salt solution 0.2 % (w/v) glucose 1 mM MgSO ₄ 0.1 mM CaCl ₂ 1 µg thiamine
SOC (Super Optimal Broth)	20 g tryptone 5 g yeast extract 10 mM g NaCl 2.5 mM KCl 10 mM MgCl ₂ 10 mM MgSO ₄ 20 mM glucose in 1 l H ₂ O
TB (Terrific Broth)	12 g tryptone 24 g yeast extract 4 ml (v/v) glycerol 72 mM K ₂ HPO ₄ 17 mM KH ₂ PO ₄ in 1 l H ₂ O
Top-agar	0.7 g agar in 100 ml LB medium

Table 5: Media for mammalian cell culture

Cell type	Composition	Reference
COS-7	High glucose (4.5 g/l) DMEM with 4% (w/v) L-glutamine 10% (v/v) FCS 100 U/ml penicillin-streptomycin	[140]
Glia cells	Minimum Essential Medium (MEM) with 10% HS 0.6% glucose (w/v) 1 mM L-glutamine 100 U/ml penicillin-streptomycin	[141]
HEK293	High glucose (4.5 g/l) DMEM with 4% (w/v) L-glutamine 10% (v/v) FCS 100 U/ml penicillin-streptomycin	[142]
HEK293-FT	High glucose (4.5 g/l) DMEM with 4% (w/v) L-glutamine 10% (v/v) FCS 100 mM MEM non-essential amino acids 500 µg/ml geneticin 100 U/ml penicillin-streptomycin	[142]
Neuronal maintenance medium	MEM with 0.6% glucose (w/v) 1 mM sodium pyruvate 100 µM putrescine 30 µM selenium dioxide 20 µM progesterone 0.1 mg/ml bovine transferrin 5 mg/ml insulin	[141]
PC-12	DMEM with 4 mM L-glutamine 10% HS 5% FCS 100 U/ml penicillin-streptomycin	[143]

2.1.3 Molecular Kits

For quantitative preparation of genetic material as well as for biochemical analyses, several kits were used during this project. In Table 6, those kits are listed together with the corresponding manufacturer. Unless specified otherwise in section 3, all kits were used according to the manufacturer's instructions.

Table 6: Commercial kits for molecular biology used in the project

Kit	Purpose	Manufacturer
GeneJET Mini Prep	Plasmid isolation from bacteria	Thermo Fisher Scientific, Waltham, MA, USA
Novagen® BCA Protein Assay	Quantitative determination of protein concentrations	Merck, Darmstadt, Germany
NucleoBond® Xtra Midi	Large-scale plasmid isolation from bacteria	Machery-Nagel, Düren, Germany
QIAquick® Gel Extraction	Extraction of genetic material from agarose gels	Quiagen, Venlo, Netherlands
QIAquick® PCR purification	Removal of protein contaminations from DNA preparations	Quiagen, Venlo, Netherlands
RNeasy® Mini	RNA isolation from white blood cell preparations	Quiagen, Venlo, Netherlands
SuperScript™ III One-Step RT-PCR	Reverse transcription from total RNA preparations	Thermo Fisher Scientific, Waltham, MA, USA
SuperScript™ IV First-Strand Synthesis System	Reverse transcription from total RNA preparations	Thermo Fisher Scientific, Waltham, MA, USA

2.1.4 Antibodies

The primary and secondary antibodies used in the project are listed in Table 7 and Table 8.

Table 7: Primary antibodies used in IF staining and for comparative studies

Antibody target	Clone name / product code	Dilution	Source
Homer-1	160 011	1:100	Synaptic Systems, Göttingen, Germany
SNAP-25	clone 71.1 / 111 011	1:100	Synaptic Systems, Göttingen, Germany
SNAP-25	111 002	1:100	Synaptic Systems, Göttingen, Germany
Synaptophysin	101 004	1:200	Synaptic Systems, Göttingen, Germany
Syntaxin 1A	HPC-1	1:50	Abcam, Cambridge, UK
Syntaxin 1A	110 302	1:100	Synaptic Systems, Göttingen, Germany
Syntaxin 1A	clone 78.2 / 110 011	1:100	Synaptic Systems, Göttingen, Germany

Table 8: Fluorescently labeled secondary antibodies used to detect primary antibodies

Antibody target	Clone name / product code	Conjugation	Dilution	Manufacturer
FLAG-tag / DDDDK-tag	clone M2	DyLight®650	1:500	Abcam, Cambridge, UK
Guinea pig IgG	706-545-148	Alexa488	1:200	Jackson ImmunoResearch, Newmarket, UK
HA-tag	clone 16B12	DyLight®650	1:500	Abcam, Cambridge, UK
Mouse IgG	2-0002-005-1	Star580	1:100	Abberior, Göttingen, Germany
Mouse IgG	715-165-150	Cy3	1:100	Dianova, Hamburg, Germany
Mouse IgG	50185	atto647N	1:100	Sigma-Aldrich, St. Louis, MO, USA
Mouse IgG	610-156-121	atto647N	1:100	Rockland, Limerick, PA, USA
Phage protein pVIII	27-9421-01	HRP	1:5000	GE Healthcare, Little Chalfont, UK
Rabbit IgG	715-165-152	Cy3	1:100	Dianova, Hamburg, Germany
Rabbit IgG	611-156-122	atto647N	1:100	Rockland, Limerick, PA, USA

Antibodies against SNAP-25 and syntaxin 1A (#111 011 and #110 011, respectively, both from SynapticSystems, Göttingen, Germany) were used in PBS containing 3 % BSA at the recommended dilution of 1:100 for 1 h. After 3 x 10 minutes washing with PBS, primary antibodies were detected by fluorescently labeled secondary antibodies (goat anti guinea pig coupled to AlexaFluor488, Jackson ImmunoResearch, #706-545-148; donkey anti rabbit coupled to Cy3, Dianova, #715-165-152; goat anti mouse coupled to atto647N, Rockland, #610-156-121) as described before [144,145]. Nanobodies directly conjugated to fluorescent dyes were typically used at a concentration of 25-50 nM.

2.1.5 Purified Proteins

Purified fractions of alternative members of the SNAP and syntaxin family were commercially purchased from Origene™ Technologies, Rockville, MD, USA to test the selected nanobodies for cross-reactivity. During the testing procedure protein purity and concentrations were kept identical for all variants. Particularly, purified SNAP-23, SNAP-29 and SNAP-47 were used to test cross-reactivity of S25-Nb10 and syntaxin 1B, syntaxin 2 and syntaxin 3 were used to check for unspecific interactions of stx-Nb6.

2.1.6 Consumables

Specific consumables deviating from standard laboratory equipment and their manufacturers are listed in Table 9.

Table 9: Specific consumables and equipment used in the project

Consumable	Used for	Manufacturer
48 well glass bottom plates	High-throughput microscopy screens	Sigma-Aldrich, St. Louis, MO, USA
96-well round bottom plates	Growing individual colonies after panning	Thermo Fisher Scientific, Waltham, MA, USA
Amersham™ Protean™ Premium 0.2 µm nitrocellulose membrane	Western blotting, dot blots	GE Healthcare, Little Chalfont, UK
Baffled Erlenmeyer flasks (2 or 5 liter)	Growing bacteria cultures	Carl Roth, Karlsruhe, Germany
Electroporation cuvettes, 1 mm gap size	Library creation by electroporation	BioRad; Hercules, CA, USA
Glass-Econo columns	Custom packing of columns for chromatography	BioRad; Hercules, CA, USA
MagStrep “type3” XT beads	Antigen immobilization for panning	IBA, Göttingen, Germany
MaxiSorp®	Antigen immobilization in ELISA	Thermo Fisher Scientific, Waltham, MA, USA
NAP™-10 columns	Protein desalting	GE Healthcare, Little Chalfont, UK
NAP™-5 columns	Protein desalting	GE Healthcare, Little Chalfont, UK
Syringe-top filters (0.22 µm and 0.45 µm)	Sterile-filtration and degassing of buffers	Sartorius, Göttingen, Germany

2.1.7 Instrumentation / Equipment

Important laboratory equipment used during the project is listed below. In further descriptions of the experimental procedure, only the name for the instrument is used. Please refer to Table 10 for further details regarding manufacturer and software for operation.

Table 10: Major instrumentation and laboratory equipment used during the project. If applicable, software used to operate the device is indicated. More detailed information on the used software can be found in Table 11.

Instrument	Manufacturer	Software used
ÄKTApure25 HPLC	GE Healthcare; Little Chalfont, UK	Unicorn 7.0.2 (GE Healthcare)
Amersham™ Imager 600	GE Healthcare; Little Chalfont, UK	AI600 Control 1.2 (GE Healthcare)
arium® pro Ultrapure Water System	Sartorius; Göttingen, Germany	-
Branson Digital Sonifier S-450	Emerson; St. Louis, MO, USA	-
Cytation-3 Multi-Mode Reader	BioTek; Winooski, VT, USA	Gen5 Image+ (BioTek)
EMCCD camera	Andor; Belfast, Northern Ireland, UK	Inspector (Abberior)
Fluorescence excitation laser	Abberior Instruments GmbH	Inspector (Abberior)
F-View CCD camera	Olympus Corporation; Shinjuku, Japan	Cell^P (Olympus Corporation)
Gene Pulser® II Electroporation System	BioRad; Hercules, CA, USA	-
IXON X3897 camera	Andor; Belfast, Northern Ireland, UK	NIS-Elements AR 4.60.00 (Nikon Corporation)
Leica CM1850 cryotome	Leica; Wetzlar, Germany	-
Leica TCS SP5 STED confocal microscope	Leica Microsystems; Wetzlar, Germany	Leica Application Suite Advanced Fluorescence (Leica)
Mai Tai Titanium Sapphire tunable laser	Spectra-Physics; Mountain View, CA, USA	Leica Application Suite Advanced Fluorescence (Leica)
Mastercycler® Gradient	Eppendorf AG; Hamburg, Germany	-
Mastercycler® nexus X2	Eppendorf AG; Hamburg, Germany	-
Mini-PROTEAN Tetra Cell	BioRad; Hercules, CA, USA	-
Monolith™ NT.115Pico	NanoTemper; Munich, Germany	MO.Control MO.Affinity Analysis

Motor-driven glass-Teflon homogenizer (17 ml; 0.1–0.15 mm clearance)	Omnilab; Bremen, Germany	-
NanoDrop™ Spectrophotometer ND-2000C	Thermo Fisher Scientific; Waltham, MA, USA	ND-2000C V1.0
NanoDrop™ Spectrophotometer ND-1000	PeqLab; Erlangen, Germany	ND-1000 V3.8.1
Nikon Ti-E Epifluorescence microscope	Nikon Corporation; Chiyoda, Tokyo, Japan	NIS-Elements AR 4.60.00 (Nikon Corporation)
Olympus IX71 microscope	Olympus Corporation; Shinjuku, Japan	Cell^P (Olympus Corporation)
Olympus IX83 microscope	Olympus Corporation; Shinjuku, Japan	Inspector (Abberior)
Pulsed diode lasers	PicoQuant; Berlin, Germany	Leica Application Suite Advanced Fluorescence (Leica Microsystems)
T3 Thermocycler	Biometra; Göttingen, Germany	-
Trans-Blot® Cell	BioRad; Hercules, CA, USA	-
Waterbath WNE 14	Memmert; Schwabach, Germany	-

2.1.8 Software

For evaluation of data as well as for establishment on lab routines, several programs were used. Table 11 lists the most important software with reference to their area of application and developer. For software already listed in the previous section, additional information on the area of use is given. When mentioned in the following sections of the thesis, only the program name will be given. Please refer to this section for further details.

Table 11: Software for operation of devices and data analysis

Program Name	Purpose	Developer
Adobe Photoshop CS6	Image processing	Adobe Systems, San José, CA, USA
Adobe Illustrator CS6	Image processing and figure compilation	Adobe Systems, San José, CA, USA
ImageJ	Image analysis, ROI analyzation	National Institute of Health, Bethesda, MD, USA
CLC sequence 7	Protein sequence alignment and generation phylogenetic trees	QUIAGEN Bioinformatics, Venlo, Netherlands
Matlab R2015b	Image analysis, averaging fluorescence signal of synapses	MathWorks®, Natick, MA, USA
MarvinSketch 6.2.0	Visualization of chemical formulas and reactions	ChemAxon, Budapest, Hungary
DNASTAR 12.3.1.4	DNA sequence analysis and <i>in silico</i> cloning	DNASTAR, Madison, WI, USA
PyMol 1.7.4.5 Edu	Visualization of molecular protein models	Schrödinger Inc., New York, NY, USA
ApE v2.0.47	Plasmid analysis and <i>in silico</i> cloning	M. Wayne Davis, University of Utah, Salt Lake City, USA
Unicorn 7.0.2	Writing methods for protein purification in ÄKTA-HPLC system	GE Healthcare, Little Chalfont, UK

2.2 Methods and Protocols

The following sections lists all relevant methods and protocols used and established during the project. If applicable, references to the original protocols are given and modifications are indicated. If not specified else, all incubation and centrifugation steps were performed at room temperature.

2.2.1 Molecular Cloning / Gene Constructs

During this project, several vectors were generated for production of recombinant proteins in bacteria or for transient transfection into mammalian cell lines for IF experiments. New plasmids were designed based on backbones commonly used in the lab, which were originally modified from commercial plasmids. The plasmid typically used for large-scale protein production was derived from the LacO-pQLinkN-construct [146] and termed pNB666. It was modified to contain an N-terminal 14xHis-tag as well as a bdSUMO-domain fused to the protein of interest to increase protein solubility and expression yield. Moreover, a Twin-Strep-Tag® (tst-tag) was fused to the C-terminus of the protein for affinity purification.

Table 12 gives an overview on the most important plasmids generated and used in this project. Additionally, Figure 7 shows exemplary vector maps for bacterial and mammalian plasmids highlighting all important features of the respective construct. If the vector was not available already in the lab, it was obtained from Addgene, Cambridge, USA or ordered to be synthesized *de novo* by GeneScript, Nanking, China. Proteins of interest (POI) were inserted into the backbone vectors by enzymatic restriction and ligation and in later stages of the project by Gibson assembly as described below.

Table 12: Overview of major backbone plasmids used in the project. The vectors contain conserved regions coding for molecular tags to generate a recombinant fusion protein for further processing. The individual domains of the fusion proteins are listed in consecutive order. The position for the protein to be inserted is highlighted *in italics*.

Plasmid name	Features / fusion parts	Purpose	Origin (reference)
K40	14x-His-tag ZZ-domain scSUMO-domain <i>POI insert</i> tst-tag	Bacterial expression for large-scale production of recombinant proteins (construct for restriction cloning)	LacO-pQLinkN [146]
pNB666	14x-His-tag bdSUMO-domain <i>POI insert</i> tst-tag	Bacterial expression for large-scale production of recombinant proteins (construct for Gibson assembly)	LacO-pQLinkN [146]
pNB667	14x-His-tag bdSUMO-domain <i>POI insert</i> tst-tag cysteine	Bacterial expression for large-scale production of recombinant proteins with a C-terminal cysteine residue (construct for Gibson assembly)	LacO-pQLinkN [146]
pcDNA3.1(+)	-	Mammalian expression under CMV promotor	Addgene
pEGFP-N1	<i>POI insert</i> EGFP	Mammalian expression under CMV promotor with POI fused to the N-terminus of EGFP	Addgene
pIRES2-tst-AcGFP1	<i>POI insert</i> tst-tag / AcGFP (not fused)	Mammalian bi-cistronic vector for simultaneous expression of POI and the fluorescent protein AcGFP1 (not fused). Used for large-scale production of proteins in mammalian cells	Clontech Laboratories
pHen2_rest	pelB <i>POI insert</i> 9xHis-tag myc-tag EPEA-tag TEV-cleavage site phage pIII protein	Phage display vector for use in restriction library. Derived from pHen2 including some modifications to facilitate cloning and processing of the expressed protein (see Figure 9).	pHen2, kindly provided by [73]
pHen2_Gibson	pelB 21 bp region <i>mCherry/POI insert</i> 21 bp region TEV-cleavage site 3xFLAG-tag phage pIII protein	Phage display vector for use in Gibson library, modified from pHen2_rest vector to increase cloning efficiency (see Figure 9).	pHen2, kindly provided by [73]
pUC19 Control Vector	only ampicillin resistance	To test transformation efficiency of newly prepared competent bacteria	NEBexpress, Ipswich, MA, USA

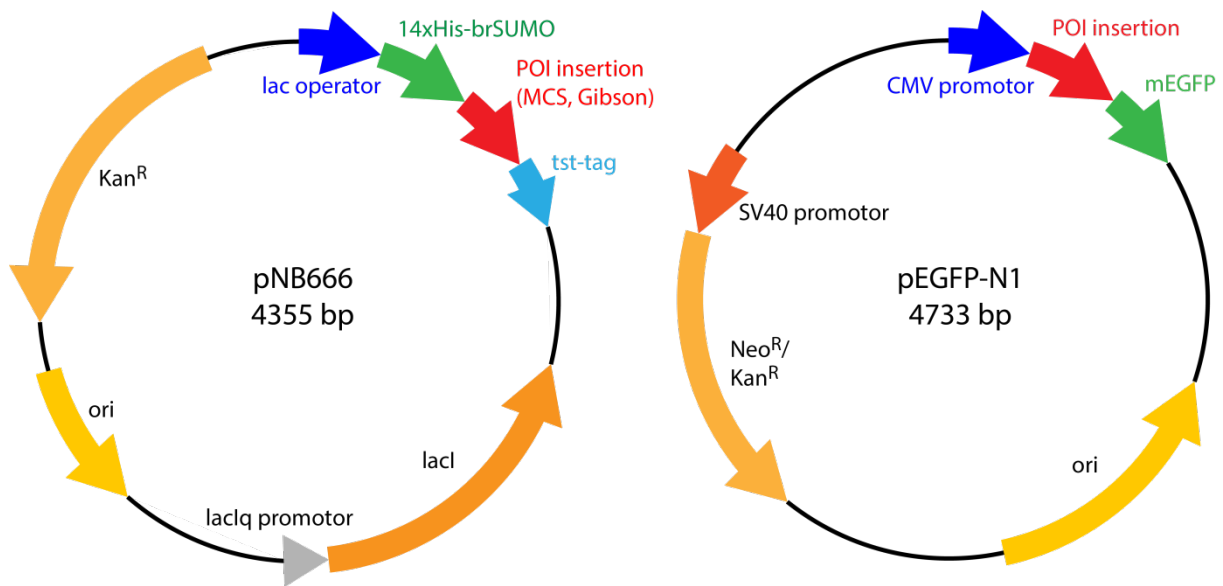


Figure 7: Main vectors for bacterial and mammalian expression systems used in the project. The vector pNB666 served as a backbone for expression in bacteria using the inducible lac-promotor to drive protein expression. For overexpression in mammalian cell lines, the pEGFP-N1 vector was commonly used expressing the protein of interest (POI) fused to EGFP at the C-terminus. Sequences coding for the POIs were cloned into the vector using restriction and ligation enzymes or Gibson assembly. Alternative expression vectors depicted in Table 12 are based on the same backbones with the modifications given in the table.

Restriction cloning

Novel plasmids for protein expression were initially generated from the backbone vectors by enzymatic restriction cloning. First, the vector backbone was amplified by growing a culture of the respective bacterial stock overnight at 37 °C. Plasmids were isolated from the bacteria using GeneJET Mini Prep kit (Thermo Fisher Scientific) or NucleoBond® Xtra Midi kit (Machery-Nagel) and resuspended in ddH₂O. 1.5 µg of the plasmid were mixed with required FastDigest™ restriction enzymes (Thermo Fisher Scientific) according to manufacturer's instructions and incubated in 1x FastDigest™ Buffer (total volume of 20 µl) for 1 h at 37 °C to linearize the vector.

The DNA-insert to be cloned into the vector was amplified by PCR using specific primers introducing the respective restriction sites for cloning. Primers were generally ordered from Eurofins Genomics (Ebersberg, Germany) or Sigma-Aldrich (St. Louis, MO, USA) and used in the PCR reaction at a concentration of 5 µM. As a template for amplification, either an existing vector containing the fragment of interest or a *de novo* synthesized stretch of DNA (GeneScript, Nanking, China) was used. Nucleotides (pre-mixed, Thermo Fisher Scientific) were added to a final concentration of 4 mM. For DNA amplification, Phusion® High-Fidelity polymerase (New England Biolabs) was used according to

manufacturer's instructions (15 sec elongation per 1,000 bp at 72 °C). Typically, 30 amplification cycles were performed; an exemplary PCR routine is depicted in Table 13.

After PCR, both the amplified fragment and the linearized vector were loaded onto a preparative 2 % agarose gel (PeqLab) casted with 1xTAE buffer and mixed with Ethidium bromide solution (Carl Roth). After running at 90 V, the gel was illuminated by UV-light in an Amersham™ Imager 600 system to visualize the DNA-bands. The bands required for cloning were cut from the gel keeping the exposure to the UV-light to a minimum to avoid damaging the DNA.

From the chunks of agarose, DNA was extracted by using the QIAquick® Gel Extraction kit (Quiagen). The eluted PCR-amplificate was digested with restriction enzymes as described above. For subsequent removal of the restriction enzymes, QIAquick® PCR purification kit (Quiagen) was used. Concentrations of the eluted DNA fragment and linearized vector were determined by absorption at 260 nm in NanoDrop spectrophotometer. 50 ng of linearized vector were mixed with three- or seven-fold molar excess of the amplified PCR product. T4 DNA ligase and corresponding buffer (both Thermo Fisher Scientific) were added filling the mixtures to a final volume of 20 µl with nuclease-free water (Carl Roth). Control ligation was set up without adding PCR product. The ligation reaction was incubated overnight at room temperature and transformed into competent *Escherichia coli* bacteria as described below.

Table 13: Typical PCR protocol used for DNA amplification. Steps 2-4 were typically repeated 30 times for quantitative amplification of the template DNA.

Step	Rationale	Temperature	Time
1	double-strand denaturation	98 °C	3 min
2	denaturation	98 °C	15 sec
3	annealing	50-70 °C, depending on primers used	20 sec
4	amplification	72 °C	15 sec per kbp
5	final amplification	72 °C	5 min
6	storage	4 °C	∞

Gibson cloning

During progression of the project, Gibson assembly was introduced as a more efficient and faster method for molecular cloning [147]. The enzymes required for Gibson assembly (T5-exonuclease, Phusion DNA polymerase, Taq DNA ligase) were produced and kindly provided by Dr. Steffen Frey (Nanotag Biotechnologies, Göttingen, Germany) in 2x reaction buffer, subsequently referred to as Gibson reaction mix. To generate new constructs, both backbone vector and insert were amplified by PCR as described above using specific primer with 21-bp overhangs. The overhangs were carefully designed not to form any hairpin or anneal unspecifically to any part of the plasmid sequence. The overhangs were designed to have an annealing temperature between 56 and 60 °C to allow specific base pairing during incubation. After amplification the PCR products were analyzed in a qualitative 2 % agarose gel and purified with QIAquick® PCR purification kit (Qiagen) as described above.

For the Gibson reaction 15 fmol of pure amplified vector were mixed with an equimolar amount of insert in a total volume of 2 µl. Another 2 µl of 2x Gibson reaction mix were added to the DNA and the reaction was incubated for 30 minutes at 48 °C. 1 µl of the mixture was diluted 1:20 in nuclease-free water (Carl Roth) and directly transformed into competent bacteria as described below.

2.2.2 Glycerol Stocks

The ligated plasmids generated for protein expression were transformed into 50 µl DH5α™ *Escherichia coli* bacteria (α-Select Chemically Competent Cells, Bioline) by heat-shock in a water bath. Bacteria were thawed on ice, mixed with the ligation reaction and incubated in the water bath at 42 °C for 35 sec followed by 3 minutes incubation on ice. 500 µl SOC medium were added to the bacteria and the transformation mixture was incubated at 37 °C for 1 h.

After transformation, bacteria were grown overnight at 37 °C on LB-agar plates supplemented with either 50 µg/ml carbenicillin (an ampicillin analog) or kanamycin, depending on the gene construct. Next day, single colonies were picked and grown in 5 ml LB medium overnight at 37 °C. From those cultures, plasmids were isolated using GeneJET Mini Prep (Thermo Fisher Scientific) kit according to manufacturer's instructions. Isolated plasmids were sent for sequencing to confirm successful in-frame insertion of the DNA fragment. Typically, 1 µg of purified plasmid was sent to SeqLab, Göttingen, Germany for sequencing.

Plasmids with correct insertion of the DNA were transformed into chemical competent *E. coli* expression strains as described above. Generally, NEBxpress bacteria (New England Biolabs) were used for cytosolic expression of proteins. For expression of nanobodies, which do require disulfide bond formation, SHuffle® express *E. coli* (New England Biolabs) were used. A culture of the re-transformed bacteria was grown in LB medium at 37 °C overnight and stored at -80 °C after adding glycerol to achieve a final concentration of 40 %.

2.2.3 Bacterial Protein Expression and Purification

Bacteria from the frozen glycerol stock were scraped with a sterile pipet tip and suspended into 50 ml of LB medium supplemented with respective antibiotic. The culture was grown overnight at 37 °C, 120 rpm and subsequently diluted 1:100 into Terrific Broth (TB) medium. Generally, 250 or 500 ml cultures were grown at 30 °C, 120 rpm in baffled Erlenmeyer flasks with a capacity of two or five liters, respectively. OD₆₀₀ was monitored using a NanoDrop™ Spectrophotometer (Thermo Fisher Scientific) in disposable plastic cuvettes (Sigma-Aldrich, St. Louis, MO, USA). When OD₆₀₀ was >1, protein expression was induced by adding IPTG to a final concentration of 1 mM. The cultures were grown overnight at 25-30 °C, 120 rpm.

On the next day, bacteria were harvested in centrifuge beakers for 20 minutes at 3200 ×g. The pellet was resuspended in lysis buffer (50 mM HEPES, 150 mM NaCl, 1 mM EDTA, 1 mM PMSF, 500 µg/ml lysozyme and 100 µg/ml DNaseI [both Sigma-Aldrich], pH 8.0). After incubation on ice for 20 minutes to degrade the cell wall and DNA, bacteria were lysed by ultra-sonication applying five times five pulses at 95 % with a Branson Digital Sonifier. Subsequently, cell debris was removed by centrifugation at 4 °C, 16,000 ×g for >1 h. The crude lysate was handled on ice and processed immediately to avoid protein degradation. To further clear the lysate it was filtered through 0.45 µm syringe top filter (Sartorius).

For affinity purification of proteins from the lysate, an ÄKTApure25 HPLC system (GE Healthcare) was used in combination with different columns as depicted in Table 14. Generally, the lysate was loaded into a 50 ml super-loop to apply it on an affinity column for a first purification step. Elution was carried out by competitive binding using specific elution buffer (see Table 14). Purity of the eluted fractions was analyzed by sodium dodecyl sulfate polyacrylamide gel electrophoresis (SDS-PAGE, see below). To further increase the purity of the eluted protein, polishing steps such as ion exchange and size exclusion chromatography were performed using the ÄKTA HPLC system. Protocols for HPLC operation were written using Unicorn 7.0.2 (GE Healthcare) and adapted individually for each purification step.

Alternatively, proteins were purified using cComplete™ His-Tag purification resin equilibrated with A500 buffer. Beads were incubated for 1-2 h with the crude bacteria lysate followed by three times washing with A500 buffer. For elution of bound proteins, B500 buffer was used. All steps were carried out on ice. The eluted protein was immediately desalted into PBS using the ÄKTApure25 HPLC to avoid protein precipitation due to high salt and imidazole concentrations. The purified protein was analyzed on a SDS-PAGE gel as described below.

To avoid any unspecific interaction evoked by the bdSUMO domain, the bdSUMO protease was produced as described above and added to cleave the desalted protein. The protease was generally incubated with the protein for >1 h at 4 °C. Subsequently, 5-20 µl cOmplete™ His-Tag purification resin was added to trap the fragment as well as uncleaved protein and the bdSUMO protease itself. After 30 minutes incubation at 4 °C, the supernatant containing the pure and cleaved protein of interest was processed. As a final step, all proteins were desalted in to PBS (see above), pH 7.4, snap-frozen in liquid N₂ and stored at -20 °C.

Table 14: Compilation of methods and column types used for protein purification using the ÄKTA HPLC system. Typical buffer compositions and sample volumes are given. The final conditions for individual protein purifications were adjusted and optimized based on the parameters given below. Mostly, columns were purchased from GE Healthcare, Little Chalfont, UK (GE).

Chromato- graphy type	Column used (manufacturer)	Running buffer	Elution buffer	Sample volume
Affinity (Step-tag)	StrepTrap HP, 5ml (GE)	50 mM HEPES 150 mM NaCl 1 mM EDTA pH 7.4	Running buffer + 7.5 mM desthiobiotin	10-20 ml lysate
Affinity (His-tag)	HiTrap HP, 5ml (GE)	50 mM HEPES 150 mM NaCl 30 mM imidazole 1 mM EDTA pH 8.0	Running buffer with 500 mM imidazole	10 ml lysate
Affinity (His-tag)	Protino® Ni-NTA, 5ml (Machery-Nagel)	50 mM HEPES 150 mM NaCl 30 mM imidazole pH 8.0	Running buffer with 500 mM imidazole	10-20 ml lysate
Anion exchange	HiTrap Q HP 16/10, 20 ml (GE)	25 mM Tris/HCl 50 mM NaCl pH 8.0	25 mM Tris/HCl 1 M NaCl pH 8.0	5-10 ml
Cation exchange	HiTrap SP HP 16/10, 20 ml (GE)	PBS, pH 7.4	PBS 1 M NaCl pH 7.4	5-10 ml
Desalting	HiTrap desalting, 5ml (GE)	PBS, pH 7.4	PBS, pH 7.4	1.5 ml
Desalting	HiTrap desalting 26/10 (GE)	PBS, pH 7.4	PBS, pH 7.4	15 ml
Size exclusion	Superdex™ 75 increase 10/300 GL (GE)	PBS, pH 7.4	PBS, pH 7.4	500 µl

2.2.4 SDS PAGE

For analysis of the protein fraction during purification, denaturing gel electrophoresis was performed as introduced by Schagger and von Jagow in 1987 [148]. The protein samples were mixed with 2x SDS-PAGE sample buffer and subsequently boiled for 5-10 minutes at 95 °C and loaded on a 10 % denaturing Tris/Tricine polyacrylamide gel (see Table 15 for gel composition). The proteins were separated by using the Mini-PROTEAN Tetra Cell system for vertical SDS-PAGE generating a discontinuous buffer system (for buffer composition see Table 3). The gels were run for approximately 15 minutes at 90 V until the proteins entered the separation gel. Afterwards, the power was increased to 120 V for another 90 minutes or until the Coomassie Brilliant Blue R-250 was running out of the bottom of the gel.

For visualization of proteins bands, the gel was incubated in SDS-PAGE gel staining buffer (for recipe see Table 3) for at least two hours or overnight followed by sequential washing in SDS-PAGE destaining buffer until protein bands became visible. The destained gels were imaged in an Amersham™ Imager 600 system for documentation.

Table 15: Recipe for casting denaturing SDS-PAGE gels

	Stacking Gel (1x)	Separation Gel (1x)
SDS-PAGE gel buffer (10x)	375 µl	1.675 ml
ddH₂O	925 µl	570 µl
NF-Acrylamid/Bis-solution (30 %)	200 µl	1.667 ml
50 % Glycerol	-	1.060 ml
10 % Ammonium persulfate (APS)	10 µl	25 µl
Tetramethylethylenediamine (TEMED)	2 µl	3 µl

2.2.5 Preparation of Competent Bacteria

For several aspects of this project, transformation of competent bacteria was required. Those bacteria were amplified from commercially available stocks (see Table 16) and purified according to the protocols given below. For transfection of bacteria used for proteins expression, chemically competent bacteria were used for economic reason. For generation of phage-display libraries as described in section 2.2.15, electrocompetent bacteria were used to maximize the transformation efficiency. As the bacteria do not contain a plasmid, they do not possess any resistance against the antibiotics commonly used in the lab. Hence, all steps were carried out in sterile conditions if possible or after thorough cleaning with 70 % ethanol to avoid any contamination of the competent bacteria. Buffers and media used for preparation of the competent bacteria are listed in section 2.1.2.

Preparation of chemically competent bacteria

The protocol for amplification of chemically competent bacteria was adapted from [149]. The stock of competent bacteria was streaked onto a LB-agar plate and incubated at 37 °C overnight. The next day, a single colony was picked with a sterile pipet tip and used to prepare an overnight liquid culture of 2.5 ml in LB medium at 37 °C and 120 rpm. That culture was used to inoculate 250 ml LB medium supplemented with 20 mM MgSO₄. The culture was grown to OD₆₀₀ = 0.6 in a baffled Erlenmeyer flask and subsequently harvested by centrifugation for 20 minutes at 3,200 ×g. The pellets were resuspended and pooled in 100 ml ice-cold TFB1 buffer. All following steps were carried out on 4 °C with pre-chilled laboratory equipment and plasticware. After incubation on ice for 5 minutes, bacteria were again pelleted for 20 minutes at 3,200 ×g, 4 °C. The pellet was gently resuspended in 10 ml ice-cold TFB2 buffer avoiding pipetting and vortexing. The bacteria were incubated on ice for another 45 minutes and finally aliquoted into pre-cooled reaction tubes. After snap-freezing in liquid N₂, bacteria were stored at -80 °C for up to 12 months.

Preparation of electrocompetent bacteria

A 10 ml overnight culture of the bacteria grown in LB at 37 °C, 120 rpm was diluted into 4 x 500 ml LB medium and grown in baffled Erlenmeyer flasks until OD₆₀₀ reached 0.6. At that point, the culture was immediately cooled down in an ice-water bath and gently shaken for another 10 minutes. All following steps were performed on ice at an ambient temperature of 4 °C with pre-cooled laboratory equipment and plasticware.

The culture was transferred to centrifuge beakers and harvested for 20 minutes at 3,200 ×g, 4 °C. The pellet was resuspended in 50 ml ice-cold sterile water by vigorous swirling. After resuspension, the culture was added to 500 ml ice-cold water and pelleted again as before. That washing procedure was repeated 3 times in total to remove all traces of bacterial medium. At each washing step, the pellets from individual beakers were combined to obtain one single pellet after the third washing. That pellet was again resuspended in 50 ml ice-cold water and mixed with 450 ml 10 % autoclaved, ice-cold glycerol. Next, the culture was pelleted and resuspended in 4 ml 10 % glycerol. From that resuspension, 50 µl aliquots were distributed in pre-cooled reaction tubes and immediately snap-frozen in liquid N₂. The aliquots were stored at -80 °C for a maximum of three months.

To determine the final competency of the bacteria, 10 µg of the pUC19 Control Vector (New England Biolabs) were used in an electroporation reaction (see below). Dilution series of the transformed bacteria were plated on LB-agar and incubated overnight at 37 °C. The number of colony forming units (cfu) indicating the competency of the bacteria was calculated according to Equation 4 indicated below. Typically, measured values for bacteria competency (colony forming units, cfu) were around 10-20 % of the value indicated by the manufacturer, which constitutes sufficient competency.

$$\frac{\text{cfu}}{\mu\text{g plasmid}} = \frac{\text{number of colonies}}{10 \text{ pg}} * \frac{10^6 \text{ pg}}{\mu\text{g}} * \frac{\text{transformation volume}[\mu\text{l}]}{\mu\text{l plated}}$$

Equation 4: Formula for estimation of colony forming units (cfu) per μg of transfected plasmid. The pUC19 Control Vector was used in a test electroporation reaction to determine the competency of the amplified bacteria. The competency reached at least 10 % of the value indicated by the manufacturer, which reflects a good quality for electroporation.

Table 16: Overview of competent *Escherichia coli* bacteria used in the project. Bacteria were purchased from manufacturer and subsequently amplified according to the protocols given above to increase the number of possible transformations.

Strain	Type	Manufacturer
NEB [®] Express	Chemically competent	New England Biolabs, Ipswich, MA, USA
SHuffle [®] Express	Chemically competent	New England Biolabs, Ipswich, MA, USA
DH5 α [™]	Chemically competent	Bioline, London, UK
TG-1	Electrocompetent	Lucigen, Middleton, WI, USA

2.2.6 Cell-Line Culture and Transfection

Round Menzel coverslips for cell culture with (15 mm diameter, <100 μm thick) were first cleaned in 1 M HCl overnight followed by 1 h cleaning with 1 M NaOH. After washing thoroughly with deionized H_2O , coverslips were stored in 70 % ethanol. Before seeding the cells, coverslips were flamed under sterile conditions and coated with 0.1 mg/ml poly-L-lysine (PLL) for 1 h followed by 3 washes with sterile H_2O for 5 minutes. For this project, COS-7, HEK293 and PC-12 cells were used for IF experiments and HEK293-FT cells were used for production of recombinant antigens in mammalian cells. All cell lines were cultured in sterile polystyrene petri dishes (\varnothing 145 mm, CellStar) at 37 °C, 5 % CO_2 . The composition of different media is depicted in Table 5. When the confluence of the petri dish reached >80 %, the cell culture was split and seeded on coverslips pre-coated with PLL. For this, cells were washed once carefully with sterile PBS (Dulbecco's PBS, Sigma-Aldrich) before applying 3 ml Trypsin/EDTA solution (Lonza) for two minutes to promote detaching of the cells. Trypsin was deactivated by adding 10 ml culture medium and cells were suspended into the medium by gentle pipetting. After centrifugation at 200 $\times g$ for 4 minutes, the cell pellet was resuspended in 10 ml culture medium and seeded into the wells at a dilution of 1:100 – 1:250. Typically, after 12-16 h incubation at 37 °C and 5% CO_2 , seeded cells were transfected with plasmids to induce overexpression of proteins.

Per well, 1 µg of purified plasmid was mixed with 2 µl of Lipofectamin® 2000 reagent (Thermo Fisher Scientific) in 100 µl Opti-MEM™ (Thermo Fisher Scientific) and incubated for 20 minutes at room temperature. Afterwards, the mixture was carefully added dropwise onto the cells. The transfected cells were incubated for 8-16 h at 37 °C, 5 % CO₂ and subsequently used for immunostaining experiments or protein purification.

2.2.7 Immunostainings

Cells growing on coverslips were first fixed in 12-well plates by incubation with 4 % paraformaldehyde (PFA) dissolved in PBS for 45 minutes on an orbital shaker at 100 rpm. After fixation, PFA was aspirated and residual aldehyde was quenched by washing for 10 minutes with 100 mM glycine, pH 7.4. To improve epitope accessibility, cells were permeabilized for 10 minutes using PBS-Tx buffer and subsequently blocked with PBS-BSA for 1 h, 100 rpm. All steps were carried out in a 12-well plate using 1 ml liquid for each step.

For immunostaining, the primary antibody or nanobody was diluted accordingly into PBS-BSA and a 100 µl droplet of that dilution was spotted onto a stripe of parafilm®. The coverslips were incubated upside down in a dark humidifying chamber. After 1 h, coverslips were washed 3 times with PBS followed by incubation with secondary antibody (if applicable) for 45 minutes as described above. After incubation with secondary antibody, the coverslips were washed 3 times with PBS and once with HS-PBS to remove unspecific binding. If performed, nuclear staining was conducted at this point by adding 1:5,000 Hoechst Solution in one of the washing steps.

For mounting the samples, coverslips were carefully embedded in 10 µl Mowiol solution on a glass slide and dried overnight at room temperature in the dark. The samples were stored at 4 °C until imaging.

2.2.8 Fluorescence Imaging

To confirm binding of selected novel affinity probes and to detect their target antigen in biological contexts, different types of IF imaging were used. General binding of the probes was detected by epifluorescence microscopy. Confocal microscopy was subsequently used to analyze the cellular antigen in more detail. For detection of subcellular structures in high detail, STED-microscopy was used to achieve super-resolution imaging.

Epifluorescence

For fast evaluation of novel affinity molecules or for high-throughput validation of nanobody candidates, a Nikon Ti-E epifluorescence microscope (Nikon Corporation) was used. For imaging, either an S plan fluor ELWD 40x 0.6 NA DIC N1 objective or a plan apochromat λ 60x 1.4 NA oil-immersion objective was used. The microscope was equipped with an HBO-100W lamp and an IXON X3897 camera (Andor) and operated with the NIS-Elements AR software, version 4.60.00 (Nikon Corporation).

Alternatively, an inverted epifluorescence Olympus IX71 microscope (Olympus Corporation) equipped with a 60x 1.35 NA oil-immersion objective, a 100W mercury lamp and an F-View II CCD camera (Olympus Corporation) was used. That system was operated by the Cell[^]P software (Olympus Corporation) and mainly used, if no high-throughput screening of nanobodies was required.

Confocal and STED microscopy

Confocal and STED images were acquired with a Leica TCS SP5 STED confocal microscope (Leica Microsystems) equipped with an HCX plan apochromat 100x 1.4 NA oil-immersion objective, operated by the Leica Application Suite Advanced Fluorescence software (Leica Microsystems). The fluorophores were excited with pulsed diode lasers (PicoQuant) at their corresponding wavelength. For multichannel image acquisition, laser lines were used as follows: Argon laser for excitation at 488 nm (GFP), Helium-Neon laser for excitation at 543 nm (Cy3, mCherry) and a Helium-Neon laser for excitation at 633 nm (atto647N, Cy5, DyLight[®]650). The detection range was set by adjusting the AOTF filters of the microscope in operation software of the microscope. The STED depletion beam was generated using a Mai Tai Titanium Sapphire tunable two-photon laser (Spectra-Physics) pulsed at 80 MHz and 750 nm with an output power of 1.6 W.

For confocal and STED images, 16 and 96 line scans were recorded, respectively, at 1,000 Hz scanning speed. Typically, images were composed of 1,024 x 1,024 pixels with a pixel size of 60.6 nm for confocal and 20.2 nm for STED images. The fluorescence signal was detected using photomultipliers for confocal and avalanche photodiodes (APD) for STED operation mode. Exemplary images displayed as results as well as corresponding control images were scaled equally.

Multicolor STED microscopy

For simultaneous detection of several fluorescent channels in STED mode, an inverse 4-channel easy3D STED setup (Abberior) was used. The setup was composed of an Olympus IX83 microscope body equipped with a plan apochromat 100x 1.4 NA oil-immersion objective (Olympus Corporation) and an EMCCD camera (Andor). Fluorescence excitation lasers (Abberior) pulsed at 40 MHz were utilized for the excitation lines 488 nm (GFP), 561 nm (Abberior Star580) and 640 nm (atto647N). For

depletion of the fluorescence signal of the Star580 and atto647N dyes, a 775 nm STED laser (Abberior) pulsed at 40 MHz with an output power of 1.250 W was applied. Both confocal and STED signal was detected using APD detectors (Abberior) in predefined channels. The operation of the setup and the recording of images were performed with the Inspector software, version 0.14 (Abberior).

2.2.9 Protein Purification from Mammalian Cell Lines

For validation of nanobody specificity, antigens were also expressed in mammalian cells to mimic the interaction of the nanobodies to their antigens under native conditions. HEK293-FT cells transfected with the recombinant protein of interest were grown in round petri dishes ($\varnothing = 145$ mm) as described above for 24-36 h or until no further increase in confluency could be observed. Per plate, 700 μ l of ice-cold cell lysis buffer freshly supplemented with 1 μ g/ml DNase, 10 μ g/ml aprotinin, 10 μ g/ml leupeptin, 1 μ g/ml pepstatin A, 100 μ M PMSF (all Sigma-Aldrich) and 0.1x Protease Inhibitor Cocktail (Roche) were added. The cells were suspended in the dish using a sterile cell scraper handling everything on ice. Afterwards, the suspension was transferred to a sterile 1.5 ml reaction tube and incubated on ice for 45 minutes with occasional vortexing. Next, cells were disrupted by sonication on ice using the Branson Sonifier at 70 % power, 5 pulses of 3 sec each followed by another incubation on ice for 15 minutes. Subsequently, cell debris was removed by centrifugation for 45 minutes at 4 °C, 16,000 \times g. The supernatant containing the soluble cell lysate was snap-frozen in liquid N₂, unless it was purified further.

For purification of tst-tagged recombinant proteins from mammalian cell lysates, StrepTactin® Spin Columns (IBA) were used according to instructions of manufacturer. The quality of the purification was analyzed by SDS-PAGE as described above.

2.2.10 Primary Neuronal Culture

Primary hippocampal neuron cultures used in this project were cultured according to Kaech and Banker [141]. P1-P2 rats were decapitated and the brains were removed. Before starting the neuronal culture, glia cells prepared from cortex were seeded directly into 12-well cell culture plates in glial medium (see Table 5). To obtain primary neurons, hippocampi were extracted and pooled in HBSS (Thermo Fisher Scientific) followed by enzymatic digestion in hippocampi digestion solution (see Table 3) for 1 h at room temperature. After washing with Neurobasal-A medium (Thermo Fisher Scientific), hippocampi were incubated for 15 minutes with enzyme inactivation solution (for recipe see Table 3). After another washing step with Neurobasal-A, cells were dissociated by gentle pipetting.

Glass coverslips for culturing were cleaned with nitric acid and coated with 1 mg/ml PLL. A few small paraffin dots on the coverslips were added to ensure spatial separation of the two cultures. Around 30,000 neurons were seeded per coverslip to obtain low-density facilitating the analysis of individual synapses. Typically, neurons were seeded four days after the glia preparation with the cells facing each other. The culture medium was replaced by neuronal maintenance medium and incubated at 37 °C, 5 % CO₂ in a cell culture incubator as described by Kaech *et al.* [141]. Approximately 12-18 days after preparation, neurons on coverslips were used for IF experiments.

2.2.11 Brain Slice Preparation

Brain slices were prepared from adult (6-8 weeks old) Wistar rats, by perfusion with PBS to remove blood, followed by 4 % PFA in PBS for fixation. The brains were removed from the skull and incubated in 4 % PFA in PBS at 4 °C overnight. On the following day, the brains were transferred to a solution of 30 % sucrose in PBS on 4 °C until they sank to the bottom of the solution, before freezing and storing them at -80 °C until sectioning. For that, the brains were cut into 30-35 µm thick slices on a Leica CM1850 cryotome.

2.2.12 Tissue Isolation

To test the binding specificity of my selected nanobody candidates, I isolated various tissues from an adult mouse to perform qualitative binding assays. An adult mouse was anaesthetized and killed by CO₂ gas and different tissue samples (heart, muscle, liver, testis and brain) were carefully dissected. The brain was further dissected to obtain isolated fractions of the hippocampi, cerebellum and cortex. All tissues were immediately put in ice-cold PBS supplemented with 1 mM EDTA to block protease activity. The tissues were homogenized using a motor-driven glass-Teflon homogenizer (17 ml with 0.1–0.15 mm clearance; Omnilab) at 900 rpm, 30 strokes and subsequently directly snap-frozen in liquid N₂. For usage in binding assays, the total protein concentration of each tissue sample was determined by Novagen® BCA Protein Assay kit (Merck).

2.2.13 Western Blotting

For testing the nanobody binding specificity in a biochemical context and to compare nanobody performance to conventional antibodies, Western blotting was used. Typically, 30-50 µg of mammalian cell lysate (see section 2.2.9) were loaded onto a 10 % SDS-PAGE gel (see section 2.2.4) and subsequently transferred to a 0.2 µm nitrocellulose membrane by wet Western blotting. For that, a Trans-Blot® Cell system (BioRad) filled with WB transfer buffer was used. Transfer to the membrane was typically carried out at 400 mA for 2.5 h. The membrane was then blocked for 1 h with PBS-T/milk, and subsequently incubated with the directly fluorescently labeled nanobody or a primary antibody plus labeled secondary antibody for detection in 5 % milk/PBS-T. The following steps were done as described in section 2.2.7. The membrane was finally imaged in an Amersham™ Imager 600.

2.2.14 Animal Immunization

White blood cell isolation

To generate a biological repertoire of target-specific antibodies, an alpaca (*vicugna pacos*) was immunized with a mixture of purified protein produced in bacteria. Modified versions of the three SNARE proteins SNAP-25, syntaxin 1A and VAMP2 (see Figure 8) were mixed with incomplete Freund's adjuvant and injected into the animal (performed by preclinics GmbH, Potsdam, Germany). In total, six injections containing each 300 – 500 µg purified protein were given to the animal at an interval of 7 days. 5 days after the last injection, 50 ml of blood were drawn and directly processed by preclinics to isolate the white blood cells. A discontinuous Ficoll-gradient was used to separate the white blood cells from the serum by ultracentrifugation. Afterwards, the isolated cell preparation was mixed with ice-cold RNeasy Lysis Buffer and immediately shipped to Göttingen where it was directly processed to avoid any degradation of the RNA.

After several months, the same alpaca was again immunized once with 500 µg of the same mixture of proteins to trigger its adaptive immune response. After 5 days, 50 ml blood were taken and processed as described before to isolate RNA from the memory B cells. This immune-boost was expected to evoke the production of highly specific affinity probes generated by the animal. Due to the immunological memory and somatic hypermutation of antibodies, the obtained antibody sequences are expected to contain a new set of specific binders [150].

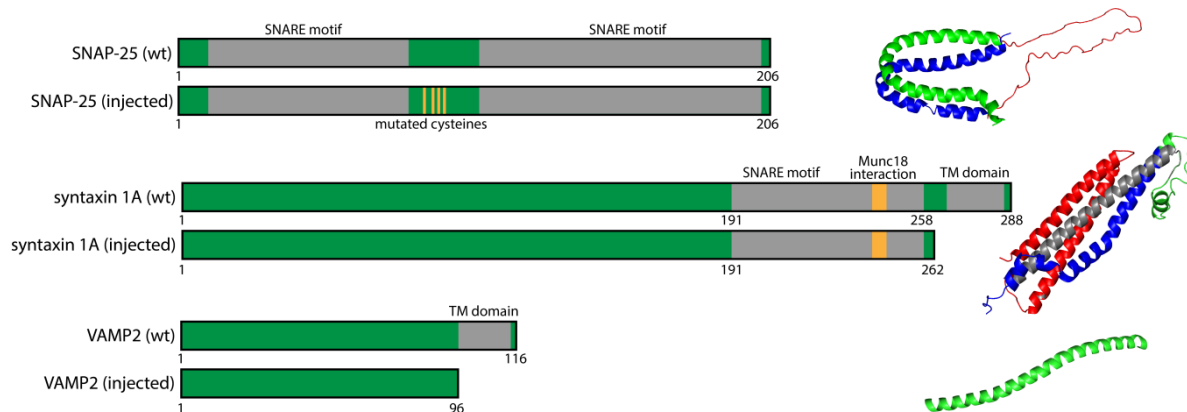


Figure 8: Schematic and cartoon model of recombinant antigens used for immunization. The cysteine moieties of wild-type (wt) SNAP-25 were mutated to serine residues to facilitate recombinant production of the full protein. Syntaxin 1A and VAMP2 were produced and injected into the animal lacking the hydrophobic transmembrane (TM) domain as that domain is not accessible for affinity probes in IF under native conditions. The position of the TM domains and the SNARE motifs are marked in grey. Structure models were created with PyMOL based on deposited data from the Protein Data Bank. The accession numbers are: 1kil (SNAP-25), 1ez3 (syntaxin 1A) and 1n7s (VAMP2).

RNA-extraction

Before starting with the RNA preparation from white blood cells, all surfaces and required lab equipment were cleaned with RNaseZAP™ (Sigma-Aldrich). Common disposable plasticware was replaced by sterile, RNase-free reaction tubes and pipet tips (STARLAB, Hamburg, Germany) for the time of the preparation.

For isolation of RNA, the RNeasy® Mini kit (Qiagen) was used. To avoid saturation of the columns, a total of 10 spin columns were used in each preparation. The optional on-column digestion with DNase described in the manual was performed to avoid contamination of genomic DNA. The extracted RNA was dissolved in nuclease-free water and snap-frozen in liquid N₂ for complementary DNA (cDNA) synthesis and nanobody library preparation.

2.2.15 Nanobody Library Construction

From white blood cell RNA, nanobody sequences were extracted to build recombinant libraries for affinity selection of nanobodies. As this was established *de novo* in the lab, several optimization steps were needed. Below the workflow to generate the final libraries used in this project is shown. All PCR reactions were set up as described in section 2.2.1 using Phusion® polymerase (New England Biolabs) unless specified otherwise.

Nanobody sequences were either cloned into the target vector by restriction cloning or Gibson assembly, resulting in different libraries with different biochemical properties.

Restriction library

20 µg total RNA were reverse-transcribed into cDNA using SuperScript™ III One-Step RT-PCR kit (Thermo Fisher Scientific). Instead of random hexamer primers, specific primers annealing to the conserved nanobody framework (forward) and hinge region (reverse) were used. As the heavy-chain IgG2 and IgG3 subtypes differ in composition of their hinge region, two different reverse primers were used simultaneously. Table 17 shows the sequence of the primers used highlighting the sites introduces for restriction cloning. The forward primer introduces two different hexameric restriction sites (*NcoI* and *PstI*) to bypass loss of sequence diversity if one of the restrictions sites also coincidentally is present in the nanobody sequence. In contrast, the reverse primers only possess a *NotI* - restriction site, as this enzyme cuts at an octameric palindromic stretch of DNA, which is very unlikely to occur elsewhere in the nanobody sequence. The primer sequences were modified from Olichon *et al.* [85].

The optimal annealing temperature was determined for each amplification attempt by gradient PCR (58 – 68 °C annealing) in Mastercycler® Gradient thermocycler and found to be 61 °C for Alp_F1+/Alp_R1+ and 65 °C for Alp_F1+/Alp_R2+. After 40 cycles of amplification by PCR, the cDNA was purified from a preparative 2 % agarose gel using QIAquick® Gel Extraction kit (Quiagen). The eluted DNA was pooled and divided in two tubes where it was either digested with *NcoI/NotI* or *PstI/NotI* FastDigest restriction enzymes (Thermo Fisher Scientific) for 3 h at 37 °C and subsequently cleaned from restriction enzyme using QIAquick® PCR purification kit.

In parallel, the phagemid vector (see also Figure 9) to generate the restriction library was amplified and purified as described in 2.2.1. 50 µg of the purified vector were digested with *NcoI/NotI* or *PstI/NotI* for 2 h at 37 °C. After that, 2 ml of FastAP /Thermo Fisher Scientific) were added and the mixture was incubated for another 2 hour at 37 °C. The digested phagemid was purified in a preparative 2 % agarose gel using QIAquick® Gel Extraction kit (Quiagen) and reconstituted in nuclease-free water. The vector was mixed with the insert at a molecular ratio of 1:3 and ligated overnight using T4 ligase (Thermo Fisher Scientific) as described before.

Table 17: Primers used for generating nanobody library by restriction cloning. Sequences are depicted from 5' to 3' end. Additional base pairs are added to the 5' end to facilitate cleavage by restriction enzymes. Palindromic sites for restriction are highlighted, complementary regions annealing to the nanobody sequences are underlined in red.

Sequence (5' to 3')	Name	Type	Restriction
attaCCATGGCTGCAGAGKTGCAGCTCGTGGAGTCNGGNGGAGGC	Alp_F1+	Forward	NcoI / PstI
attattattcagattattagtGCGGCCGC <u>CACTAWTGGGGTCTTCGCTGTGGTGCG</u>	Alp_R1+	Reverse	NotI
attattattcagattattagtGCGGCCGC <u>CACTAGTTTGTGGTTTTGGTGTCTTGGG</u>	Alp_R2+	Reverse	NotI

Gibson library

In later stages of the project, I decided to generate another nanobody library by Gibson assembly to increase cloning efficiency and thus, nanobody diversity. That library was generated from novel RNA obtained after boosting the alpaca's immune response (see above). 20 µg of total RNA were transcribed into cDNA using the SuperScript™ IV First-Strand Synthesis System. The primers used were adapted from [67] or designed *de novo* and are depicted in Table 18. In total, a three-step nested PCR was performed. In a first step, parts of the variable chain of the overall IgG repertoire were amplified using the Call001/Call002 primer set. In a second PCR, overhangs for Gibson assembly were introduced to primers specifically binding to the nanobody framework and hinge regions. A variety of degenerated primers was used to encounter for biological variety of the genetic code in the constant region of the nanobody sequence. As a final step, the sequence repertoire was amplified using the primer set Gibson1/Gibson2 (see Table 18) to increase the efficiency of subsequent Gibson assembly. An overview on the subsequent PCR steps is shown in Table 19 and Figure 13. Between individual steps and after the final PCR, the amplified DNA was purified by QIAquick® PCR purification kit (Quiagen). The quality of each amplification step was controlled by running 2 µl of the PCR products on a qualitative 2 % agarose gel imaged with an Amersham™ Imager 600. Optimal annealing temperatures for nested PCR steps were determined empirically by gradient PCR in a Mastercycler® Gradient thermocycler as described above.

For generation of the Gibson library, the pHen2 phagemid was modified to contain the overhang sequences used to amplify the nanobody repertoire. Moreover, the vector size was minimized to increase the efficiency of subsequent transformation. The template phagemid used further contains the fluorescent protein mCherry at the foreseen position of the nanobody. The expression of the red mCherry protein allows to identify colonies without a nanobody insert and hence to monitor cloning efficiency. A schematic view of the pHen2_Gibson vector is shown in Figure 9. The vector was amplified by PCR (30 cycles, annealing at 55 °C) using the primer set Gib_vec_f/Gib_vec_rv depicted in Table 18. The linear PCR product was cut from a preparative 2 % agarose gel using the QIAquick® Gel Extraction kit (Quiagen). A total of 1.5 µg amplified pHen2_Gibson vector was mixed with an equimolar amount of nanobody PCR product. Cloning of the nanobody sequences into the vector was done as described in section 2.2.1, except the ligation mixture was not diluted before transformation to maintain high sequence diversity.

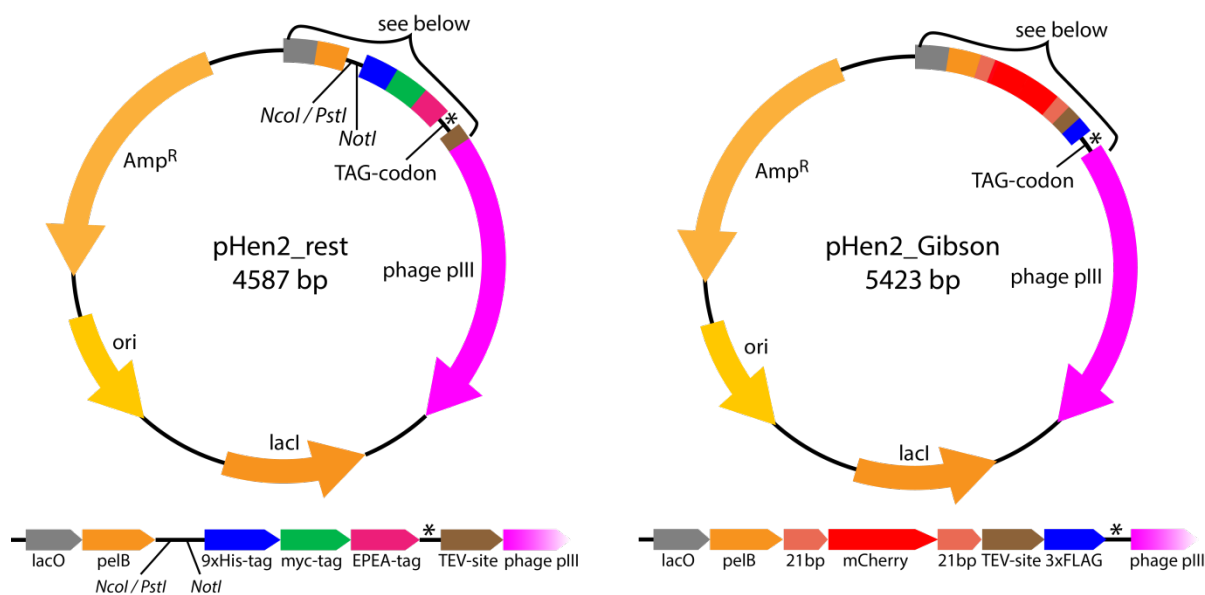


Figure 9: Vectors generated and used to create phage display libraries. Segments relevant for cloning and molecular engineering are highlighted in color and depicted below the vector map. The pHen2_rest vector was originally used as a phagemid for generation on nanobody libraries based on restriction cloning. For generation of libraries by Gibson assembly, the pHen2_Gibson vector was designed.

Table 18: Overview of primers used for the generation of nanobody libraries by Gibson assembly. The overhangs for Gibson assembly are highlighted in green, complementary regions annealing to the nanobody sequences are underlined in red. The nanobody inserts were successively used as a template for the next PCR reaction indicated in the rightmost column.

Sequence (5' to 3')	Name	Type	Template
GTCCTGGCTGCTCTTCTACAAGG	Call001	Forward	cDNA
GGTACGTGCTGTTGAACTGTTCC	Call002	Reverse	cDNA
<u>TCTGGTGATGCATCTGACAGC</u> GAGGTGCAGCTGSWGGAGTCTGG	F1_Gibson	Forward	product PCR 1
GTTTTCCCCAGTGGATCCAGAACTAWTAGGGTCTTCGCTGTGGTGC	R1_Gibson	Reverse	product PCR 1
GTTTTCCCCAGTGGATCCAGAA <u>AGTTTGTGGTTTTGGTGTCTTGGG</u>	R2_Gibson	Reverse	product PCR 1
<u>TCTGGTGATGCATCTGACAGC</u>	Gibson_for	Forward	product PCR 2
<u>GTTTTCCCCAGTGGATCCAGAA</u>	Gibson_rev	Reverse	product PCR 2
<u>TCTGGATCCACTGGGGAAAAC</u>	Gib_vec_f	Forward	phagemid
<u>GCTGTCAGATGCATCACCAGA</u>	Gib_vec_rv	Reverse	phagemid

Table 19: Nested PCR steps for cDNA amplification to clone into Gibson library. The number of cycles for each PCR reaction is given together with the corresponding annealing temperature (T_{anneal}) optimized for the respective primer set.

Step	Rationale	Primers used	PCR cycles, T_{anneal}
1	Amplification of total IgG repertoire	Call001 + Call002	8 cycles, 60 °C
2	Amplification of nanobody sequences and introduction of overhangs for Gibson assembly	F1_Gibson + R1_Gibson/R2_Gibson	3 cycles, 63 °C, 5 cycles, 68 °C
3	Final amplification to increase quality of PCR product as long primers from step 2 result in low cloning efficiency	Gibson_for + Gibson_rev	3 cycles, 58 °C, 15 cycles, 60 °C

Both libraries generated by enzymatic restriction cloning and Gibson assembly were cloned into electrocompetent *E. coli* TG-1 bacteria (Lucigen) freshly prepared as described in section 2.2.5. The ligation mix was divided into several individual reactions to ensure transformation efficiency and to avoid saturation of the bacteria electroporation capacity. Typically, 30-50 transformations using up to 100 ng ligated DNA per reaction were carried out to generate one library. The DNA was gently mixed on ice with an aliquot of freshly prepared TG-1 bacteria and transferred to an electroporation cuvette (BioRad) with a gap size of 1 mm. The optimal conditions for electroporation were determined empirically in previously performed test ligations. For the electroporation reactions to generate the library, a capacity of 25 μF and a resistance of 400 Ω were used at a voltage of 1.25 kV. To monitor the electroporation efficiency, the time constant for each individual reaction was monitored. Only reactions resulting in values higher than 9 (instrument scale ranging from 1 to 10) were used in subsequent steps (typically, 95 % of all reactions would meet that criterion indication successful electroporation).

Immediately after electroporation, 500 μl Recovery Medium (Lucigen) were added and the culture was incubated for 1 h at 37 °C, 500 rpm. Subsequently, all transformation reactions of one library were pooled and plated on LB-agar containing 100 $\mu\text{g}/\text{ml}$ ampicillin in 16 square bioassay dishes (245 x 245 mm, Sigma-Aldrich). Dilution series of the transformed bacteria were plated to estimate total colony numbers reflecting library diversity. The bacteria were incubated overnight at 37 °C and next day scraped off the agar using LB medium and pelleted for 15 minutes at 4000 $\times\text{g}$. The pellet was resuspended in 20 ml LB and glycerol was added to a final concentration of 25 %. Finally, the library was aliquoted in 2 ml fractions, snap-frozen in liquid N_2 and stored at -80 °C.

2.2.16 Phage Display

To identify those nanobodies, which specifically bind to the target antigen of interest, molecular display of the nanobodies on lysogenic M13 phages was established in the laboratory [151]. This method directly links the biochemical properties of the expressed nanobody to its genetic code encapsulated in the phage. The nanobody is expressed as a fusion protein with the phage minor coat protein pIII, which is also used by the phage for infection. Each phage possesses five copies of the pIII protein controlling the number of displayed nanobodies. Most steps for phage display were determined empirically, however during the progression of this project, also several protocols describing similar approaches became available [67,152–154].

Generally, the phage display procedure can be divided into 3 parts: Phage production, binding of phages to the target protein and finally elution of specifically bound phages. A full cyclic repetition of these steps is commonly referred to as one panning round as depicted in Figure 10. To avoid contamination of common bacteria used in the lab, especially the competent bacteria stocks, all steps involving handling of bioactive phages were carried out in separate rooms or under the fume hood.

Helper Phage Preparation

Before starting the actual phage display selection, MK13KO7 Helper Phages (NEB) were amplified for further use during panning rounds as described by Lee *et al.* [154]. An overnight culture of TG-1 *E. coli* bacteria in 5 ml 2-YT medium was diluted 1:100 into 5 ml fresh 2-YT medium and grown at 37 °C until OD₆₀₀ reached ≈ 0.5. A serial dilution of MK13KO7 Helper Phages ranging from 10⁴ to 10¹² phages/ml was prepared in PBS. 10 µl of those dilutions were added to 200 µl TG-1 culture each and incubated at 37 °C in a water bath for 30 minutes. Each reaction was carefully mixed with 3 ml top-agar at 42 °C and poured on 2-YT agar plates. After solidification, plates were incubated overnight at 37 °C. Plaques in the top-agar indicated locations of phage-production. One plaque was picked with a sterile pipet tip and used to infect a 5 ml culture of TG-1 bacteria at OD₆₀₀ ≈ 0.5. After 2 h at 37 °C, 120 rpm, the culture was expanded to 500 ml 2-YT medium supplemented with 50 µg/ml kanamycin and grown overnight in a baffled Erlenmeyer flask at 30 °C, 120 rpm. Next day, the culture was pelleted in disposable 50 ml tubes and the supernatant was filtered through 0.45 µg syringe-top filters (Sartorius). PEG-8000 was added to a final concentration of 4 % (w/v) to precipitate the phages from the supernatant (see below for detailed description). The phage titer was estimated by measuring absorbance at 260 nm (A₂₆₀) and using the empirical Equation 5 postulated by Lee *et al.* [154].

$$\frac{\text{phages}}{\text{ml}} = A_{260} * \text{dilution factor} * 22.14 * 10^{10}$$

Equation 5: Formula to determine the phage titer after precipitation of phage particles. As phages contain a substantial amount of DNA, the absorbance at 260 nm (A_{260}) can be used to measure their concentration. The multiplier of 22.14×10^{10} is an empirical value determined by Lee *et al.* [154].

Production of phages

An aliquot of the frozen library was diluted into 500 ml 2-YT medium supplemented with 4 % glucose and 100 µg/ml ampicillin. The culture was grown in a baffled Erlenmeyer flask to $OD_{600} \approx 0.5$ at 37 °C, 120 rpm. Thereupon, 2×10^{12} helper phages were added to achieve a multiplicity of infection (MOI, i.e. ratio of total phages to bacteria) higher than 10, thus maximizing phage infection efficiency. For the first round of panning, commercially obtained hyperphages M13 K07ΔpIII were used to generate multivalent display of the nanobody. For infections in subsequent panning steps, classical MK13K07 Helper Phages were used, which had been amplified as described above. The infected culture was incubated another 45 minutes at 37 °C, 30 rpm. After that, bacteria were pelleted in disposable 50 ml tubes for 10 minutes at 3,200 ×g. The bacteria pellet was resuspended in 500 ml 2-YT medium supplemented with 100 µg/ml ampicillin and 50 µg/ml kanamycin. The culture was grown overnight at 30 °C, 120 rpm in a baffled Erlenmeyer flask.

The next day, bacteria were pelleted again and discarded. To the supernatant containing the phages secreted from the bacteria, PEG-8000 was added to a final concentration of 4 % (w/v). The mixture was incubated for at least 2 h on ice to precipitate the phages. The phages were pelleted by centrifugation for 30 minutes at 4 °C, 3200 ×g in 50 ml tubes and resuspended in ice-cold PBS. After pooling all pellets, phages were again precipitated by adding to 4 % PEG-8000 for 1 h on ice in a single 50 ml tube to obtain a single phage pellet. After another centrifugation for 30 minutes at 4 °C, 3200 ×g, the phage pellet was dissolved in 2 ml PBS. To remove insoluble debris, the phages were centrifuged for 5 minutes at 3200 ×g without prior adding of PEG. The supernatant containing the phages was filtered through a 0.45 µm syringe-top filter (Sartorius) to remove remaining particles. The phage titer was estimated by measuring absorbance at 260 nm and using the empirical Equation 5 given above.

Antigen immobilization

Purified protein prepared as described in the sections 2.2.3 and 2.2.9 was either immobilized unspecifically on MaxiSorp® flat-bottom 96-well plates (Thermo Fisher Scientific) or via the tst-tag on MagStrep “type3” XT beads (IBA). Typically, 3 – 10 nmol of antigen per affinity selection were immobilized. The amount of antigen was gradually reduced during subsequent panning to increase the stringency of the selection (see also Table 22). For immobilization, the antigen was incubated for 1 h with the matrix in PBS-T. Unbound protein was removed by washing twice with PBS-T. If the antigen was immobilized on plates, free binding sites on the plastic of the plate were blocked with PBS-T/milk.

Affinity selection

Purified phages were incubated with the immobilized antigen for 2 h. Unbound phages were removed and the beads/wells were washed with PBS-T. The total number and individual duration of the washing steps was increased during subsequent panning rounds, to select for nanobodies with a high affinity as shown in Table 22. For selections yielding final nanobody candidates, up to 10 washing steps with of up to 4 h were performed. To elute bound phages after washing, 100 µg/ml trypsin in TBSC were used to disrupt the interaction between the antigen and the affinity molecule by enzymatic degradation. Alternatively, the whole phages were eluted specifically from the magnetic beads using BE Strep-Tactin® Elution Buffer (IBA). Elution was carried out for 1 h with gentle mixing of the reaction. The eluted phages were subsequently used to infect a freshly prepared culture of TG-1 bacteria to perform the next panning round.

Reinfection of bacteria culture

TG-1 bacteria were grown on M9 minimal medium glucose plates without antibiotics for 36 hours at 37 °C. The minimal medium contains only amino acids essential for the bacteria. This way the bacteria are forced to express the genes required for synthesis of proline and other amino acids. Those genes are located on the same episome as the F'-pilus of the bacteria, which is required for docking and infection of phage particles. Hence, growing the bacteria on M9 minimal medium makes them susceptible for phage infection. From the plate a single colony was used to grow a liquid culture of TG-1 bacteria in 50 ml 2-YT medium at 37 °C.

The phages eluted from the affinity selection were added to the TG-1 bacteria and incubated for 1 h at 37 °C, 30 rpm. The bacteria were pelleted and resuspended in 1-2 ml of 2-YT medium and distributed onto LB-agar plates supplemented with 100 µg/ml ampicillin. Additionally, a serial dilution of the infected culture was plated to estimate the total number of infected colonies and monitor the progress of selection. The plates were incubated at 37 °C overnight. The following day,

bacteria were scraped off the agar using 2-YT medium and diluted into 500 ml 2-YT medium total. That culture was supplemented with 4 % glucose and 100 µg/ml ampicillin and grown in a baffled Erlenmeyer flask for the next panning round as described above.

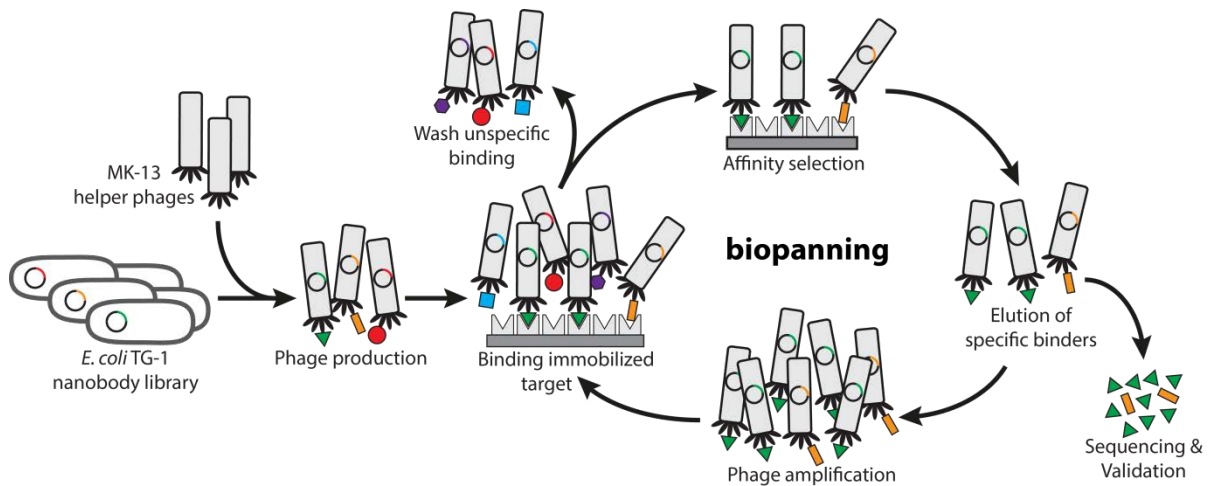


Figure 10: Schematic representation of the phage display procedure. Phages were produced by growing the library in 2-YT medium overnight infecting the culture with helper phages. Phages displaying different nanobodies were purified by precipitation and selected for affinity to an immobilized target antigen. Bound phages were eluted and used to infect a new bacteria culture for the next round of affinity selection, a procedure also referred to as biopanning. After the final panning round, individual nanobody populations displayed on phages were isolated for a subsequent validation procedure.

Screening of individual clones by ELISA

After 2-3 rounds of panning, individual colonies from re-infected TG-1 bacteria were screened by soluble fragment ELISA to identify nanobody families. 80 single colonies were picked from plated dilution series using sterile pipet tips and dipped into the wells of a 96-well round-bottom plate filled with 200 µl 2-YT medium supplemented with 100 µg/ml ampicillin. The remaining wells were used for internal controls during subsequent screening procedure. Cultures were grown at 37 °C, 120 rpm overnight in a humidifying chamber to avoid evaporation of the medium. On the next day, a duplicate of the plate was created using 5 µl bacteria from the overnight cultures. The cultures of the original plates were added to 20 % glycerol and frozen at -80 °C for storage. The new plate was grown at 37 °C, 120 rpm for 3 h followed by infection with MK13KO7 Helper Phages at a MOI of >10. For infection, the plate was incubated 1 h at 37 °C, 30 rpm. Infected cultures were pelleted in the plate for 15 minutes at 3,200 xg. Pellets were resuspended in 200 µl fresh 2-YT medium (supplemented with 100 µg/ml ampicillin and 50 µg/ml kanamycin) and phages were produced overnight at 30 °C, 120 rpm in a humidifying chamber.

On the following day, bacteria were pelleted as before and the supernatant containing the monoclonal phages was transferred to a clean 96-well plate. The antigen used during the affinity selection was immobilized using a MaxiSorp® flat-bottom 96-well plates (Thermo Fisher Scientific) as described above. Free binding sites on the plastic of the plate were blocked carefully by incubation with PBS-T/milk overnight to avoid false-positive results due to background binding of the phages. Per well, 25 µl of the phage supernatant mixed with 75 µl PBS-T/milk were transferred in the antigen-coated wells and incubated for 1 h, 100 rpm. The wells were washed 3 times 10 minutes with PBS-T. To detect the bound phages, an antibody directed against the phage major coat protein pVIII conjugated to horseradish peroxidase (HRP, obtained from GE Healthcare) was used at 1:5000 dilution in PBS-BSA. After 1 h incubation, 100rpm, wells were washed 3 times for 10 minutes with PBS-T. To detect binding, 100 µl of 1-Step™ Ultra TMB-ELISA Substrate Solution (Thermo Fisher Scientific) were added to each well. The plate was incubated until dark blue color developed in positive control wells. At that point, the reaction was stopped by adding 50 µl of 1 M sulphuric acid to each well. The absorbance at 430 nm was read in a Cytation-3 Multi-Mode Reader (BioTek). Specific binding of the displayed nanobody was considered if the readout was at least 10-fold over the background signal. Positively tested candidates were subjected to a stepwise validation procedure to further validate specific binding of the nanobody.

2.2.17 Validation and Characterization of Nanobody Candidates

For positively tested wells, an overnight culture in 5 ml 2-YT medium was grown (37 °C, 120 rpm) from the glycerol stock plate stored at -80 °C. The phagemids were extracted using the GeneJET Mini Prep kit (Thermo Fisher Scientific) and sent for sequencing (SeqLab, Göttingen). The sequences obtained were grouped into families according to their CDR-composition. Identification of the conserved nanobody framework was based on consensus data provided in the literature [155]. One nanobody sequence of each family was then extracted by PCR and cloned into an expression vector (K40 or pNB666, see section 2.2.1) for cytosolic expression of the nanobody in SHuffle® Express bacteria. A FLAG-tag was fused to the nanobody to allow detection by secondary antibodies in the following validation steps which are depicted in section 3.3.2.

Validation in dot blot

For a first validation step of the nanobody candidates, up to 1 µg of the purified antigens was spotted on a 0.2 µm nitrocellulose membrane for a dot blot assay. After blocking for 1 h with PBS-T/milk, the membranes were incubated with crude lysate from bacteria overexpressing the nanobody, prepared as described in section 2.2.3 for 1 h, 100 rpm. After 3 washes with PBS-T, bound nanobodies were detected with a secondary Anti-DDDDK tag antibody conjugated to DyLight®650 (Abcam, clone M2) for 1 h, 100 rpm in PBS-BSA. After 3 washes with PBS-T, the signal was detected in Amersham™ Imager 600.

Validation in IF

To test whether selected nanobody candidates do not only bind the native but also the chemically fixed antigen, the crude lysate containing the nanobody was incubated on COS-7 cells overexpressing the target antigen fused to EGFP (see section 2.2.6). The cells grown on coverslips were fixed, quenched permeabilized and blocked as described in section 2.2.7 before incubation. After 3 PBS washes, Anti-DDDDK tag antibody conjugated to DyLight®650 (Abcam, clone M2) was used at a dilution of 1:500 to detect bound nanobodies. Alternatively, COS-7 cells were directly grown and handled on 48-well glass bottom plates and automatically imaged with a Nikon Ti-E epifluorescence microscope or Cytation-3 Multi-Mode Reader. If the fluorescent signal of the secondary antibody was clearly colocalizing with the EGFP signal without notable background signal, the nanobody was identified as a positive candidate. Those candidates were considered to be suitable for IF experiments and were expressed again in large scale followed by purification and covalent conjugation to a fluorophore.

2.2.18 Labelling of Nanobodies

To exploit their full potential, nanobodies were directly coupled to fluorescent molecules following different strategies. Chemically functionalized fluorophores were ordered commercially and coupled to the protein adapting the protocols given by the manufacturer. In Table 20, major fluorophores used for coupling reactions are shown. Typically, atto647N (Atto-tec) was used for conjugation to nanobodies, as that molecule shows a high quantum yield and can also be used for STED-microscopy. Dyes were usually delivered lyophilized and dissolved in anhydrous DMSO under protective gas atmosphere (N₂ or Ar). Aliquots of ~100 nmol dye were frozen at -20 °C until used for labeling reactions. The individual strategies for labeling are described below. A schematic overview of the underlying reaction mechanisms is depicted in Figure 11.

Table 20: Selection of fluorophores used for conjugation to affinity molecules. The commercially obtained fluorophores were functionalized with an N-hydroxysuccinimide (NHS) ester or a maleimide group for chemical conjugation.

Fluorophore	Functionalization	Manufacturer
Alexa488	Maleimide	Thermo Fisher Scientific, Waltham, MA, USA
Alexa546	Maleimide	Thermo Fisher Scientific, Waltham, MA, USA
Alexa594	Maleimide	Thermo Fisher Scientific, Waltham, MA, USA
Alexa647	NHS-ester	Thermo Fisher Scientific, Waltham, MA, USA
Alexa647	Maleimide	Thermo Fisher Scientific, Waltham, MA, USA
atto488	Maleimide	Atto-tec, Siegen, Germany
atto532	Maleimide	Atto-tec, Siegen, Germany
atto532	NHS-ester	Atto-tec, Siegen, Germany
atto647N	NHS-ester	Atto-tec, Siegen, Germany
atto647N	Maleimide	Atto-tec, Siegen, Germany
CF647	Maleimide	Sigma-Aldrich, St. Louis, MO, USA
Cy3B	Maleimide	GE Healthcare, Little Chalfont, UK
Cy5	Maleimide	GE Healthcare, Little Chalfont, UK
Cy5	NHS-ester	GE Healthcare, Little Chalfont, UK
Star580	Maleimide	Abberior, Göttingen, Germany
Star635P	Maleimide	Abberior, Göttingen, Germany
Star635P	Maleimide	Abberior, Göttingen, Germany
StarRed	Maleimide	Abberior, Göttingen, Germany

NHS-ester labeling

This method was used to label nanobodies or antibodies stochastically at exposed lysine residues. 10-30 nmol purified protein were desalted into PBS and added to 100 mM NaHCO₃ using 1 M stock solution of pH 8.6 to increase the pH value for activating the lysine reactivity (total volume of 0.5-1.0 ml). The dye was slowly added in 5-10-fold molar excess compared to the protein while constant stirring. After mixing for 1 h on ice in the dark, the reaction was quenched by adding 20 µl freshly prepared 1.5 M hydroxylamine solution, pH 8.5. For separation of labeled protein from free dye, the reaction was passed through a 20 cm custom-made gel filtration Econo-Column® (BioRad) packed with Sephadex™ G-25 superfine resin (GE Healthcare) and equilibrated with PBS. Fraction of the eluted protein were taken and measured in NanoDrop spectrophotometer for absorption at 280 nm and the corresponding wavelength of the dye moiety. The degree of labeling (DOL) was calculated according to the Equation 6 given below.

The extinction coefficient of the protein ϵ_{prot} was calculated using the online ProtParam tool from ExPASy (<http://web.expasy.org/protparam/>). The extinction coefficient of the fluorophore ϵ_{max} and the factor to correct for its absorbance at 280 nm (CF_{280}) were employed as provided by the manufacturer.

Typically, DOL values greater than 100 % labeling were obtained for NHS-ester labeling indicating the presence of more than one dye moiety per nanobody. The labeled nanobody was added to 50 % glycerol and stored at -20 °C.

$$\text{DOL} = \frac{A_{280} * \epsilon_{\text{prot}}}{(A_{280} - A_{\text{max}} * CF_{280}) * \epsilon_{\text{max}}}$$

Equation 6: Formula to determine the degree of labeling (DOL). The absorbance of the protein and the dye are measured at 280 nm (A_{280}) and its specific wavelength (A_{max}), respectively. The extinction coefficient ϵ_{prot} was calculated using the online ExPASy ProtParam tool (<http://web.expasy.org/protparam/>). The extinction coefficient of the dye ϵ_{max} and the dye-specific correction factor for absorbance at 280 nm (CF_{280}) were taken from the material data sheets of the fluorophores.

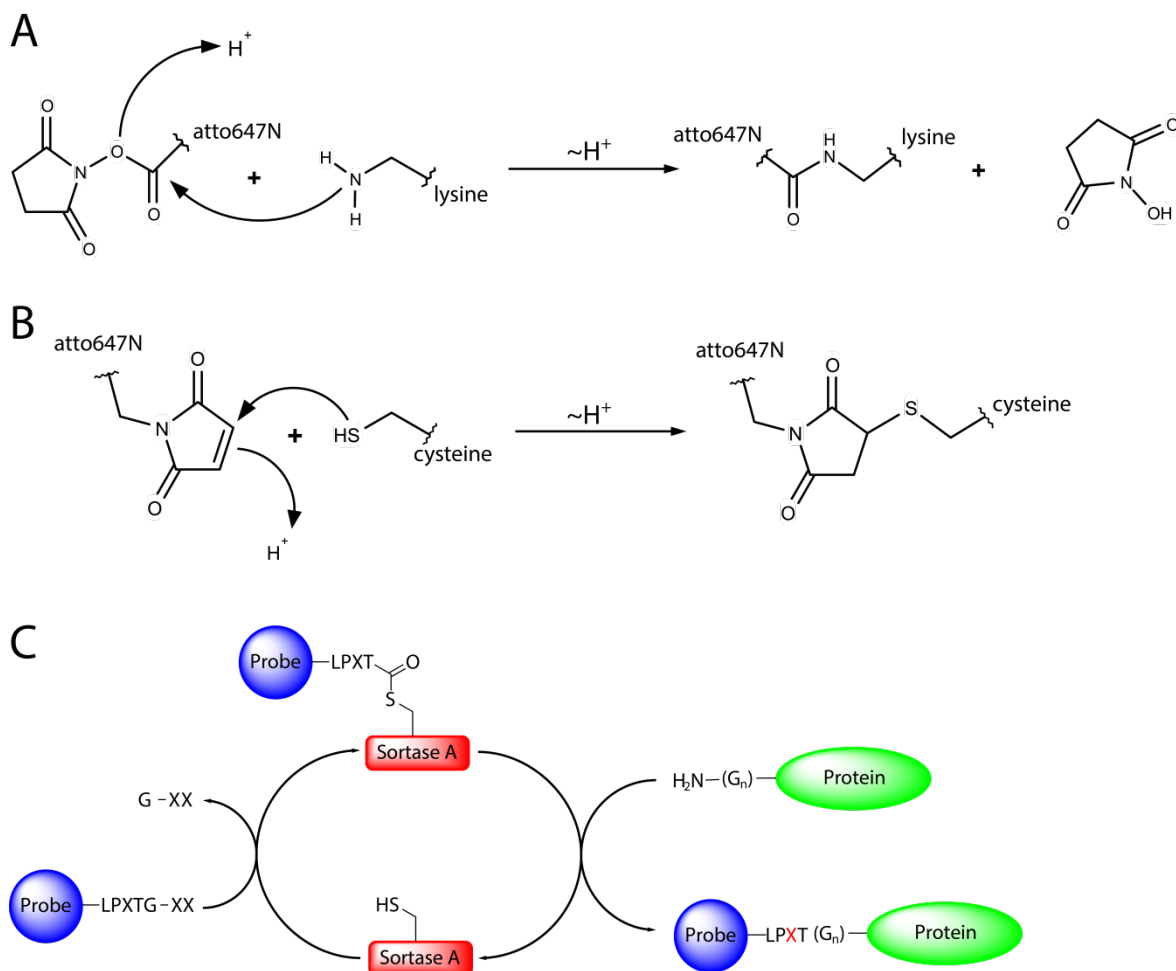
Maleimide labeling

To label nanobodies in a more quantitative way compared to NHS-ester labeling, they were expressed in a plasmid adding a C-terminal cysteine residue (see Table 12). These terminal cysteine moieties can specifically be attacked by maleimide-functionalized fluorophores. TCEP was added to the purified nanobody in 50-fold molar excess to break intermolecular disulfide bridges formed during the purification process. After mixing for 30 minutes, unreacted TCEP was removed via NAP™-5 or NAP™-10 columns (GE Healthcare) equilibrated with PBS. 10-30 nmol reduced protein were used in volume of 0.5-1.0 ml. Maleimide-functionalized dye was slowly added in 3-5-fold molar excess and mixed with the protein for 3 h on ice, in the dark. After that, free dye was removed by gel filtration as described above. Alternatively, the ÄKTApure25 HPLC system was used for removal of free dye loading the labeled sample on a Superdex™ 75 increase 10/300 GL column (GE Healthcare, see Table 14). Typically, a DOL of >85 % was obtained after labeling with maleimide-functionalized fluorophores. Glycerol was added to final concentration of 50 % and the labeled probe was stored at -20 °C.

Sortase A-mediated labeling

As an alternative way to specifically label expressed nanobodies, enzymatic labeling using sortase-mediated formation of a covalent bond was performed according to [156]. To generate a substrate for sortase A, atto647N was coupled to the amino acid motif leucine-proline-glutamate-threonine-glycine-glycine, which resulted in a conjugate termed atto647N-LPETGG-NH₂ to be detected by the

enzyme. The nanobody sequence in turn was modified to express a motif of at least three glycine residues at its C-terminus for coupling of the dye conjugate. The enzyme sortase A was expressed and purified from bacteria as described before. 40 μM purified nanobody was mixed with 1 mM dye conjugate and 80 μM sortase in sortase buffer to drive the reaction towards the coupled protein. The reaction was carried out overnight with slow stirring. Free dye was removed using 20 cm custom-made gel filtration Ecnocolumns[®] as described above. As the DOL regularly did not exceed 40 %, I therefore primarily focused on alternative approaches as also shown in section 3.4.2.



adapted from Theile, CS *et al.*, Site-specific N-terminal labeling of proteins using sortase-mediated reactions, *Nat. Prot.*, **2008**, 8, 1800-1807

Figure 11: Different strategies for labeling nanobodies with fluorophores. **A:** Dye molecules functionalized with NHS-ester groups react with lysine residues exposed at the nanobody surface. **B:** Maleimide-functionalized fluorophores specifically react with reduced cysteines added to the C-terminus of the nanobody. **C:** Enzymatic labeling using sortase A detecting a specific amino acid motif added to the fluorophore for subsequent site-directed labeling to the nanobody. Comparing the different labeling approaches, I decided to generally perform the labeling reaction based on maleimide-functionalized fluorophores (see section 3.4.2).

2.2.19 Affinity Measurements

After successfully passing the validation steps listed above, the final nanobodies were tested for their actual affinity to their target antigen. This was done by microscale thermophoresis (MST) in a Monolith™ NT.115Pico instrument determining the K_D -values of the nanobody-antigen complexes. The fluorescence of the directly labeled nanobody was measured in PBS containing 0.05 % Tween®20. To determine the affinity, different nanobody samples were mixed with a dilution series of the purified antigen in Premium Coated Capillaries to avoid background binding to the capillary surface. For operation of the instrument and evaluation of affinity data, the MO.Control and MO.Affinity Analysis software (NanoTemper) was used.

2.2.20 Image Analysis and Evaluation

Generally, microscopy images were analyzed by measuring the intensity of regions of interest (ROI) and line scans in ImageJ. The fluorescence intensity was measured in a line scan for each pixel or as average of the ROI and normalized according to the maximum value in the line scan or ROI.

To identify and average the fluorescence of nanobodies and antibodies in synapses as conducted in section 3.5.5, the Matlab R2015b software was used. The macro used for the analysis was kindly provided by Prof. Dr. Silvio Rizzoli using the first channel for identification and the second channel for alignment of synaptic boutons.

2.2.21 Molecular Modelling

Molecular models of affinity probes and antigens used for affinity screening were based on structures from the Protein Data Bank (www.pdb.org). The corresponding accession numbers are given in the figure legends. Graphic representations of the model were created using PyMol version 1.7.4.5 Edu. Secondary structures of the proteins were differentially colored to facilitate the visualization of the molecule.

3. Results

Fluorescence microscopy is a major technique to analyze the subcellular organization of synaptic proteins. The observation of subcellular protein distribution is though limited by the usage of conventional antibodies. Especially in super-resolution techniques, antibodies have been reported to cause artifacts and impair the resolution. Smaller probes such as nanobodies have in contrast been shown to overcome most of the problems caused by antibodies in molecular imaging techniques.

The rationale of this project was to generate novel nanobodies, which specifically bind synaptic proteins for their use in super-resolution microscopy. Using nanobodies for molecular imaging, I aimed to detect a higher number of epitopes in the sample, thus increasing imaging accuracy and attainable resolution. I successfully identified and characterized two novel probes binding SNAP-25 and syntaxin 1A with high affinity and specificity.

I could further show that those probes reveal a subcellular organization in high detail deviating from observations made with classical antibodies in super-resolution. Due to their advantages in fluorescence imaging, I consider my novel nanobodies to be versatile tools for future studies in the field of synaptic physiology.

3.1 Establishing the Workflow for Protein Production

As a first part of this project, I established several protocols for the expression and purification of recombinant proteins. The three major neuronal SNARE proteins SNAP-25, syntaxin 1A and VAMP2 were chosen as POI for generation of new nanobodies. Those antigens were produced in bacteria using inducible plasmids commonly used in the laboratory practice. Different plasmids for expression were tested to optimize the yield for each protein. After comparing various expression conditions, I decided to use the vectors K40 and pNB666 derived from the LacO-pQLinkN-construct for protein production in bacteria [146].

Moreover, I tested different bacteria media and expression conditions. Quantifying protein yield under varying conditions, I decided to produce recombinant proteins in large scale for 8 to 12 h at 30 °C, 120 rpm in TB medium. Notably, growing the culture in baffled Erlenmeyer flasks tremendously increased protein yielded up to 5-fold compared to a culture of the same volume grown in plain Erlenmeyer flasks. After establishing the bacteria cultures, different approaches for bacteria lysis were tested including alkaline lysis, freeze-thaw cycles, French press and sonication. A combination of short sonication pulses at high power and enzymatic digestion of the bacterial cell wall and DNA was found to be most efficient.

Finally, I compared different strategies to purify the recombinant proteins from the crude lysate. First, all proteins were purified via their His-tag using affinity resin loaded with Nickel ions. However, after several optimizations, that procedure was found to result in rather poor purity of the eluted protein, despite using high salt (500 mM NaCl) buffers for washing as shown in Figure 12. Hence I decided to introduce an ÄKTApure25 HPLC system in the laboratory for automated and large-scale production of proteins. The commercial His-tag affinity columns used with that system improved the purity of the eluted protein. Nevertheless proteins purified via a His-tag frequently still required a second polishing step to remove remaining contaminants from the elution.

The best results for protein purity and recovery rate were obtained when immobilizing the protein via a recombinant Twin-Strep-Tag® instead of the His-tag. Due to very specific elution using d-desthiobiotin, purity rates of >95 % could be obtained on a regular basis. After purification, SUMO-protease was added to the expressed protein to cleave off the SUMO domain and to reconstitute the protein to its native state. The cleaved SUMO fragment, the SUMO-protease and remaining uncleaved protein were immobilized and removed upon binding to His-tag affinity resin. The HPLC was also used for fast desalting of the eluted fractions to remove the high salt elution buffer and thus to prevent protein precipitation in the course of time. All purifications were evaluated by SDS-PAGE to evaluate the protein quality. Exemplary analyses of protein purification using different approaches are shown in Figure 12.

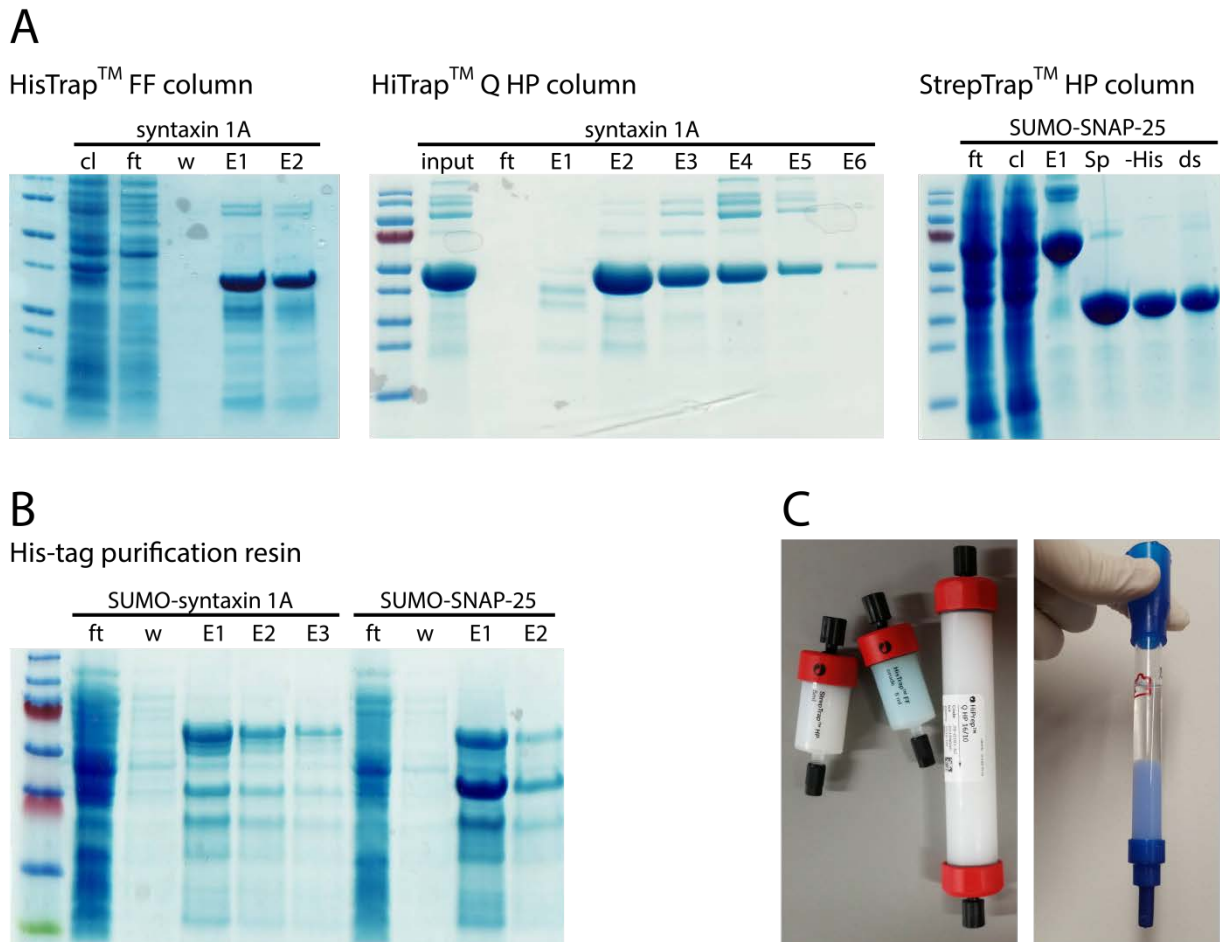


Figure 12: Compilation of different protein purification strategies. **A:** Protein purification using commercial pre-casted columns designed for the ÄKTA HPLC system. HisTrap™ FF columns were used to immobilized proteins via a recombinant poly-histidine tag. However, eluted fractions frequently showed some contaminations requiring an additional polishing step such as ion-exchange chromatography. Using HiTrap™ Q/SP HP columns removed most of the contaminations as shown in the middle panel. Alternatively, proteins were purified via a Twin-Strep-Tag® (tst-tag) using StrepTrap™ columns, which resulted in a high degree of protein purity as seen in the gel. **B:** Using affinity resin binding to the His-tag of the protein frequently resulted in impure elution fraction of the purified protein and thus required an additional polishing step to remove protein contaminations. **C:** Examples for columns used with the HPLC (left) or custom-packed (right). To avoid protein precipitation, pure eluted fraction were pooled and desalted into PBS pH 7.4. cl = crude lysate, ft = Flowthrough, w = wash, E1-3 = eluted fractions, Sp = treated with SUMO-protease, -His = after removal of cleaved fragment, ds = after desalting into PBS.

3.2 Creating the Nanobody Libraries for Phage Display

After purification, the antigens were used to immunize an alpaca to evoke an immune response and thus to generate novel affinity molecules. The immunization procedure and extraction of white blood cells was carried out by preclinics GmbH, Potsdam, Germany. Briefly, the frozen purified proteins (SNAP-25, syntaxin 1A, VAMP2) were shipped to the company and injected to the animal together with incomplete Freud's adjuvant as described in section 2.2.14. After seven weeks, I received a

pellet of extracted white blood cells. The isolated blood cells were typically stored and shipped in RNeasy[®] to preserve the RNA.

In several trial extractions the conditions for the total RNA extraction procedure were optimized to minimize degradation and loss of sample quality. Isolation of peripheral B-cells from blood using Ficoll-gradient centrifugation rather than lysis of the erythrocytes turned out to yield best results (data not shown). For further preparations, the samples were shipped directly on the same day of extraction to the lab to minimize the time of transportation.

To isolate the total RNA from the cells, I used the RNeasy[®] Mini kit (Qiagen). To avoid diversity loss by saturation of the column, I used 8 columns per extraction providing a total capacity of 800 µg RNA. After extraction, the RNA was retro-transcribed using initially the SuperScript[™] III and later the SuperScript[™] IV system (Thermo Fisher Scientific). Although it was recommended to use random hexamer primers annealing to the RNA for reverse transcription, using directly site-specific primers for the IgG sequences significantly improved the cDNA yield about 10-fold. The first nanobody libraries were created by direct amplification of the nanobody sequences from IgG2 and IgG3 cDNA introducing peripheral restriction sites by PCR (Alp_F1+ and Alp_R1/2+ primers, see Table 17). However, in subsequent experiments I realized that this method resulted in a rather low diversity of the library and thus in a limited number of specific nanobodies. Therefore I decided to set up a new approach omitting the inefficient cloning by restriction enzymes. All IgG heavy variable regions were first amplified in a nested PCR reaction (using the Call001 and Call002 primers) followed by specific amplification of nanobody sequences (using primers Gibson_F1 and Gibson_R1/2) as described by Pardon *et al.* [67]. At that second amplification step, 21 bp overhangs for Gibson assembly were introduced instead of the restriction sites. The phagemid was modified and amplified accordingly to allow insertion of the nanobody sequences by Gibson assembly resulting in an up to 20-fold higher cloning efficiency.

In various test reactions it turned out that the quality of TG-1 bacteria as well as the stoichiometric ratio of bacteria compared to plasmid concentration is crucial for an efficient electroporation. To maximize the efficiency of transformation, competent TG-1 bacteria were thus prepared freshly before each library generation. The medium used after electroporation was as well observed to have a great impact on the colony number. For the final libraries, I used Recovery Medium (Lucigen) to resuspend the electroporated cells, which resulted in a more than 10-fold higher number of colonies compared to SOC or LB medium. Table 21 provides an overview on different libraries for phage display created by electroporation.

Additionally, the ionic strength of the electroporation mixture was found to be very critical for the transformation. Ligated plasmid DNA therefore needed to be cleared from protein contaminants and eluted into pure water to minimize the salt concentration. A maximum of 1.5 µl of the ligation

reaction could subsequently be used to electroporate 50 μ l of TG-1 bacteria without destroying the cells. As each TG-1 aliquot is further capable of internalizing only a limited number of plasmids, I empirically determined the best ratio of ligated plasmid versus bacteria not to exceed the competency of the bacteria. A maximum of 250 ng ligated plasmid DNA was used per reaction, which corresponds to \sim 150 fmol or 4.5×10^{10} molecules. Consequently, 40-50 individual electroporation reactions needed to be performed for each library as depicted in section 2.2.5.

A common way to determine the diversity is based on counting individual colonies after diluting the total library. With that, the diversity of my libraries ranges between 6.5×10^6 clones for restriction-based and 4.5×10^{11} for Gibson-based cloning as shown in Table 21.

Table 21: Overview on different libraries created for nanobody selection by phage display. The primer sets used to extract the nanobody sequences from total white blood cell preparations are indicated. To avoid overloading of the bacteria, successive electroporation reactions were performed using a maximum of 150 fmol DNA per reaction. The library diversity was estimated by counting individual colonies of plated bacteria dilution series after electroporation. After optimization the protocol, the amount of input RNA was increased to create the restriction-final library used for initial screen by phage display. As no novel nanobody families were revealed from the restriction library, I decided to create new libraries using Gibson cloning to maximize cloning efficiency and thus the sequence diversity in the library.

Library name	RNA input	Primers	PCR cycles	Competency of TG-1 bacteria	Electroporations	Apparent diversity
Test conditions	200 ng	F1 + R1/R2 Call001/002	35	3.8×10^8 cfu/ μ g	3	-
Mock library	500 ng	F1 + R1/R2	40	1.2×10^8 cfu/ μ g	12	Not tested
Restriction-small	500 ng	F1 + R1/R2	40	1.0×10^9 cfu/ μ g	8	6.5×10^6
Restriction-final	12 μ g	F1 + R1/R2	40	1.0×10^9 cfu/ μ g	48	1.12×10^8
Gibson-1	10 μ g	Call001/002	8	2.5×10^8 cfu/ μ g	40	4.0×10^7
		F1+R1/2_Gibson Gibson_for/rev	8 8			
Gibson-2	20 μ g	Call001/002	8	1.6×10^9 cfu/ μ g	40	4.5×10^{11}
		F1+R1/2_Gibson Gibson_for/rev	8 8			

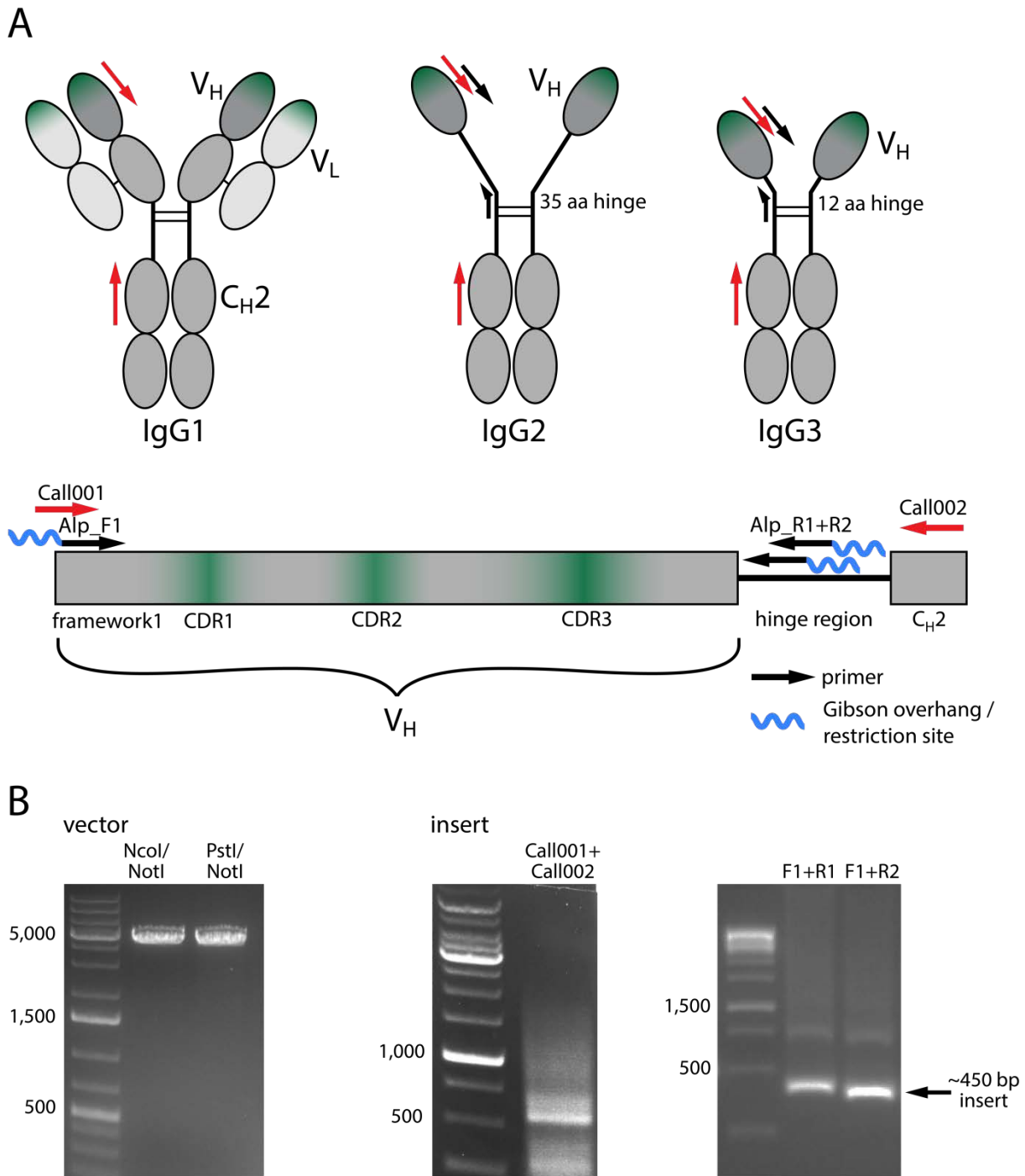


Figure 13: Extraction of nanobody DNA sequences from alpaca IgG antibodies for cloning into phagemid vectors. **A:** Primer sets (black and red arrows) align to conserved elements of the IgG antibodies as described in Table 17 and Table 18. Degenerated primers were used to amplify the nanobody sequences in subsequent PCR reactions. Overhangs were added to the primers to create sites for enzymatic restriction or complementary sequences for Gibson cloning. **B:** Examples of PCR reaction to amplify the backbone vector (left) and the nanobody sequences (middle and right).

3.3 Selection of Nanobodies from Phage Display Libraries

After their sequences had successfully been integrated into a bacterial library, specific nanobodies were selected by phage display. The basic principles of this method had been established in the laboratory in a previous project using a naïve library of human domain antibodies [65].

3.3.1 Screening for Nanobodies via Phage Display

A common way for the affinity selection of nanobodies is based on the absorption of antigens to the plastic surfaces of tubes or plates based on polar or hydrophobic interactions. Yet, the absorption of the protein to the plastic might disrupt its molecular fold and thus the epitope conformation. This method is nevertheless commonly used for ELISA assays, which were also used for validation of positive binders. However the aim of this project was to select for nanobodies to be used in IF studies. Therefore, a more comprehensive validation protocol eliminating affinity molecules, which do not bind to the native epitope, needed to be established.

My first screens of the libraries were entirely carried out in tubes coated with the target antigens as described above. I found that the first round of panning is most crucial for the outcome of the screen as that step comprises the highest level of competition among displayed nanobodies. To reduce stringency in the first panning round, I used hyperphages to infect the initial library [157]. This leads to polyvalent display of nanobodies, thus facilitating the binding of phages present in lower copy number or having a lower affinity as illustrated in Figure 14. The titer of purified phages was measured during panning rounds to monitor the progress of affinity selection.

As expected, the amount of phages decreased after the first panning but increased again as specific binders were selected (see Figure 14). Due to amplification of only few genetically different phage populations during the panning rounds, the number of new candidates after each screen is typically limited, depending on the selection conditions in the panning. To increase the number and also select for alternative probes, the conditions of the pannings were modified along with new screenings. Particularly, I modified the amount of antigen to bind more phages during the affinity selection step. The amount of antigen was still reduced in successive panning rounds to enforce the competitive selection procedure as summarized in Table 22. In consecutive screens, the washing steps were adjusted to be less stringent allowing also the selection of molecules with lower affinities. The time of individual washing steps was further reduced from overnight in the initial screens to 10 minutes in the latest screens resulting in identification of yet new nanobody families.

After up to three rounds of phage display, 80 clones were picked and tested in a monoclonal phage-ELISA assay. A HRP-coupled antibody directed against the major coat protein of the phage was used for detection of bound candidates. When the fluorescent readout of the subsequent enzymatic reaction described in section 2.2.16 was at least 10-fold over the background signal, binding of tested candidates was considered positive. Those positive clones were grown in liquid culture for plasmid isolation followed by sequencing. As expected, several redundant sequences were identified, which indicates the enrichment of particular phage populations due to specific antigen binding. The obtained sequences were grouped into nanobody families according to the composition of their CDR regions. If only a single amino acid in CDR1 or CDR2 was different, two nanobody sequences were still considered to belong to the same family. However, differences in the composition of the CDR3 were generally considered a separate family as the CDR3 is known to be an important factor for epitope binding [51].

Each family contained from 4 to 33 clones indicating the amplification of particular sequences. To map the CDR regions, the conserved framework sequences of the nanobodies were aligned according to Maass *et al.* [155]. Figure 15 shows exemplary sequences marking the complementary regions determining the nanobody specificity. As expected, the framework region is highly conserved among all selected nanobodies, regardless of the antigen used for screening. This is in line with observations from Maass *et al.* [155]. Notably, the selected nanobody candidates possess either two or four cysteine residues promoting the formation of one or two disulfide bridges. Nanobodies requiring the formation of two disulfide bridges were occasionally reported to show low expression yields in bacteria and impaired functionality. However these candidates were not discarded at this point as I was following a dedicated strategy to validate the nanobody function.

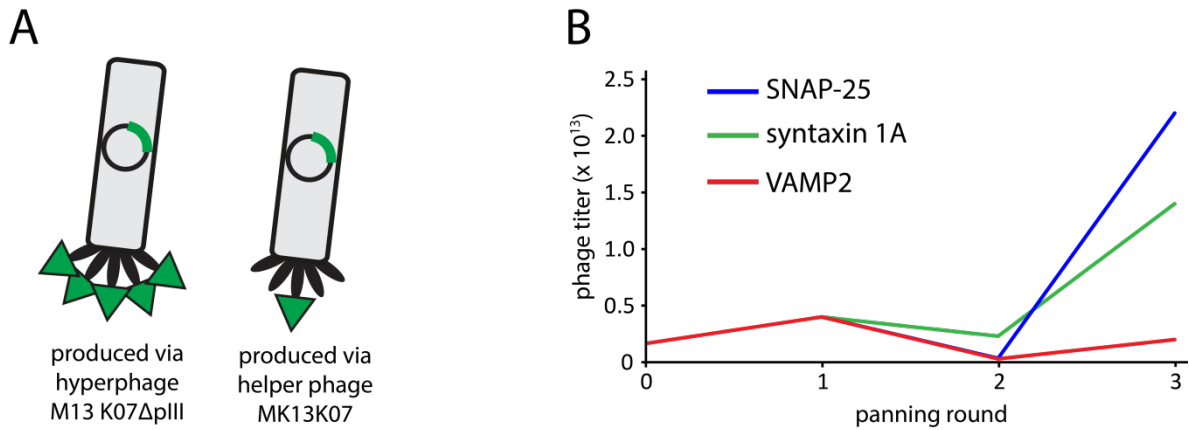


Figure 14: Titer of amplified phages during subsequent panning rounds. **A:** Schematic illustration of phages produced upon infection with M13 K07ΔpIII hyperphages for polyvalent display in the first panning round and classical MK13K07 helper phages in the subsequent panning rounds. Each phage expresses 5 copies of the phage minor coat protein pIII (black ellipse). The nanobody (green triangle) is expressed from a phagemid (circle) as a fusion construct together with the pIII protein. Depending on the phage type used, either one or five copies of the nanobody are displayed by the phage mediating the affinity selections. **B:** Phage titer for exemplary panning rounds against SNAP-25, syntaxin 1A and VAMP2. An initial decrease of the phage titer indicates the elimination on unspecific phages. In the third panning for syntaxin 1A and SNAP-25, the phage concentration considerably increased due to selection and amplification of specific phage candidates. Notably, the phage titer for panning against VAMP2 did not rise significantly, which indicates that no positive candidate was selected and amplified.

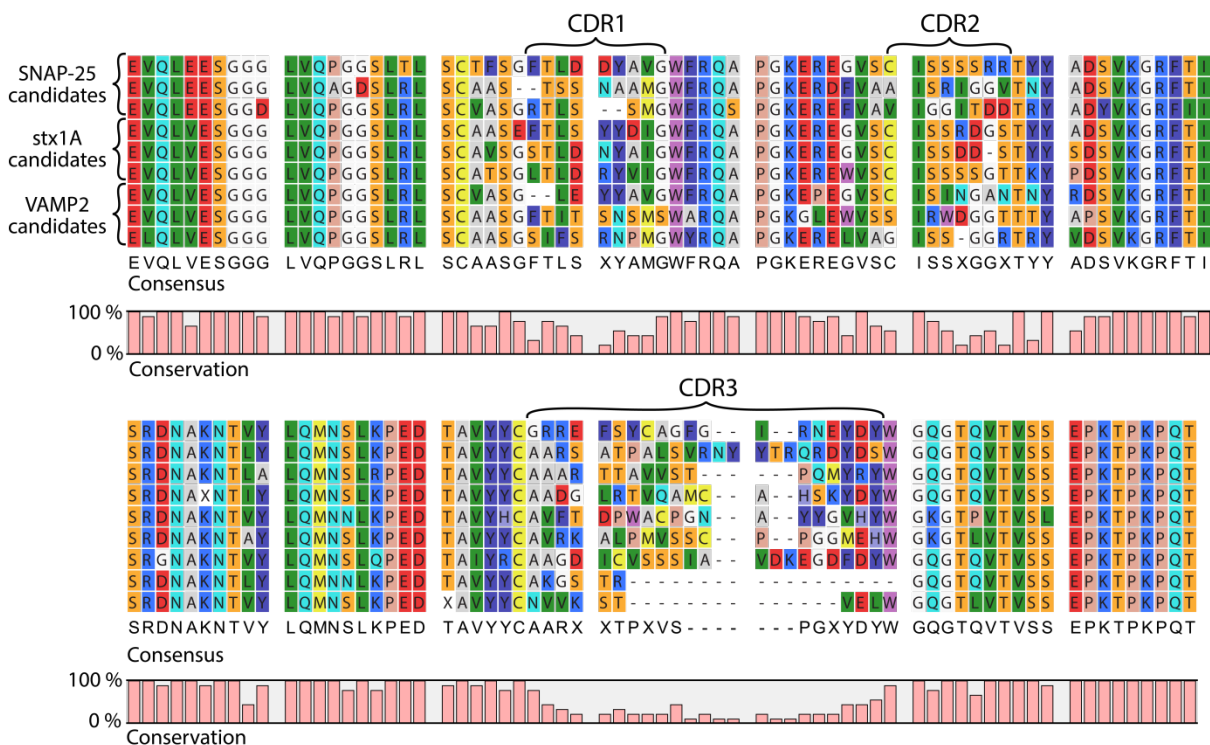


Figure 15: Sequence alignment of selected nanobody candidates. Three randomly picked sequences per antigen are shown out of several hundred. After alignment, the conserved framework as well as the three CDR regions can be identified. CDR1 and CDR2 were found to show only little variation in both length and composition. In contrast, the CDR3 region typically playing the major part in epitope detection exhibits high diversity in different nanobodies.

3.3.2 Establishing a Robust Validation Protocol

As I was aiming to select nanobodies suitable for microscopy, the functionality of selected candidates needed to be confirmed not only in phage-ELISA but also under native conditions. Therefore I established a routine composed of several validation steps, which allowed me to test the specificity and functionality of my candidates under defined conditions in an efficient manner. A flow scheme of the selection procedure of nanobodies against SNAP-25 is shown in Figure 16 indicating the individual validation steps. Nanobodies against other targets were selected and validated accordingly.

First, one representative candidate of each nanobody family was produced in bacteria and tested in immunoblot and IF experiments. Some nanobodies could not be expressed in bacteria even if fused to domains improving the solubility of the protein. As large-scale production of nanobodies for subsequent experiments was required, those candidates were discarded at that point.

Second, candidates that could readily be produced in bacteria were tested in a dot blot assay. I found that only a subset of the expressible candidates was capable of detecting the native purified antigen spotted on a membrane, despite tested positively in ELISA. As before, only those candidates showing specific binding to the antigen were considered for the next validation step.

As a third step, I tested if the nanobodies are also capable of binding their antigen in a cellular environment after chemical fixation. In IF stainings, candidates were detected with a secondary antibody directed against a recombinant tag fused to the nanobody to facilitate parallel screening. As expected, the formaldehyde fixation of the cells impaired the binding capability of some candidates. I excluded those candidates from further analyses to only consider nanobodies able to bind to antigen fixed with PFA, as I was aiming to use the nanobodies mainly in IF studies on fixed cells.

To exploit the full potential of nanobodies in microscopy, it is beneficial to directly conjugate them to a fluorescent molecule rather than detecting them indirectly with an antibody as performed during validation (see section 1.5). As a final validation step, purified nanobodies were thus chemically conjugated to a single fluorophore and tested again in IF to rule out unspecific binding caused by the labeling procedure. All candidates passing this last validation step were analyzed in MST assays to determine the dissociation constant k_D indicating the affinity.

A summary of all phage display selections and the resulting new nanobody families is shown in Table 22. It can also be seen that the number of functional nanobodies successively decreased during subsequent validation steps. In the course of different screens I was thus optimizing the selection procedure to maximize the success rate for identification of specific candidates.

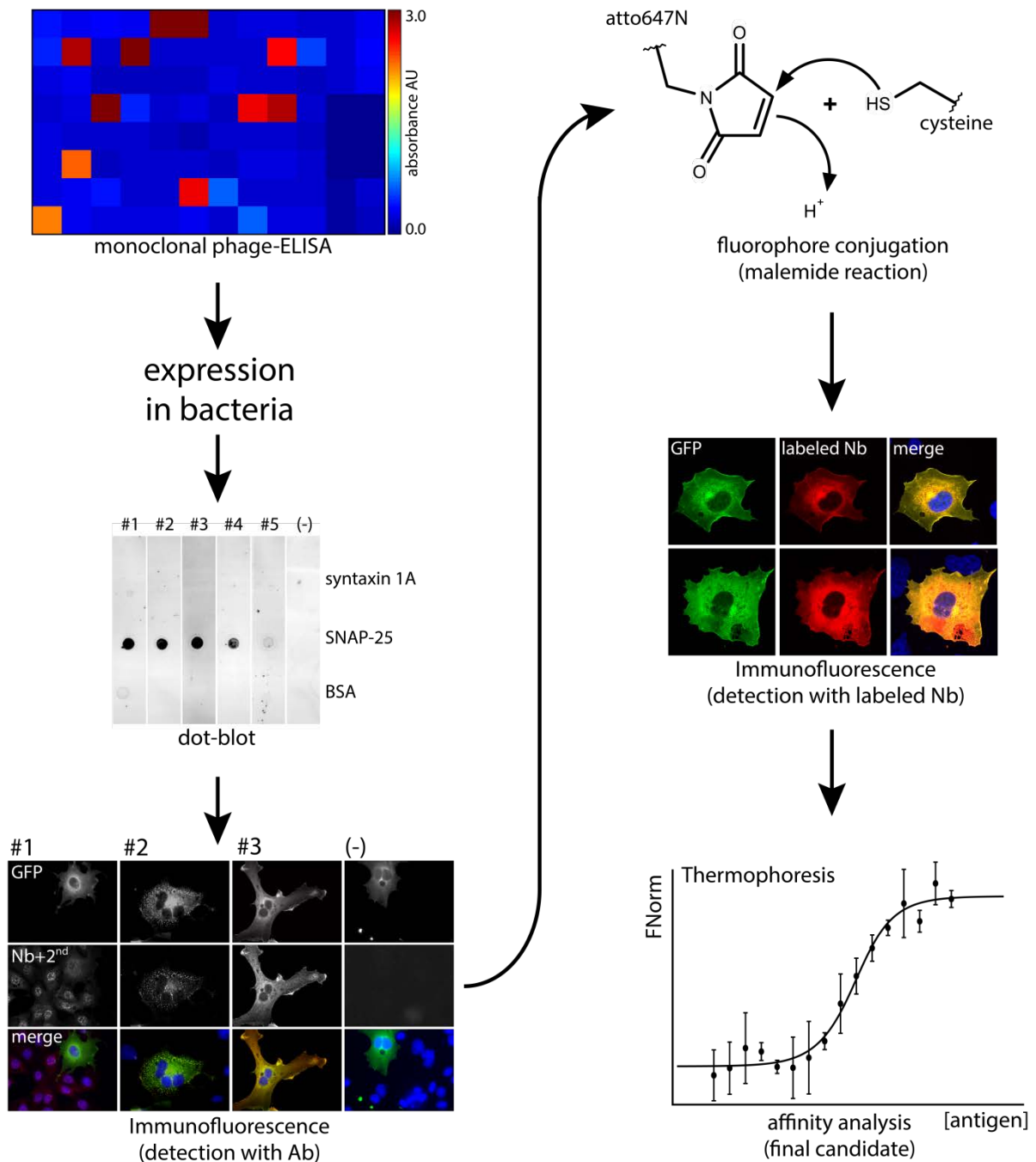


Figure 16: Flow-scheme for stepwise validation procedure of nanobody candidates. Monoclonal phage ELISA was used as a first validation step. The corresponding cartoon represents the fluorescent readout of a 96-well plate including negative controls (two rightmost columns). After expression in bacteria, the bacterial lysate was used to detect the antigen spotted on a nitrocellulose membrane in a dot blot. Binding was revealed using a fluorescently labeled secondary antibody directed against a recombinant FLAG-tag fused to the nanobody. Analogously, the candidates were tested on COS-7 cells overexpressing the target antigen fused to EGFP. If passing these validation steps, nanobodies were purified adding a recombinant cysteine moiety at their C-terminus for direct conjugation to maleimide-activated fluorophores. The functionality of directly labeled nanobodies was again confirmed in IF on COS-7 cells overexpressing the antigen. The affinity of the final candidates used in subsequent experiments was determined by MST. The figure shows exemplary results of a screening for nanobodies binding to SNAP-25.

3.3.3 Optimizing the Selection Procedure

As shown in Table 22, conditions in consecutive screens were adapted to obtain alternative candidates after the affinity selection. In later screens the washing conditions were modified as intensive washing 10 times for an hour or more dramatically reduced the amount of final candidates. Thorough washing was in turn found to favor the selection of nanobodies with a high affinity. As this is a feature desired for IF, I decided to keep the number of washings constant but to reduce the time to 5 minutes per washing step.

Another change I introduced was the use of antigen purified from mammalian systems rather than from bacteria. I was aiming to select directly for nanobodies capable of binding antigen in a cellular context. At the same time candidates only detecting bacterial protein without a proper folding or including post-translational modifications should be omitted.

After implementing the modification, I identified yet novel nanobody families from the restriction library, although it had been screened intensively before as can be seen in Table 22. Subsequent screens did not reveal any new nanobody families and only few candidates passed all validation steps indicating a low success rate of the screening procedure. However it should be noted, that the screening and validation procedure as well as the protocol for library generation were constantly improved during the project.

For this reason, I decided to generate a new library for screening based on Gibson assembly to increase the chances of selecting candidates suitable for IF microscopy. As expected, I could identify yet new nanobodies passing all validation steps due to a higher diversity achieved in the Gibson library.

In addition to establishing a standard validation procedure, I also introduced a protocol for automated analysis of multiple candidates. After testing in ELISA, positive candidates were expressed in bacteria and directly tested in IF omitting the dot blot at the first place. For this, COS-7 cells were grown not on glass coverslips but in glass-bottom 96-well plates for automated analysis using the Cytation-3 Multi-Mode Reader or the Nikon Ti-E epifluorescence microscope. The protocol was successfully tested by screening the Gibson-2 library for nanobodies binding SNAP-25 as shown in Table 22.

All in all, I established a protocol applicable for parallel validation of multiple candidates after phage display selection. The selection itself was further optimized as described above to obtain high-affine nanobodies specifically binding to the native target molecule. Applying those procedures, novel functional nanobodies for IF can now be routinely identified from a phage display library within approximately 2 weeks.

Table 22: Compilation of different nanobody families identified via phage display. Each screen included 2-3 rounds of panning concluding with the isolation and sequencing of individual clones. The amount of antigen presented to the phages in succeeding panning rounds was reduced to achieve competitive selection of high-affinity binders. The number of different nanobody families is indicated for the different validation steps. Only if a candidate passed one validation step, it was tested for the next criterion.

Screen	Library used	Antigen presented in 1 st / 2 nd / 3 rd panning [nmol]	Immobilization	Washing steps	Positively validated in		
					ELISA	Dot blot	IF
SNAP-25							
1	Restriction-final	7 / 7 / 3.5	MaxiSorp®	10x PBS-T 2x HS-PBS 3x PBS	3	2	none
2	Restriction-final	7 / 7	MaxiSorp®	10x PBS-T 2x PBS (overnight)	2	1	none
3	Restriction-final	7 / 3.5	tst-type2 beads	10x PBS-T 2x PBS	5	2	1
4	Restriction-final	5.8 / 1.4 (mammalian)	tst-type3XT beads	6x PBS-T 2x HS-PBS 2x PBS	2	2	1
5	Gibson-1	10 / 5 / 2.5	tst-type3XT beads	10x PBS-T 2x HS-PBS 2x PBS	8	7	3
6	Gibson-2	30 / 30 (automated screening)	tst-type3XT beads	3x PBS	2	2	1
syntaxin 1A							
1	Restriction-final	5 / 2.7	MaxiSorp®	10x PBS-T 3x PBS	4	2	1
2	Restriction-final	3.8 / 2.8 (mammalian)	tst-type2 beads	6x PBS-T 2x HS-PBS 2x PBS	1	1	none
3	Gibson-1	3 / 3	tst-type3XT beads	10x PBS-T 2x HS-PBS 2x PBS	4	1	none
4	Gibson-2	3 / 3	tst-type3XT beads	2x PBS-T 2x HS-PBS 8x PBS	2	2	2
VAMP2							
1	Restriction-final	13 / 6.5	MaxiSorp®	10x PBS-T 3x PBS	3	1	none
2	Restriction-final	13 / 13	MaxiSorp®	5x PBS-T 2x PBS	2	1	none
3	Restriction-final	13 / 6.5	tst-type2 beads	10x PBS-T 3x PBS	1	none	none
Total					39 (100 %)	23 (59 %)	9 (23 %)

3.4 Final Nanobody Candidates

Out of all positively validated candidates revealed by different phage display screens, I was aiming to select one candidate to use in subsequent super-resolutions studies on synaptic physiology. Thus, the successful implementation of nanobody candidates into IF experiments, was the main quality criterion for the final candidates. Unless specified else, nanobodies were used in a concentration of 50 nM.

3.4.1 Qualitative Selection for Final Candidates

As indicated before in Table 22, 23 % of all nanobody families passed the final validation step of application in IF staining COS-7 cells overexpressing the target antigen. In addition several fluorescently labeled nanobodies showed some background staining of non-transfected cells when used in stainings. Therefore, I decided to continue the screening process until nanobodies giving a specific staining would be selected.

In the course of consecutive screening, I did not identify any candidate binding VAMP2 in dot blots or IF experiments. Moreover, the potential candidates for VAMP2 also repeatedly yielded low signal in monoclonal phage ELISA validation screens compared to SNAP-25 and syntaxin 1A. In contrast, screens for nanobodies binding SNAP-25 and syntaxin 1A regularly resulted in identification of positive hits in ELISA shown in Figure 17. I therefore focused on the characterization of those candidates to ultimately obtain a specific nanobody binding with high affinity in biochemical assays and IF experiments.

As the animal was immunized with a combination of antigens, the same library was used to screen for both SNAP-25 and syntaxin 1A binding nanobodies. I therefore included both antigens in the dot blot validation steps to consider only nanobodies specific to one antigen. Figure 17 shows the validation steps for the two final candidates binding SNAP-25 and syntaxin 1A used in further experiments. Both nanobodies were selected from the Gibson-2 library and named in consecutive order of their selection. Hence, these nanobodies are referred to as **S25-Nb10** and **stx-Nb6**. Alternative candidates selected previously either did not pass one of the mentioned validation steps or generated non-reproducible results in IF experiments. The validation results of the final nanobodies S25-Nb10 and stx-Nb6 are displayed in Figure 17.

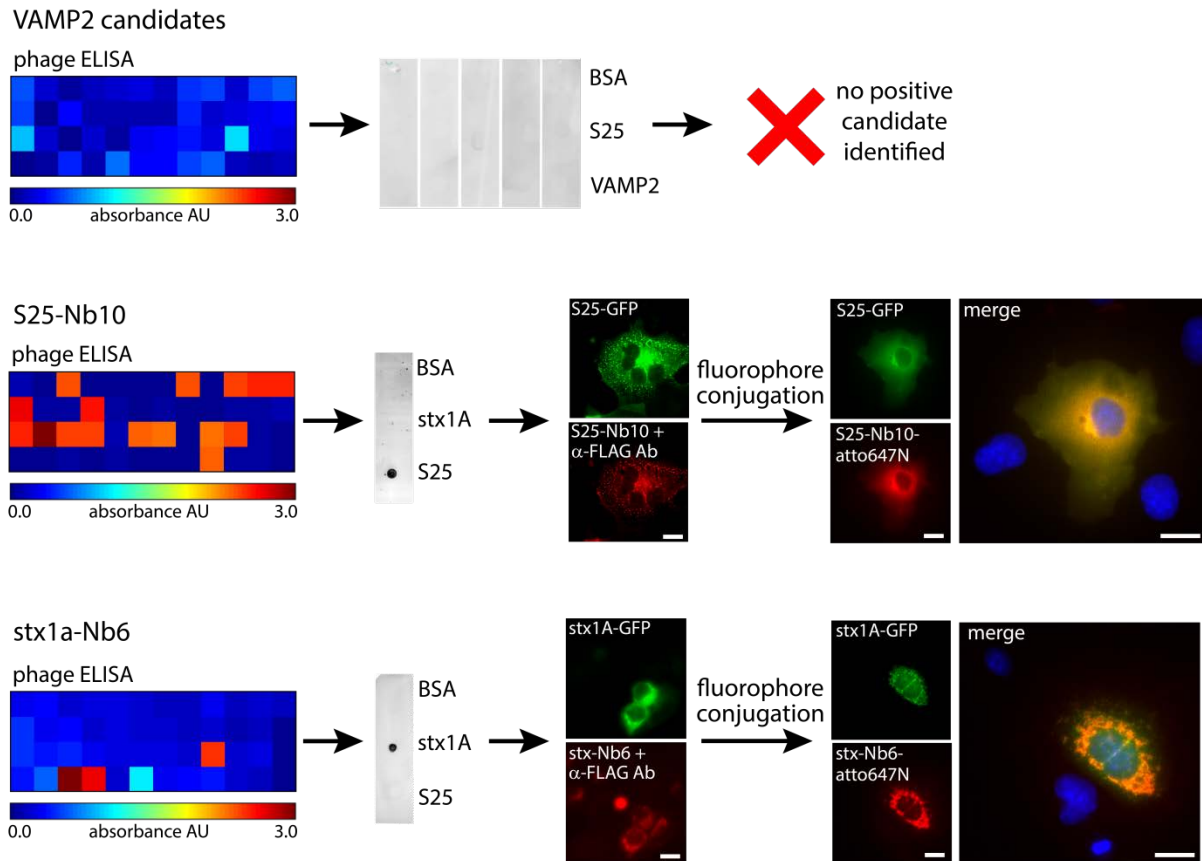


Figure 17: Validation steps of final candidates used for further experiments. Consecutive screens for VAMP2 binding nanobodies did not result in any positive candidate. In turn, for both SNAP-25 and syntaxin 1A specific nanobodies were obtained. The results of the stepwise validation procedure are shown for the final candidates S25-Nb10 and stx-Nb6 used for subsequent experiments. After tested positive in phage ELISA and dot blot, the nanobodies were applied in IF using a fluorescently labeled secondary antibody for detection. Subsequently, the nanobodies were covalently coupled to atto647N for direct detection of the antigen in IF microscopy. Both S25-Nb10 and stx-Nb6 labeled with atto647N selectively bind to COS-7 cells overexpressing the antigen but do not stain untransfected cells in proximity revealed by Hoechst-staining. Fluorescence images were recorded with Olympus IX71 epifluorescence microscope. Scale bars represent 20 μm .

3.4.2 Conjugation of Nanobodies to Functionalized Fluorophores

I explored several options to covalently couple fluorescent molecules to purified nanobodies. Initially, a 4 amino acid peptide (LPET) was chemically coupled the fluorophore and used as a substrate for the enzyme sortase A. As illustrated in Figure 11C, the sortase A covalently binds the LPET-peptide via a thioester bond. Subsequently, the activated enzyme hands over the substrate by linking it to an N-terminal poly glycine tag added to the target nanobody.

Unfortunately, the enzymatic reaction mediated by sortase A was found to be rather inefficient (DOL = 30-40 %). Increasing the substrate amount several orders of magnitude also did not shift the equilibrium substantially to form more conjugated product. As this problem was also reported in the literature, I decided to rely on chemical coupling reactions instead [158].

A common way is the utilization of fluorophores functionalized with NHS-ester or maleimide groups for coupling as described in section 2.2.18. When using NHS-ester chemistry, I observed a partial loss of nanobody functionality, presumably caused by blocking of the nanobody paratope after attachment of a dye moiety. To compensate for that effect, I added a total of 4 lysine residues to the C-terminus of the nanobody stochastically driving the reaction to that position of the nanobody. Albeit, after labeling an increased rate of precipitation of the labeled nanobody was observed, probably due to increased hydrophobicity of the molecule introduced by the attached fluorophores.

Therefore, I decided to use maleimide-functionalized fluorophores instead, which reacted with a cysteine residue added to the C-terminus of the nanobody yielding a stoichiometric labeling ratio of the entire sample. Different dyes listed in Table 20 were tested as the labeling efficiency was found to depend on the manufacturer to a significant extend. Eventually I decided to use atto647N as the default label of the nanobody as a high DOL were obtained in the coupling reactions (> 90 %). Furthermore atto647N is known to be a stable molecule with a high quantum yield well suited for STED-microscopy [159]. To ensure a high DOL, the functionalized fluorophore was used in 2-3-fold molar excess and free dye molecules were subsequently removed by size exclusion chromatography. Figure 18 shows an exemplary HPLC run following the protein absorbance at 280 nm and the dye at its corresponding wavelength of 647 nm.

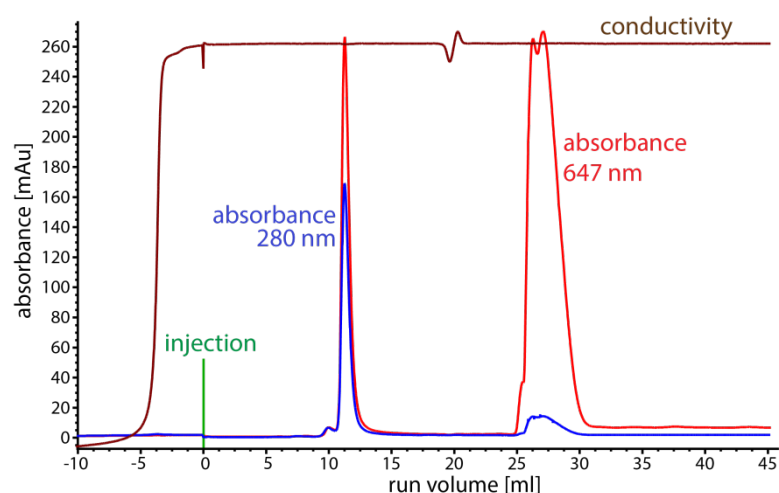


Figure 18: Exemplary HPLC run to remove excess of unreacted dye after nanobody labeling. A Superdex™ 75 increase 10/300 GL column equilibrated with PBS was used for the chromatography. A clean separation of the labeled protein (blue and red peak, left) and free dye molecules (red peak, right) was achieved. The smaller rightmost peak to the right indicating absorbance at 280 nm is caused by unspecific absorbance of the functionalized dye.

3.4.3 Affinity Determination of the Nanobodies S25-Nb10 and stx-Nb6

After identification of nanobodies specifically binding SNAP-25 and syntaxin 1A, I aimed to measure their affinity in relation to nanobodies reported in the literature and other affinity probes. Initially, I used surface plasmon resonance (SPR) to determine both thermodynamic and kinetic parameters of the binding event. A major problem when setting up the measurements was imposed due to long incubation times to observe dissociation of the nanobody-antigen complex. A single measurement including proper controls lasted around 12 h, frequently resulting in precipitation or degradation of the antigen as the measurements could only be performed at room temperature. Moreover, the interaction of the nanobody was found to be comparably strong requiring even longer incubation times to observe dissociation. In consequence, I could estimate the K_D value to be in the nanomolar range, but was not able to determine any other parameter with the setup at hand. Therefore I decided to use MST as a different approach to determine the affinity of S25-Nb10 and stx-Nb6 to their target proteins.

The fluorescently labeled nanobodies mixed with a dilution series of purified antigen were analyzed on a MST Monolith™ NT.115Pico instrument to maximize the sensitivity of the measurement. I used Premium Coated Capillaries, which resulted in the lowest level of unspecific binding of my proteins to the glass surface. The dissociation constant (K_D) of the two nanobodies S25-Nb10 and stx-Nb6 was found to be 15.5 ± 3.3 nM and 5.0 ± 1.2 nM, respectively as shown in Figure 19. Unlike in SPR, the kinetic parameters of the interactions cannot be determined by MST. However, the rather high affinity values obtained for both S25-Nb10 and stx-Nb6 suggest a slow dissociation rate of the nanobody from the antigen.

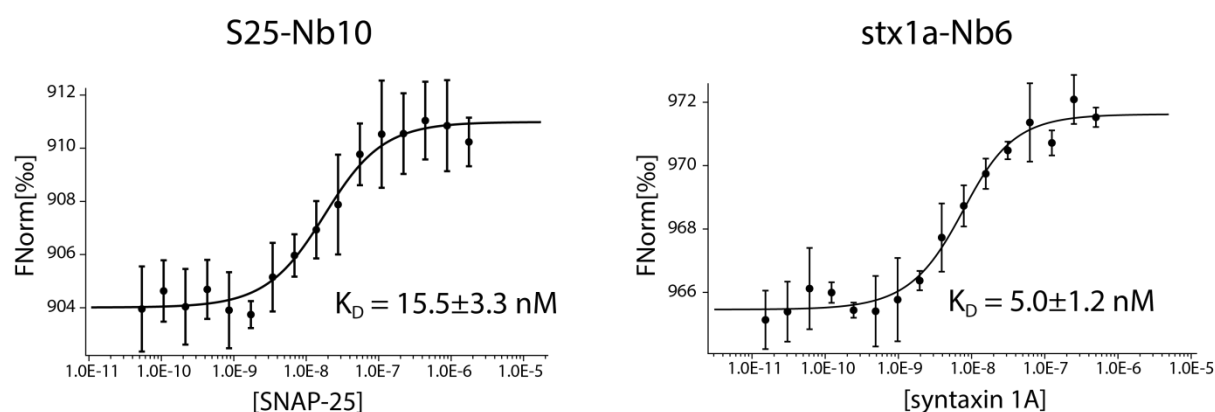


Figure 19: Affinity analysis of S25-Nb10 and stx-Nb6 by MST. Fluorescently labeled nanobody was mixed with a dilution series of its corresponding antigen. FNorm reflects the ratio of fluorescence measured in the hot area defined by the MST-pulse divided by initial fluorescence measured in the capillary. As the movement of the fluorescent nanobody in the temperature gradient changes upon antigen binding, this value can be used to fit a binding curve as a function of the antigen concentration. The resulting dissociation constants (K_D) of the two nanobodies S25-Nb10 and stx-Nb6 were found to be 15.5 ± 3.3 nM and 5.0 ± 1.2 nM, respectively.

3.4.4 Specificity Analysis of S25-Nb10 and stx-Nb6

Although both nanobodies were shown to bind their target with a high affinity using purified antigen, it also needed to be confirmed that they do not cross-react with other proteins on cells. First, I tested if the nanobodies also bind to other SNARE proteins of the same family. Equimolar amounts of native recombinant protein (purchased from Origene™ Technologies, see also section 2.1.5) were spotted on a nitrocellulose membrane without adding reducing or denaturing agents (see Figure 21). Three members of the SNAP and syntaxin protein family were chosen out of which two variants share the highest level of conservation with SNAP-25 and syntaxin 1A.

After detection with my fluorescently labeled nanobodies, I could confirm that S25-Nb10 detected SNAP-25 but not the related proteins SNAP-23, SNAP-29 and SNAP-47 as shown in Figure 21. Similarly, stx-Nb6 bound to syntaxin 1A as expected, but not to syntaxin 1B and syntaxin 2. Notably, the nanobody seems to have a weak affinity to syntaxin 3, which shares a certain sequence identity with syntaxin 1A. The observed binding rate to syntaxin 3 was in the range of 7% compared to the syntaxin 1A binding and therefore can be considered as a negligible interaction, especially in IF methods for microscopy.

After confirming the binding specificity under native conditions, I tested if the nanobodies are also capable of detecting the antigen in a Western blot after denaturing SDS-PAGE. As nanobodies have the tendency to prefer structural epitopes (refer to section 1.4.4), they might not detect a denatured form of the antigen [51]. To my surprise, both S25-Nb10 and stx-Nb6 were able to detect their antigen also after denaturation and transfer to a membrane.

This feature was used to test if the nanobodies are specific for protein lysates and tissue samples not tested during the validation. For this, I performed a Western blot using neuronal and cell-line lysates as well as tissue samples isolated from an adult mouse. Equal amounts of total protein were loaded on a denaturing SDS-PAGE gel and blotted on a nitrocellulose membrane for detection with fluorescently labeled nanobody. As shown in Figure 20, both S25-Nb10 and stx-Nb6 did not reveal any bands in tissue samples of cell lysates lacking the expression of SNAP-25 and syntaxin 1A, respectively. I therefore conclude that my novel nanobodies S25-Nb10 and stx-Nb6 bind their antigens with both high affinity and high specificity also in complex protein lysates even after separation with denaturing SDS-PAGE.

To confirm the specificity of my nanobodies in IF microscopy, I once more used COS-7 cells expressing the antigen fused to EGFP detecting it with directly labeled nanobody. I used cells transfected with the contrary EGFP fusion construct to rule out binding of the nanobody to EGFP, which has not been tested so far.

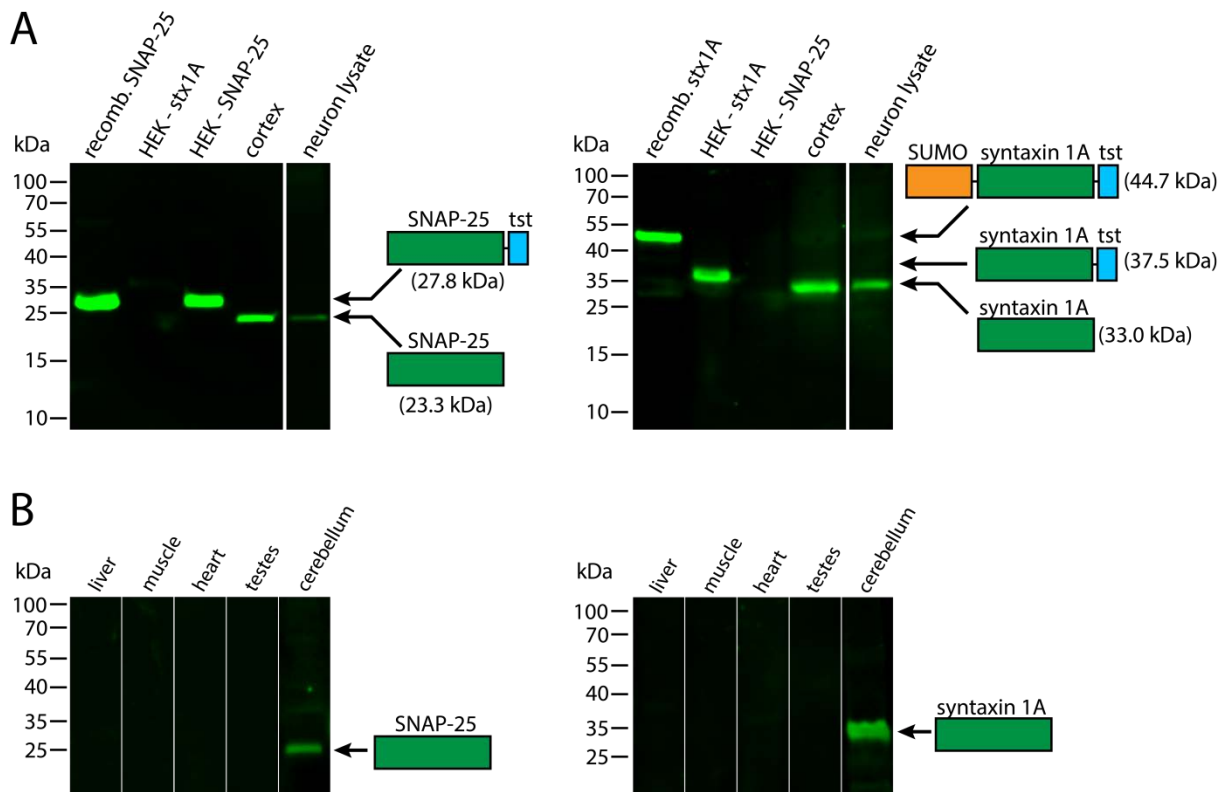


Figure 20: Specificity analysis of S25-Nb10 and stx-Nb6 by Western blotting. **A:** 5 μ g of purified recombinant protein, 20 μ g of HEK-cell lysate containing overexpressed antigen and 20 μ g lysate from primary cultured neurons were loaded on a denaturing SDS-PAGE gel and subsequently blotted onto a nitrocellulose membrane. Protein concentration was determined using BCA-assay. **B:** 20 μ g of isolated tissue sample (determined via BCA assay) were loaded on a denaturing SDS-PAGE gel and blotted as previously. After blocking, all membranes were incubated with nanobodies conjugated to atto647N for detection of the target antigen. Since recombinant proteins expressed in bacteria or mammalian cell lines possess additional tags, the expected molecular weight differs from the native protein as indicated in the schematic representations of the antigens. Both S25-Nb10 and stx-Nb6 show a single band in the blot indicating specific detection of their respective target antigen while showing no cross-reactivity to other proteins in lysates or tissue samples.

Figure 22 shows that both nanobodies specifically detect cells transfected with their target antigen but virtually show no background signal in non-transfected cells or expressing the complementary construct. This also confirms that the nanobodies bind to the overexpressed antigen and not to EGFP also overexpressed in the cells. This is an important control as EGFP was used as a common reporter also in further experiments conducted in this project. In addition to the specific binding of the nanobodies, Figure 22 shows a different cellular localization of SNAP-25 and syntaxin 1A. Whereas SNAP-25 is distributed all over the cell, the overexpressed syntaxin 1A accumulates in a perinuclear region. Previous studies showed that syntaxin 1A accumulates in the endoplasmic reticulum (ER) region if cofactors such as Munc-18 are not present [160,161]. This would explain the phenotype observed in cells overexpressing only syntaxin 1A fused to EGFP as in Figure 22.

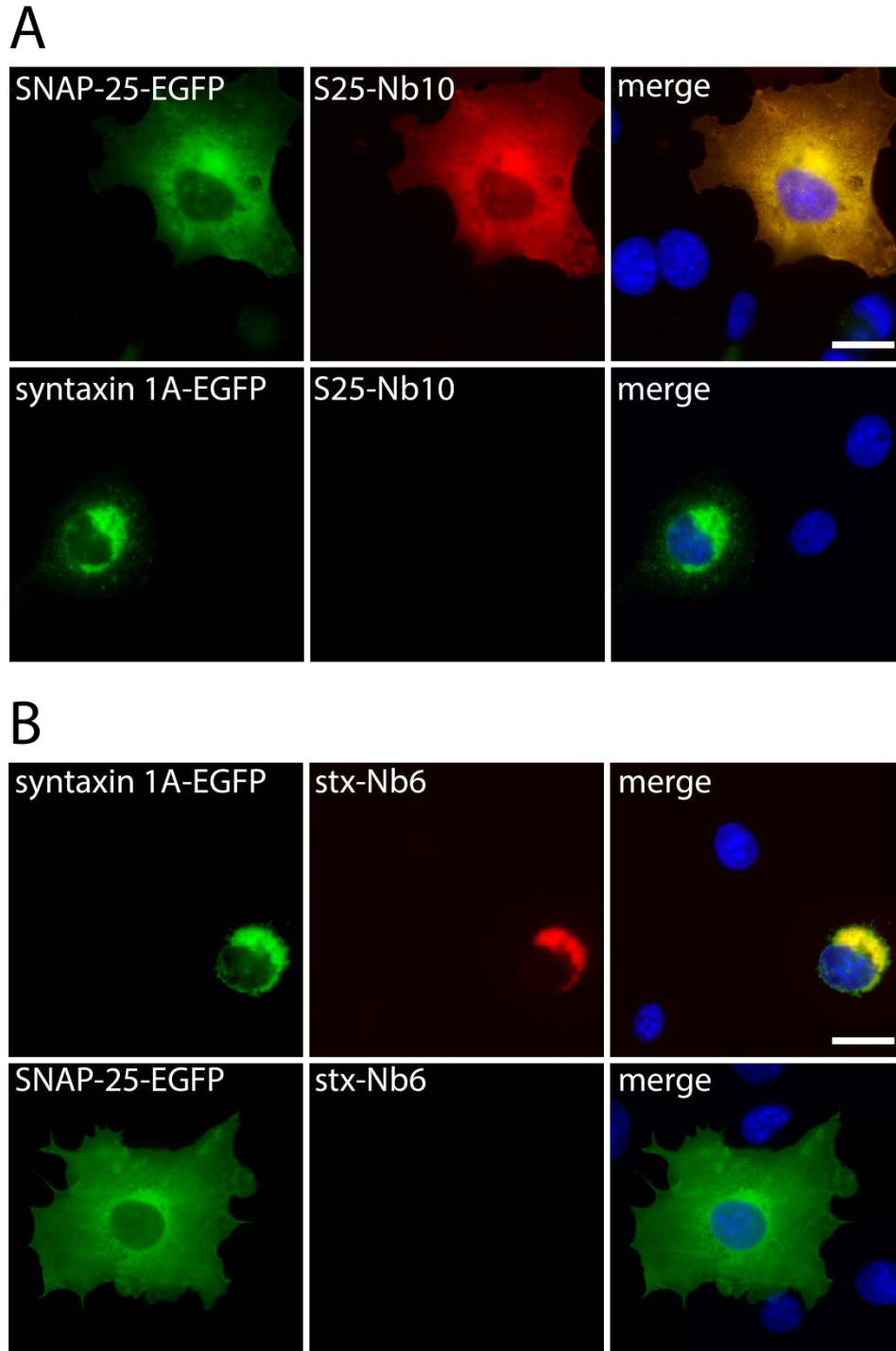


Figure 22: Specificity analysis of S25-Nb10 and stx-Nb6 by IF microscopy. COS-7 cells were transfected with SNAP-25 of syntaxin 1A fused to EGFP. Nanobodies conjugated to atto647N were applied at a concentration of 50 nM to detect the antigens. **A:** The fluorescence signal from S25-Nb10 overlaps with the fluorescence of the SNAP-25-EGFP construct but does not show any binding to syntaxin 1A EGFP. **B:** Complementarily, stx-Nb6 only detects syntaxin 1A-EGFP but not the SNAP-25 fusion protein. These results confirm the specificity of both nanobodies for their target antigen, also confirmed by no background signal on non-transfected cells (Hoechst-staining). Images were recorded with a Nikon Ti-E epifluorescence microscope. Scale bar represents 20 μ m.

3.4.5 Epitope Mapping

After the confirmation of the nanobody affinity and specificity, I was interested to identify the region within the antigen to which the nanobodies S25-Nb10 and stx-Nb6 bind. Structural methods like nuclear magnetic resonance (NMR) or crystallization would deliver the most accurate information as also discussed in section 4.4. NMR requires peptides substantially smaller than the full protein which is why I first ought to narrow down the region of the epitope.

To pinpoint that region within the antigen, I generated different truncation constructs from the full-length proteins. The separate domains of SNAP-25 and syntaxin 1A that form secondary structures were expressed individually in bacteria to perform a qualitative binding analysis on a nitrocellulose membrane. After the purification of all truncated variants, the protein concentrations were determined using a BCA assay. Equimolar amounts were spotted on a nitrocellulose membrane and detected with fluorescently labeled nanobodies. As expected, each nanobody detected the recombinant target protein SNAP-25 and syntaxin 1A used as immunogen, ranging from amino acid 1-206 and 1-264, respectively. Interestingly, both nanobodies detected only one of the truncated variants of their target protein while showing no binding to the other regions (see Figure 23). This strongly suggests that the epitope of the nanobodies is located within that respective truncated domain.

Notably, S25-Nb10 specifically binds a truncated constructs which contains one of the two SNARE domains of SNAP-25. Generally, the SNARE domains are known to form stable helices, which presumably create a specific interaction surface for the S25-Nb10 to bind [162]. In turn, stx-Nb6 binds to a truncation construct containing the N-terminal H_{abc} domain which is involved in syntaxin 1A trafficking and clustering [160].

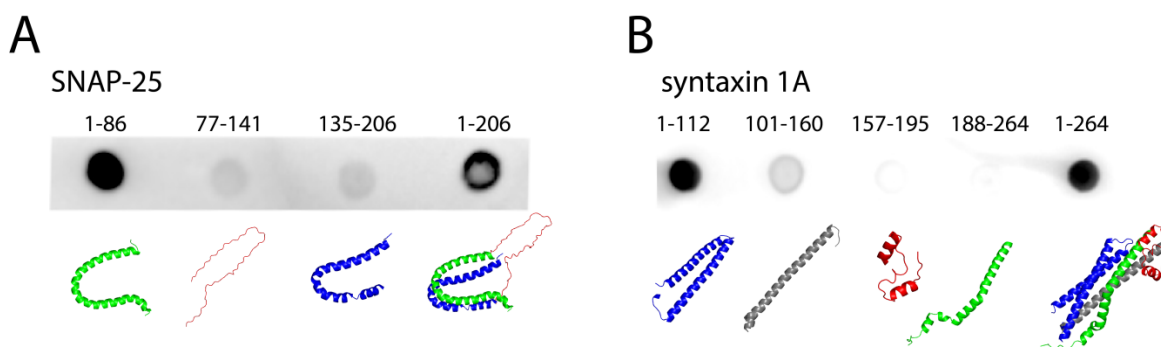


Figure 23: Mapping the epitope of S25-Nb10 and stx-Nb6. The numbers indicate the amino acid residues from the full length protein constituting the truncation construct. A cartoon of the respective truncation construct is depicted below the blot. Equimolar concentrations of purified proteins were spotted on a nitrocellulose membrane and detected with nanobody conjugated with atto647N. **A:** S25-Nb10 binds to the full-length SNAP-25 as expected (1-206). Additionally, the nanobody detects the SNARE-domain ranging from amino acid 1-86 indication this domain to contain the epitope for S25-Nb10. **B:** Similarly, stx-Nb6 detects the full-length syntaxin 1A (without the transmembrane domain) from aa 1-264 and a truncated construct from aa 1-112. As for SNAP-25, this domain also constitutes the functional SNARE domain or the protein. The images were scaled to optimize the signal to noise ratio of the dot blot.

3.5 Comparison of Novel Nanobodies to Conventional Probes in IF

To exploit the features of my nanobodies and to implement them into IF experiments, I compared their performance to full IgG molecules. For comparative studies, I decided to use two monoclonal antibodies well established in the field of SNARE protein.

Particularly, the clone 71.1 and the clone 78.2 (both from Synaptic Systems GmbH), which bind SNAP-25 and syntaxin 1A, respectively, were used. I used those antibodies as in classical IF protocols, which means detection with a fluorescently labeled secondary antibody.

3.5.1 Test for Epitope Competition

Before using my nanobodies and antibodies in immunostainings, I tested if both affinity molecules compete for the same epitope region as this would influence the result if both antibody and nanobody binding the same proteins are used simultaneously.

According to the manufacturer, the whole SNAP-25 protein was used as antigen for the clone 71.1 and the epitope is localized in the N-terminal domain between aa 20 and 40. For the case of the clone 78.2 the antibody recognized the N-terminal domain of syntaxin 1A and 1B.

To test if the antibodies compete with my nanobodies for the same epitope, I spotted the purified antigens on a nitrocellulose membrane and blocked subsequently with unlabeled nanobody for one hour.

Subsequently, the fluorescently labeled nanobody was incubated with the membrane. As expected, the fluorescent signal detected significantly less in the membrane pre-blocked with nanobody compared to the unblocked control (see Figure 24A).

In contrast the binding of the antibodies 71.1 and 78.2 was not impaired after pre-blocking with unlabeled nanobody (Figure 24A). Therefore, I concluded that both of my nanobodies do not compete with the tested antibodies for the same epitope in the target protein and thus can be used together in IF experiments without mutual interference.

Interestingly, syntaxin 1A present endogenously in the neuroendocrine cell line PC12 used in following experiments can be only poorly detected by clone 78.1 (data not shown). However it is known in the field that the antibody clone HPC-1 is able to detect syntaxin 1A also in PC-12 cells [163].

When performing the assay to test for epitope competition, some impairment of HPC-1 binding was observed upon blocking with stx-Nb6, as shown in Figure 24B. Therefore, that antibody was solely used for qualitative IF on PC-12 cells and not for comparative studies between general nanobody and antibody performance.

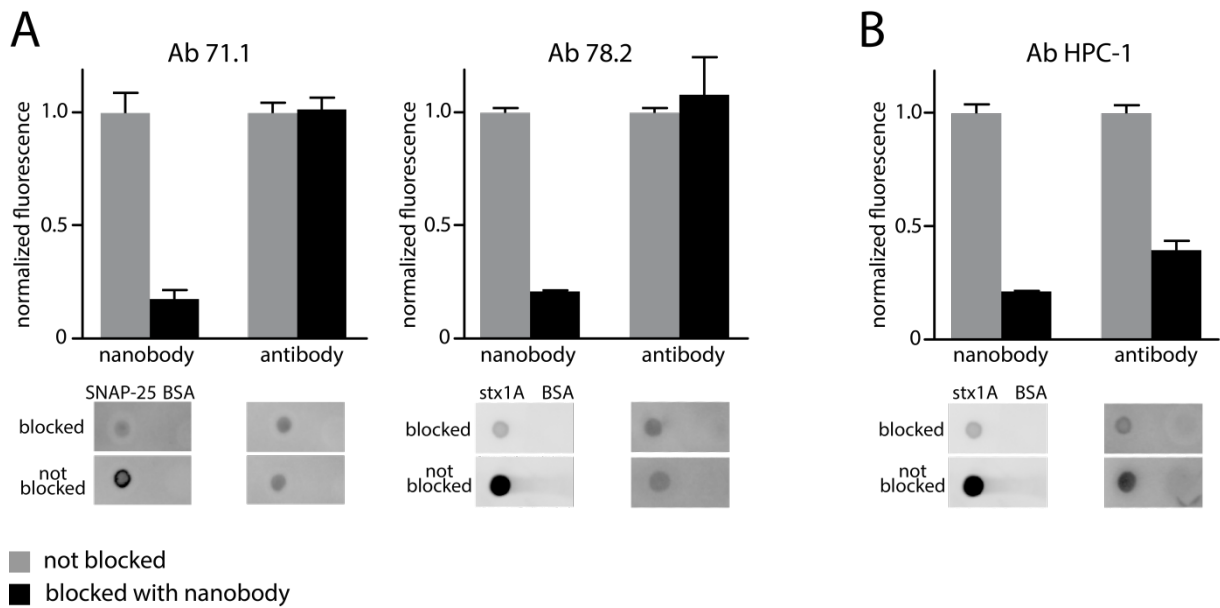


Figure 24: Dot blot analysis to investigate epitope competition of antibodies and nanobodies. Purified antigen was spotted on a nitrocellulose membrane, blocked with unlabeled nanobody and detected with fluorescently labeled nanobody (atto647N) or primary + secondary antibody (atto647N). **A:** The antibody clones 71.1 and 78.2 detected the antigen independent of prior blocking with unlabeled nanobody indicating binding to a different epitope. **B:** The HPC-1 antibody was found to be impaired by stx-Nb6 indicating epitope overlap of these two probes. BSA was immobilized on the membrane as a negative control. Error bar represent standard error of the mean (SEM), n = 3.

3.5.2 Comparative Staining in Cell Lines

Similar to the validation procedure, I first used COS-7 cells transiently expressing the target antigen fused to EGFP to perform a comparative staining with the nanobodies and the conventional antibodies. Nanobodies were directly coupled to atto647N and primary antibodies were detected with a secondary coupled to a Cy3 fluorophore. As shown before, both nanobody and antibody only seemed to bind to transfected cells overexpressing the antigen-EGFP construct, but did not show any background signal on cells not expressing the EGFP fusion construct (see Figure 17).

Overall, both antibody and nanobody stainings generally followed the location of the EGFP-signal. However the nanobodies seemed to resemble the levels of overexpressed protein more accurately than the antibody. This was particularly acute in protein-dense areas like the perinuclear region as shown in Figure 25.

To analyze this effect, I drew a line through the respective area and displayed the fluorescence intensity profile of each pixel below the line. As shown in Figure 25, the nanobody signal follows the EGFP-fluorescence quite precisely, whereas the antibody fails to follow the EGFP-fluorescence in the protein-rich regions. The phenotype was observed for both antigens, albeit slightly less clear for

syntaxin 1A. As described in section 3.4.4, syntaxin 1A shows the propensity to accumulate in the ER if its interaction partners such as MUNC-18 are not present [160,161]. This explains the massive accumulation of syntaxin 1A and the less apparent phenotype in cells expressing SNAP-25.

To further evaluate this phenotype, the average fluorescence of the whole cell, of the cytoplasm and of the perinuclear region was measured and normalized to the EGFP-fluorescence of the corresponding region, which indicates the level of expressed protein. Both S25-Nb10 and stx-Nb6 were found to significantly detect more antigens in the perinuclear region than the corresponding antibody. In addition, S25-Nb10 signal in the entire cell overlapped with the EGFP fluorescence significantly better than the antibody as shown in Figure 25C. For syntaxin 1A expressing cells, both nanobody and antibody followed the EGFP signal outside the perinuclear in somewhat lower extend. Presumably, this effect was caused by the accumulation of syntaxin 1A in the ER as mentioned above whereas the detected fluorescence in the EGFP channel might be generic autofluorescence of the cell, as the overexpressed protein is not present there.

In conclusion, I hypothesized that the size of a conventional IgG molecule prevents it from entering into protein-rich areas and detection of its antigen.

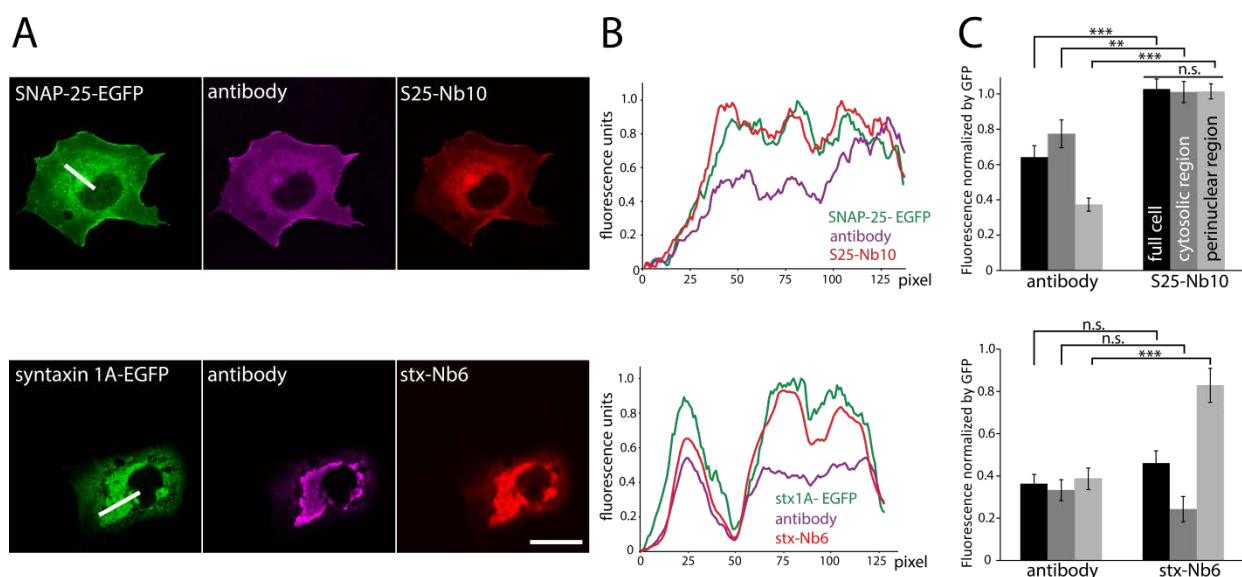


Figure 25: Binding of nanobodies to COS-7 cells overexpressing the target antigen fused to EGFP. Images were recorded in Leica TCS SP5 microscope used in confocal mode. **A:** The nanobody and EGFP signal show a high level of overlap whereas the antibody does not detect its target protein in protein-dense regions. **B:** Line scans were drawn through the perinuclear region revealing the difference in fluorescence signal of the nanobodies and antibodies (white bars in A). **C:** To quantify this effect, average fluorescence of the whole cell (black bar) as well as the cytosol (dark-grey bar) and perinuclear region presumably including the ER (light-grey bar) was measured. Analysis of the data was done using unpaired *t*-test, $n = 37$ for SNAP-25-EGFP and $n = 36$ for syntaxin 1A, ** $p < 0.01$, *** $p < 0.001$. Error bars represent SEM, scale bar represents $10 \mu\text{m}$.

3.5.3 Penetration into Tissue Sections

To follow up the previous observation that the antibodies might not be able to reach epitopes in crowded regions due to their size, I aimed to investigate the ability of antibodies and nanobodies to penetrate biological tissue samples. Brain slices of approximately 35 μm thickness were used for comparative staining of endogenous SNAP-25 and syntaxin 1A. The secondary antibodies used were coupled to atto647N as well as the directly labeled nanobodies to exclude unspecific binding of the fluorophore in the tissue. Confocal optical sections of 700 nm thickness were acquired throughout the slice.

When measuring the average fluorescence of each frame, I could clearly observe a decrease of antibody signal when imaging deeper into the tissue, depicted in Figure 26. The antibody signal increased again when the opposite periphery of the tissue sample was reached. In contrast, the average nanobody fluorescence remained relatively constant throughout the whole tissue depth. Figure 26 also shows the total fluorescence of each frame while imaging through the sample. It is important to keep in mind that due to scattering of light the fluorescent signal will decrease slightly when imaging deeper into the tissue sample increasing the distance between the focal plane and the objective.

In control experiments inverting the sample and repeating the imaging procedure, the same effect was observed. This implies that the loss in fluorescence signal is caused by the reduced amount of light reaching the objective while increasing imaging depth and not by inhomogeneous or incomplete staining. All in all, I observed that both S25-Nb10 and stx-Nb6 in contrast to their antibody counterpart showed a more continuous staining throughout the entire tissue sample. This adds to my hypothesis that indeed antibodies are limited to reach their epitopes by their comparably large size and thus may detect only a subset of all epitopes.

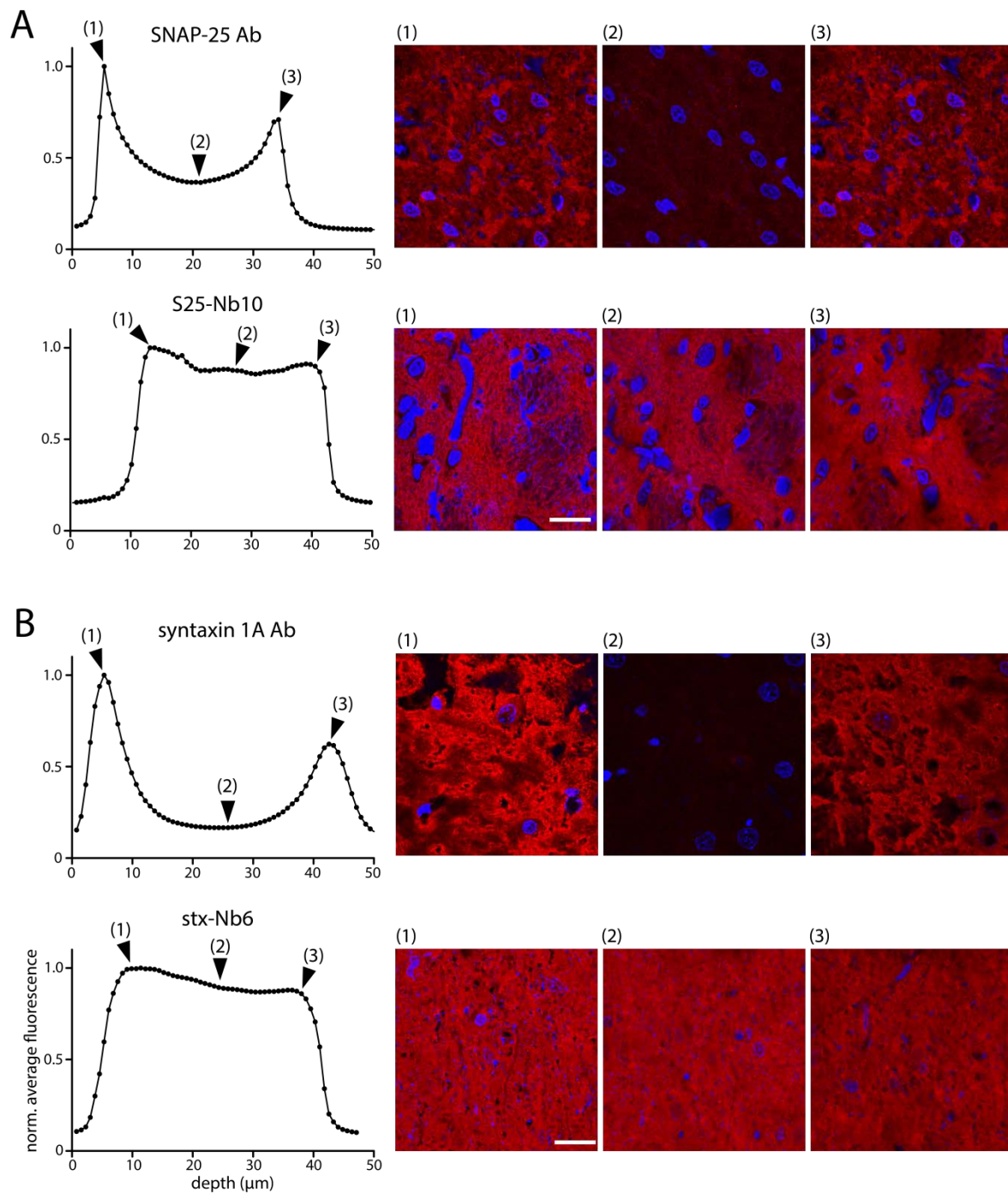


Figure 26: Tissue penetration of nanobodies and antibodies in thin sections of rat brains. The sample was either stained with primary antibody overnight followed by detection with a fluorescently labeled secondary nanobody or with directly labeled nanobody overnight. **A:** Staining for SNAP-25 using either S25-Nb10 conjugated to atto647N or the antibody clone 71.1 revealed with a secondary antibody conjugated to atto647N. **B:** Comparison of stx-Nb6 conjugated to atto647N and antibody clone 78.2, revealed as in **A**. Samples were imaged in confocal optical section of 700 nm throughout the entire slice covering approximately 35 μm . For each condition, exemplary images of different depths in the tissue were chosen, indicated by the numbers (1)-(3). In deeper regions of the tissue, the fluorescent signal of the antibodies dropped almost to zero whereas nanobody fluorescence remained constant throughout the whole brain slice. Scale bars represent 20 μm .

3.5.4 Staining of Endogenous Antigens in PC-12 Cells

As transient overexpression of proteins may be associated with artifacts, I intended to investigate endogenously expressed synaptic proteins in their native context. For this I used a cultured pheochromocytoma (PC-12) cell line derived from the adrenal medulla of *Rattus norvegicus* [164]. PC-12 cells originate from the neural crest and thus possess a similar set of proteins associated to synaptic vesicle recycling including neuronal SNARE proteins.

I performed a co-staining of antibody and nanobody as described in section 3.5.2. As expected, I observed both classes of affinity molecules to colocalize and primarily stain the plasma membrane where SNAP-25 and syntaxin 1A are located under conventional conditions shown in Figure 27. Notably, the fluorescence signal of the nanobody was generally lower compared to the antibody staining, presumably due to lack of signal amplification by secondary antibody. Analogously to the phenotype observed in overexpressing COS-7 cells, the nanobody signal localized to the perinuclear region and plasma membrane of the cells, but not to the cytoplasm or nucleus.

To exclude the possibility that the nanobodies were binding alternative molecules in PC-12 cells, which express a variety of other neuronal proteins, I additionally tested both nanobodies and antibodies on a Western blot. As also shown in Figure 27, both affinity molecules showed a single band in the blot for SNAP-25 and syntaxin 1A. As the molecular weight of that band matched the expected weight of the respective antigen, I concluded specific binding of the nanobody and the phenotypes in IF experiments to be specific staining.

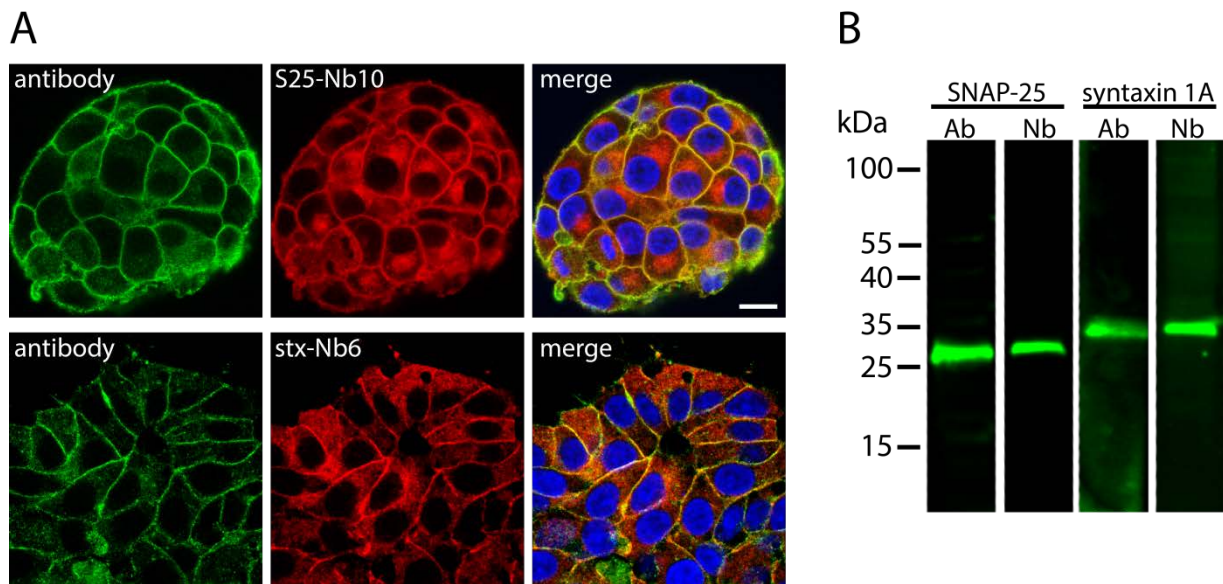


Figure 27: Staining the endogenous levels of SNAP-25 and syntaxin 1A in PC-12 cells. **A:** Nanobodies S25-Nb10 and stx-Nb6 directly conjugated to atto647N were used together with antibody clone 71.1 (SNAP-25) and HPC-1 (syntaxin 1A) detected with a secondary antibody coupled to Cy3. Both antibodies and nanobodies detect the corresponding target residing at the plasma membrane. Furthermore, the nanobodies reveal specific structures in the perinuclear region, which the antibodies did not detect. **B:** The specificity of the affinity probes on PC-12 lysate was confirmed by a Western blot loading 50 μ g of total cell lysate (determined by BCA assay). Membranes were developed with directly conjugated nanobodies (atto647N) or primary antibodies (clone 71.1 and HPC-1) detected by a secondary antibody coupled to atto647N. To compensate for the putative epitope overlap of stx-Nb6 and HPC-1 (see Figure 24), the cells were first incubated with the HPC-1 primary antibody adding the nanobody only together with the secondary antibody.

3.5.5 Staining of Endogenous Antigens in Primary Cultures Neurons

I could demonstrate that my new nanobodies are able to detect a larger set of target proteins within the specimen and thus they might provide a more accurate phenotype compared to antibodies while perpetuating antigen specificity.

So far, studying synaptic composition almost exclusively relied on antibodies to detect endogenous levels of SNAP-25 and syntaxin 1A due to the lack of alternative probes. Thus, I intended to use my new probes in combination with super-resolution microscopy to investigate the distribution of neuronal SNAP-25 and syntaxin 1A in more detail. As the synapses represent the major platform for those proteins to perform their function, I focused on synaptic boutons for the analysis. Figure 28A shows epifluorescence images of neurons stained with directly conjugated nanobody. Both S25-Nb10 and stx-Nb6 detect their target antigen along the neuron. As expected, the fluorescence signal is enriched in synaptic boutons, which were marked using an antibody against the synaptic vesicle protein synaptophysin.

As a negative control, I used a GFP-nanobody in equimolar amount and coupled to the same fluorophore (atto647N), which should not bind any protein in a hippocampal culture under the same conditions [80]. This control nanobody did not show any staining, excluding unspecific binding of the nanobody due to the hydrophobic atto647N moiety.

Next, I aimed to analyze the synapses more closely using super-resolution microscopy. To identify the synaptic regions, antibodies against synaptophysin and Homer-1 were used as markers for the pre- and postsynaptic region, respectively. As shown in Figure 28B+C, I observed that the antibodies reveal a phenotype suggesting the clustering of syntaxin 1A and to some lower extent also of SNAP-25. Those findings are generally in line with the observations previously reported in the literature [134,135,165].

When using my nanobodies to detect SNAP-25 or syntaxin 1A, those clusters were found to be substantially smaller and less evident as depicted in Figure 28. Although patterns could still be observed in the synaptic regions, the overall distribution of the target antigens seemed to be considerably more continuous than observed using antibodies (see Figure 28). That continuity was also observed for the entire neurite, whereas both SNAP-25 and syntaxin 1A were still enriched at synapses.

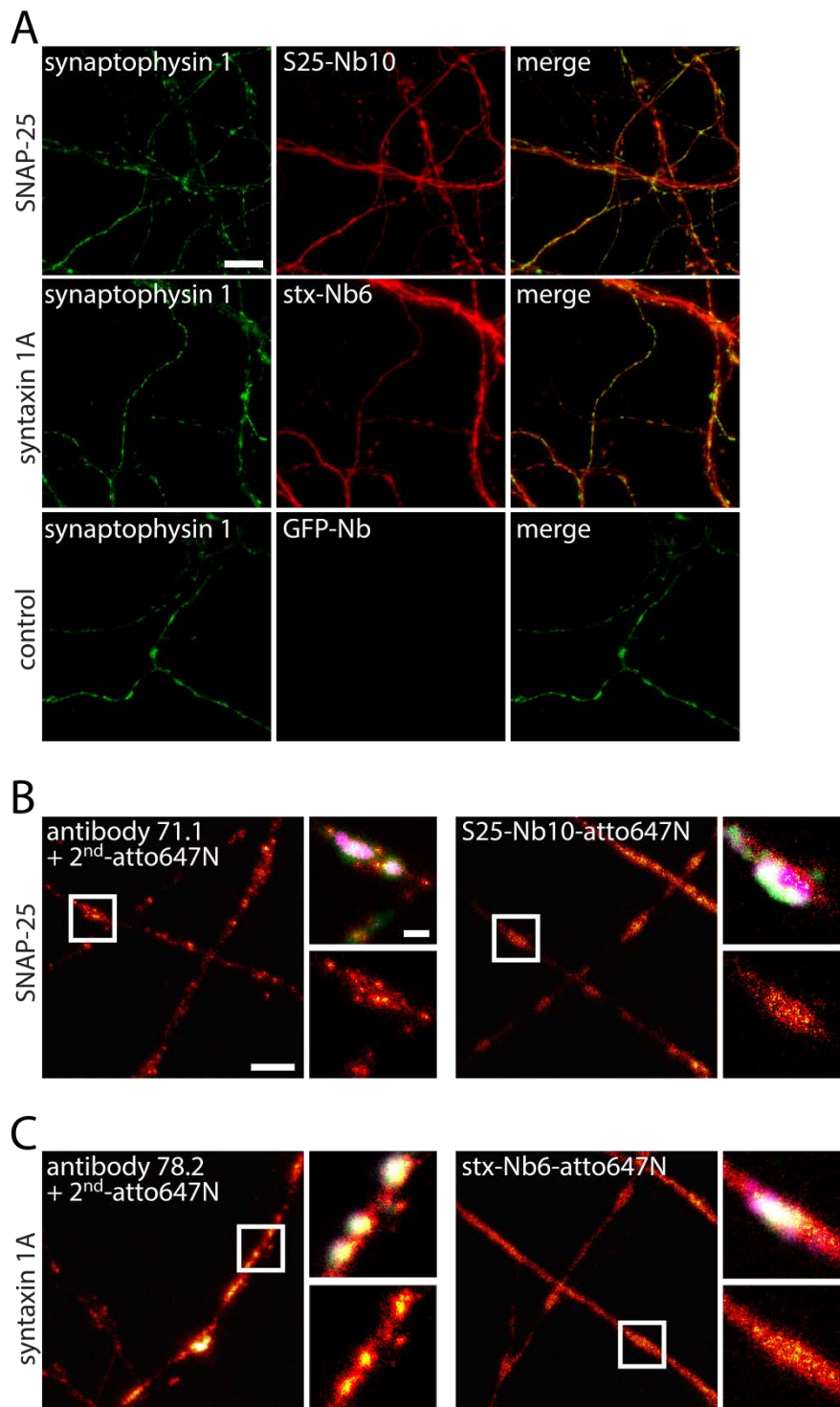


Figure 28: Comparative staining of primary cultured neurons using antibodies or nanobodies. **A:** Qualitative detection of nanobody binding. Synaptophysin antibody (see Table 7) was used for the identification of synaptic boutons. All nanobodies were directly conjugated to atto647N and used in a concentration of 50 nM. A GFP nanobody was used as a control to exclude unspecific binding due to the fluorescent label [80]. Both S25-Nb10 and stx-Nb6 stain the neuron while being enriched at synapses. Images were recorded with a Nikon Ti-E epifluorescence microscope. Scale bar represents 10 μ m. **B+C:** Direct comparison of monoclonal antibody and nanobody detecting endogenous SNARE proteins in neurons. The staining with primary and secondary antibody results in a spotty pattern of fluorescent signal along the neuron. In contrast, the directly conjugated nanobody indicates a more continuous distribution of both SNAP-25 and syntaxin 1A. Both antibody and nanobody showed their target protein to be enriched in the synapse, indicated by staining for synaptophysin (green) and Homer-1 (magenta). Antibodies were detected using secondary antibodies conjugated to Alexa488 (synaptophysin), Cy3 (Homer-1) and atto647N (SNAP-25 and syntaxin 1A). Nanobodies were used directly conjugated to atto647N. Scale bars represent 2 μ m in the large and 500 nm in the zoomed image.

For a representative and quantitative analysis of the SNAP-25 and syntaxin 1A distribution in the synaptic region, the fluorescent signal of several hundred synapses was averaged. The Homer-1 signal was used to center the synapse and the synaptophysin signal was used to align the synapse horizontally (for detailed description refer to section 2.2.20). The averaged fluorescent signal from the nanobody or antibody channel imaged in STED-resolution shows a comparably spotty pattern for the antibodies whereas the average nanobody signal indicates a more continuous staining of the synapse.

This is also reflected by a line scan drawn through the center of the averaged analysis shown in Figure 29 (white line in Homer-1 panel). The spikes in the graph represent areas with increased fluorescence indication cluster formation.

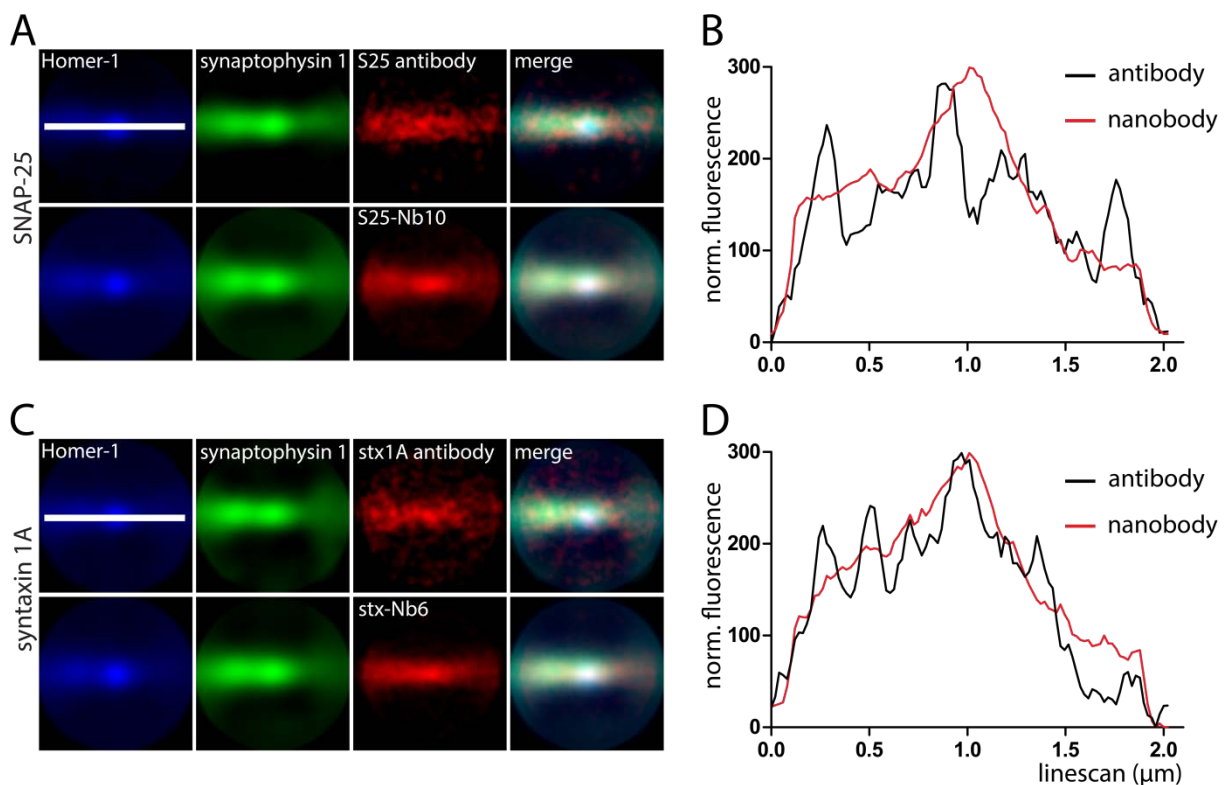


Figure 29: Synaptic distribution of SNAP-25 and syntaxin 1A revealed by antibodies or nanobodies. **A+C:** Synapses were identified by the Homer-1 fluorescence signal (blue) and aligned according to synaptophysin fluorescence (green). The fluorescence signal in the antibody or nanobody channel was averaged and normalized to correct for variation in absolute fluorescence intensity (red). It can be seen that the pattern obtained after nanobody staining is considerably more homogenous than using antibodies; $n > 100$ synapses, $N = 5$ coverslips for all conditions. **B+D:** A line profile in the center region of the averaged synapses was created (white line) analyzing the normalized fluorescence of the antibodies (black) and nanobodies (red). The spikes in the profile represent spots of high fluorescence indicating molecular clustering.

3.5.6 Imaging SNAP-25 and Syntaxin 1A in Dual Color STED Microscopy

As my novel nanobodies reveal the organization of SNAP-25 and syntaxin 1A in high detail, I aimed to image both proteins simultaneously in super-resolution to analyze their relative localization. To my knowledge, until now no study could clearly demonstrate the colocalization of SNAP-25 and syntaxin 1A at the synapse, although those proteins are known to interact to promote synaptic vesicle fusion with the plasma membrane. The small size of nanobodies was expected to promote the detection of epitopes in the protein-dense synaptic region, thus detecting colocalization, which might not be observable using conventional antibodies.

The nanobodies S25-Nb10 and stx-Nb6 were directly coupled to AbberriorStar580 or atto647N to stain endogenous SNAP-25 and syntaxin 1A in primary cultured neurons. Figure 30 shows the result of the co-staining using both nanobodies coupled to either fluorophore. To identify the synapse, I used an antibody against synaptophysin detected with a secondary antibody coupled to Alexa488 (colored in blue) as described in section 3.5.6.

The patterns revealed by the nanobody suggest microdomain organization of SNAP-25 and syntaxin 1A along the neurite and in the synapse. Although both proteins are known to interact to mediate fusion events (see section 1.6), the nanobodies reveal only little colocalization as shown in the zoom panel of Figure 30. This is also in line with current observation in the literature using antibodies to detect SNAP-25 and syntaxin-1A [166,167].

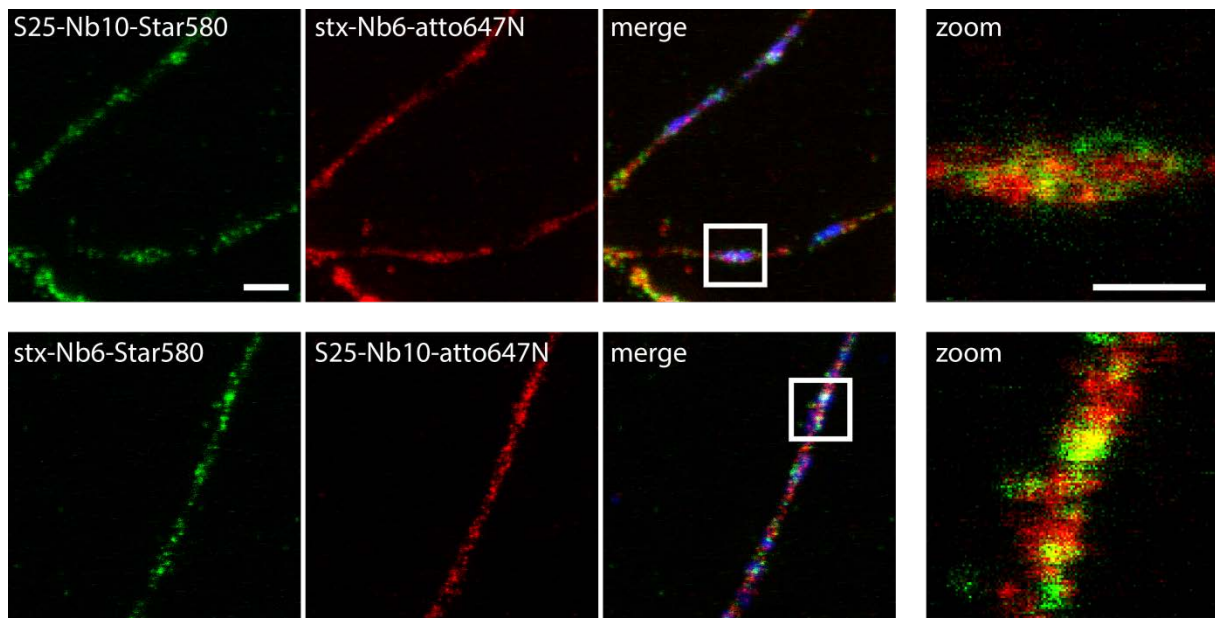


Figure 30: Dual channel STED microscopy of primary cultured neurons using nanobodies. Both nanobodies were directly conjugated to Star580 or atto647N and imaged in STED resolution. An antibody directed against synaptophysin was used to identify the synapses (blue signal in the merged panel). The nanobodies show only very little colocalization independent of the combination of conjugated fluorophores (red and green signal in the zoomed panel). Scale bars represent 1 μm in the overview and 500 nm in the zoom image.

4. Discussion

The rationale of this project was to generate new affinity probes to improve accuracy in imaging synaptic proteins with super-resolution microscopy. I successfully identified and characterized two novel nanobodies, termed S25-Nb10 and stx-Nb6, which bind with high affinity and specificity to SNAP-25 and syntaxin 1A, respectively. As this was the first project that needed the development of nanobodies in the laboratory, a major effort was laid in establishing a systematic workflow to screen for novel nanobodies. I further developed a standardized validation protocol to confirm the specificity of the selected candidates. In the long perspective, novel nanobodies are likely to be used for the analysis of various different endogenous synaptic proteins.

I confirmed nanobodies to be versatile tools in various microscopy approaches due to their flexible biochemical properties. This includes scalable expression and modification in recombinant systems, high specificity for their target antigen and easy conjugation to various labels including fluorescent dyes. By using bacterial expression strains promoting the formation of disulfide bonds, recombinant nanobodies could readily be produced in preparative amounts. Although the internal disulfide bridge of nanobodies is known to increase the stability of the scaffold, it was shown to be not required for nanobody functionality [51,110].

The general stability of nanobodies was observed during experiments carried out times at room temperature, which did not hamper the nanobody binding even if exposed to room temperature overnight. I was thus able to readily implement my nanobodies into IF experiments upon conjugation to a fluorophore.

A systematic comparison to conventional antibodies revealed remarkable differences in the observed phenotype depending on the type of affinity probe used. The large full IgG molecules were not able to detect their antigen in a protein rich environment (see section 3.5.2) and only poorly penetrated tissue slices (see section 3.5.3). My new nanobodies on the contrary were able to detect considerably more epitopes compared to the antibody as shown in Figure 25. I therefore conclude that the molecular properties of the applied probe should be considered carefully to avoid misinterpretation of the data. Small probes such as nanobodies can overcome several problems in microscopy caused by antibodies and thus provide a more realistic picture of protein distribution.

4.1 Library Generation

The design of a phage display library containing both a high number and a high diversity of nanobody candidates is essential for the selection of valuable nanobodies. Naturally, only those sequences which were originally present in the library in reasonable numbers can be amplified by phage display. Hence, I carefully optimized the procedure and conditions for library generation.

Naïve libraries, which were created from the genetic antibody repertoire without prior immunization, are regularly used for affinity probe selection [154]. Although being readily available at low costs, the lack of immunization often results in the selection of no or only very weak binders as also observed in my previous work [65].

Alternatively, synthetic libraries have been developed to screen for affinity molecules. Particularly, this approach is used for affinity molecules not based on immunoglobulin scaffolds shown in Figure 3, thus not allowing immunizations. Synthetic libraries can be designed to have a very high number of amino acid combinations in their variable region yielding up to 10^9 different sequences [71,168]. However, generation of such libraries is very expensive and despite the high number of different sequences encoded, a high affine probe binding specifically the target antigen might not be found. As nanobodies are derived from IgG molecules, I decided to generate the library for screening upon immunization of alpacas, which typically triggers a specific immune response.

In successive trial experiments, I observed that the method of white blood cell isolation as well as its transportation has a great impact on the quality and quantity of the total extracted cellular RNA. For regulatory reasons, all steps involving direct contact with the animal including white blood cell isolation were performed by preclinics GmbH (Potsdam, Germany). Originally, the company used a protocol lysing the erythrocytes for separation of the lymphocytes with subsequent overnight shipping of remaining peripheral blood mononuclear cells. Unfortunately, a very low yield of total RNA was obtained from such isolation and shipping procedure. Hence together with the company, I optimized the procedure using Ficoll-gradient centrifugation for the separation of the cells followed by storage in RNeasy[®] for protection of the RNA. All together this improved the amount of recovered total RNA substantially from an initial yield of 3 µg per 50 ml blood to approximately 180 µg in the latest RNA preparations.

Another aspect I modified from conventional protocols was the amplification of the nanobody sequences and their cloning into the phagemid. The initial restriction libraries were generated with alternative pairs of restriction enzymes to avoid internal cleavage of a nanobody sequence described in section 2.2.15 requiring dividing and parallel processing of the samples. Restriction cloning furthermore requires relatively long incubation times with multiple enzymes and purification steps

via columns. This complex procedure is likely to cause sample decline and thus a potential loss of diversity in the library.

As an efficient alternative to conventional restriction cloning, I decided to use Gibson assembly and a nested PCR approach presented in section 2.2.15 [147]. I optimized the protocol for library generation by Gibson assembly using different amounts of RNA as a starting material as shown in Table 21. By this I was able to increase the final diversity of the library by several orders of magnitude to a final value of 4.5×10^{11} colonies, which is well above the diversity obtained and reported elsewhere if using restriction cloning [169,170]. Yet it should be kept in mind that the commonly used term 'library diversity' does not reflect the real number of different sequences, but is an absolute value for the total amount of colonies after transformation. As this estimation does not take into account any redundancies, the actual diversity of the libraries is most likely substantially lower.

In another project conducted in the laboratory, my colleagues recently were able to analyze the nanobody repertoire of an alpaca by next-generation sequencing. Serial isolation of RNA from multiple alpacas repeatedly resulted in the identification of approximately 1.3×10^7 non-redundant nanobody sequences. At the same time, the sequencing was performed in a way that 10^7 sequences would not saturate the device capacity. Additionally the reproducibility of the total sequence number suggests that the common diversity of an alpaca ranges around 10^7 different nanobody clones which compares to typical diversities of immune libraries [67].

When comparing my libraries for phage display, the Gibson library was statistically expected to contain more different nanobody sequences than the restriction library due to technical improvements explained in section 2.2.15. Hence, the Gibson library also has a greater potential to yield valuable nanobodies for IF microscopy. In fact, several new candidates not found in the original restriction library were selected from the Gibson libraries. Additionally, the absolute number of candidates passing all validation steps was substantially higher in the Gibson libraries as contrasted in Table 22.

4.2 Selection Procedure by Phage Display

Similar to the library design, the actual screening and selection procedure of nanobody candidates needed to be optimized carefully. As I considered IF microscopy to be the major field of application for my nanobodies, I aimed to select nanobodies with a high affinity and a low k_{off} rate upon antigen binding. For this, I performed long washing steps ranging from 1 to 12 h in the initial panning rounds to be left with high affine binders only. As samples for IF are washed several times to remove unspecific binding in conventional protocols, I also performed up to 15 washes during one panning round.

Although several candidates were identified, I realized that such extensive washing might eventually also cause the immobilized antigen to dissociate, thus reducing the number of positive candidates. Initially, the Strep-Tag® I and II binding Strep-Tactin® (both developed by IBA, Göttingen) were used for antigen immobilization. However, the affinity of these tags was found to be in the micromolar range and immobilized proteins thus may not withstand harsh washing conditions [171]. Therefore, I reduced the number and time of washing steps in subsequent panning rounds as shown in Table 22. On top, the tag for immobilization was replaced with a more recently developed twin-Strep-Tag® (tst) binding Step-Tactin®XT. This system has been claimed to have a binding affinity in the low nanomolar range and thus does not confine as much the affinity of selected nanobodies [171].

Another advantage of immobilizing the antigen via a specific tag in a controlled orientation instead of its adsorption directly to plastic surfaces is the conservation of its native condition. In initial screens, I also used MaxiSorp® plates for unspecific antigen immobilization onto the plastic surface. As this way of antigen immobilization is known to disrupt the protein structure, most selected candidates did not bind the native antigen in IF anymore as can be seen in Table 22. Instead, magnetic MagStrep 'type3' XT beads (IBA) were used for immobilization in solution adjusting the bead volume to the amount of antigen used.

This system further provided the advantage of specific competitive elution by using biotin to release the immobilized antigen and bound phages from the solid support. In contrast, the unspecific elution performed in the conventional protocol required digestion of the antigen by trypsin to release the bound phages. Although the phages are generally considered to withstand trypsin treatment, specific elution is preferred as it essentially keeps all phage proteins required for reinfection of bacteria intact [154]. Moreover a contamination of the eluate with other proteins unspecifically bound is avoided by using a competitive agent such as d-desthiobiotin for specific elution. An even better immobilization of the antigen could be achieved via biotinylation or even covalent binding to a carrier substrate. However, an additional specific cleavage site for proteases (such as TEV protease or thrombin) should be added in that case to perform the specific elution of the antigen together with the bound phages.

The antigen used for immobilization on the beads was purified from *E. coli*, although I aimed to use the nanobodies to detect their target protein on eukaryotic samples. Moreover, the alpaca had also been immunized with proteins produced in bacteria, thus generating an immune response against these proteins. The major reason to use a bacterial expression system was the increase in yield of purified protein in comparison to cell lines such as HEK293-FT cells. Additionally, modified versions of the antigen were used, which lack the transmembrane domain (for syntaxin 1A and VAMP2) or were mutated to change the cysteine residues used for palmitoylation to serines (for SNAP-25).

Besides omitting difficulties associated with protein expression, this way I avoided to generate an immune response directed against those parts of the antigen as they would not be accessible for nanobodies in later IF experiments. However, by using a prokaryotic expression system also common post-translational modifications such as phosphorylation and glycosylation were eliminated, which are found in mammalian expression systems. It is known that conventional full length antibodies are capable of detecting such modifications allowing direct investigations of their physiological role.

Recently, even nanobodies have been reported to detect different conformational stages of an antigen upon binding of GTP as a cofactor [168]. Hence, it is very likely that also nanobodies detecting specific modifications in proteins will be reported in the future. Also the target antigens used in this project carry several modifications, which might be used as a potential target for nanobodies. Particularly, the organization of syntaxin 1A and the interaction with its binding partners has been shown to highly depend on site-specific phosphorylation of the protein [172,173]. Similarly, post-translational modifications of SNAP-25 have been reported to influence the cellular fate of that molecule [174]. More recently, a phosphorylation of SNAP-25 has also been shown to influence the synaptic vesicle cycle and neurotransmitter release [175]. Nanobodies against such specific protein modifications can presumably be obtained if using antigens derived from eukaryotic cells.

To test if the use of mammalian antigens reveals a significant number of alternative candidates, I used antigen purified from HEK293-FT cells during one selection (see Table 22). Although some new families were identified, the number of selected candidates did essentially not deviate from the number of revealed candidates using bacterial antigen. So far, screening with mammalian antigen has only been done on the restriction library. Additional rounds of phage display using mammalian antigen to screen the more diverse Gibson library still might reveal a set of novel candidates. Yet, I already identified several candidates from the Gibson library using bacterial antigen.

Typically, two panning rounds were sufficient to obtain 1-6 new nanobody families determined by sequencing the candidates tested positive in ELISA. If a third panning round was performed, often a single nanobody was found to dominate the ELISA screen suppressing all alternative candidates.

Most likely this is caused by a difference in expression efficiency of some candidates leading to a bias in phage production representing different candidates.

Thus, I concluded that two rounds of panning performed as described are sufficient to obtain new candidates from an immune library. However, this might not be the case for naïve or synthetic libraries as no predisposition for certain antigens is constituted by the animal immune system.

In parallel to the conventional selection procedure using phage display and phagemid libraries for panning, an alternative approach to obtain specific nanobodies for multiple targets in parallel was developed. Briefly, the approach is based on Illumina® next-generation sequencing of the alpaca RNA repertoire rather than cloning it into a vector. Additionally, affinity purified antibodies from the serum of the animal are subjected to mass spectrometry. The levels of nanobody-specific peptides before and after immunization are analyzed using the sequencing data as an inclusion list. A high abundance of specific peptides detected after immunization was considered to indicate the nanobody sequences contributing in specific antigen detection.

The genetic sequences of those nanobodies were ordered for bacterial expression and subsequent validation. Although being cost- and labor-intensive, the major advantage of this method is the simultaneous nanobody selection against various antigens. Interestingly, some nanobody sequences identified via mass spectrometry showed high similarity in their CDR to candidates selected by my original phage display experiments.

During validation, those nanobodies identified with both methods showed binding in dot-blot assays; however none of the candidates passed the final validation step using it into IF experiments (data not shown). Nevertheless, this observation indicates the high potential of the approach to multiplex the selection process compared to conventional phage display. A similar method has recently been introduced by Fridy and coworkers using mass spectrometry to identify nanobodies binding different epitopes on an antigen [81].

4.3 Developing a Robust Validation Protocol

After identification of novel nanobody families by either method, they were subjected to a set of validation procedures to verify their applicability for future experiments. As the candidates were originally selected based on positive signals in the ELISA only, it was required to confirm their functionality in biochemical assays and ultimately in IF microscopy. As mentioned above, ELISA screens typically rely on unspecific immobilization of the antigen to the wells of the plate. This possibly alters the protein conformation causing background binding of the phages or phages might bind to epitopes of the antigen that are not exposed under native conditions within a cellular environment. Together with the high sensitivity of the assay this might create false positive hits, which need to be eliminated in subsequent validation steps.

Even if clones were tested positively in the phage ELISA, I observed that some candidates cannot be expressed in bacteria as a recombinant protein in preparative amounts. It can be speculated that such nanobodies impose toxic side-effects on the expression host or are not soluble enough for large-scale expression in bacteria. As I was aiming to get a nanobody which can be produced in scalable amounts for multiple future applications, the nanobodies showing comparable low expression levels were discarded at that point.

After the expression of the suitable candidates, a new binding test was performed using the antigen immobilized on a nitrocellulose membrane as shown in Figure 16. In addition to the intended antigen, other purified proteins and BSA were spotted on the same membrane in equimolar amounts to serve as a negative control. In ELISA, the nanobodies had only been tested if they bind their antigen, but were not checked for binding to alternative antigens as this would exceed the capacity of this assay. By testing also other proteins in the dot blot, I could estimate if the nanobody candidate is prone to bind also to other SNARE proteins apart from its target antigen. As shown in Table 22, more than 40 % of all candidates were discarded at this step, either due to unspecific binding or because only a faint signal was detected on its corresponding antigen. I decided to use a strict threshold at this level to only continue with few, but promising nanobodies to the next laborious validation steps, namely IF experiments and affinity determination.

For the validation via IF microscopy, mammalian cells were transfected, chemically fixed with PFA and permeabilized according to conventional immunostaining protocols. However, those treatments were reported to interfere with the protein integrity and thus may cause affinity probes to fail in antigen binding [176,177]. For the validation on cells fixed with PFA, I avoided to couple every candidate to a fluorophore individually for economic reasons. Instead, I initially used a fluorescently labeled antibody to detect the DDDDK-tag (FLAG-tag) that was fused to the nanobody upon expression. This indirect detection was used to exclude those candidates from further analyses which

are not capable of binding to the chemically fixed antigen or could not withstand the IF protocol. As the direct conjugation to a fluorophore is a both expensive and time-consuming procedure, only those candidates were conjugated to a fluorophore that displayed clear colocalization between the FLAG-Antibody signal and the EGFP.

Only 23 % of initial positive families in ELISA were found to bind the antigen in IF, which highlights the importance of introducing several levels of validation including application in microscopy (see Table 22).

In a final step I confirmed the binding of the directly labeled nanobody in IF and analyzed the background binding to non-transfected cells identified by their Hoechst nuclear staining but negative EGFP signal. Occasionally, the direct labeling procedure also caused precipitation of the nanobody, particularly if using rather hydrophobic fluorophores such as atto647N [159].

Additionally, it seems that individual nanobodies have a different chemical behavior when combined with a particular fluorophore. As a consequence, some candidates were observed to precipitate after the labeling procedure or lose their function (Nanotag Biotechnologies, unpublished data). Yet the final goal of the project was to obtain nanobodies which bind their antigen specifically in IF upon direct conjugation to fluorophores such as atto647N commonly used for STED microscopy. Although several candidates might have passed the final validation, I did not optimize the immunostaining protocol for each candidate to turn selected nanobodies into a universal and practicable tool.

A potential way for direct selection of nanobodies applicable for IF is the chemical fixation of the antigen to the beads during the panning rounds to mimic the conditions in microscopy experiments. Notably, this requires also harsh elution conditions such as tryptic digestion since competitive elution will not suffice to release the antigen. In turn, the number of novel selected families is expected to decrease as epitopes can be blocked by modifications introduced via aldehyde fixation or are not accessible anymore.

When I performed test experiments using PFA-fixed antigen during the panning round, no nanobody family was revealed that had not been identified before. As I already obtained several good binders, this approach was not exploited further. However, it could still be a promising screening procedure, especially when performing it in 96-well plates using a pipetting robot to achieve a high-throughput selection. In such a case, the intermediate validation on a dot blot could be omitted to prevent false-negative nanobodies from being discarded. For now, all nanobody candidates have been expressed and validated individually restricting the number of candidates that can be handled simultaneously.

As depicted in section 3.3, no final nanobody binding to VAMP2 could be identified during the validation procedure. This may be due to a limited immunogenicity of VAMP2 not evoking a B-cell response in the animal, which triggers the production of specific antibodies. A possible explanation could be the high conservation of this protein among different species, which prevents its detection as a foreign molecule. Alternatively, the immune reaction by the alpaca might have been too low to generate a significant amount of specific IgG molecules.

Notably, the generation of conventional antibodies against VAMP2 has also been observed to be challenging resulting in a limited number of commercially available antibodies specific for this protein. Moreover, nanobodies typically bind structural epitopes due to their flexible CDR3 loop penetrating into binding pockets of the antigen [51,84]. In contrast the fold of VAMP2 is known as a rather unstructured protein lacking a tertiary structure and thus might not expose a stable conformational epitope as a target for the nanobody [178].

Therefore the positive hits in ELISA presumably resulted from transient interactions with VAMP2 or even from background binding in the assay. None of these candidates was specifically amplified over the others during the panning, indicating the lack of a specific affinity to the antigen. SNAP-25 and syntaxin 1A on the other hand acquire a more complex tertiary structure as illustrated in Figure 8, which can specifically be detected by my selected nanobodies S25-Nb10 and stx-Nb6.

4.4 Characterization of S25-Nb10 and stx-Nb6

An important parameter of the nanobodies is their affinity as it influences the quality of staining in IF experiments. The conditions during SPR measurements caused both precipitation and degradation of the antigen due to long incubation times as mentioned in section 3.4.3.

I initially decided on this method as not only the affinity, indicated by the dissociation constant K_D , but also the kinetic behavior of the nanobodies could be measured. The kinetic parameters such as association (k_{on}) and dissociation (k_{off}) provide additional information on the dynamic behavior. Those values can be used to adjust the washing conditions accordingly to minimize the loss of nanobody during washing steps.

I found most nanobodies to exhibit similar values for k_{on} causing the dissociation constant K_D to directly determine the overall affinity of the probe [81,168]. Hence, a low dissociation constant was considered to indicate a strong affinity of my nanobody. To measure the K_D value of the nanobody-antigen complex, MST was finally used as a more reliable and faster method.

The two nanobodies S25-Nb10 and stx-Nb6 binding SNAP-25 and syntaxin 1A, respectively, passed all validation criteria and bind their antigen with high affinity. Their dissociation constants were found to be in the low nanomolar range (15.5 ± 3.3 nM for S25-Nb10 and 5.0 ± 1.2 nM for stx-Nb6), which

indicates a high affinity of the nanobody comparable to other probes described in the literature [84,168]. Those nanobodies were therefore used as final probes for further experiments.

I decided to use the nanobodies in a concentration of 50 nM in immunostainings, which is well above the K_D value and thus expected to saturate the detection of the epitopes. At the same time this concentration of nanobodies was still low enough to prevent unspecific staining in cells not expressing EGFP (see Figure 22). This is shown in Figure 28 where a GFP-nanobody also conjugated to atto647N was used at equivalent conditions to determine if the fluorophore contributes to background binding (negative control).

The sequences of rat syntaxin 1A and SNAP-25 were used for both phage display selection and validation experiments. Both proteins are virtually conserved among mammals including *homo sapiens*, *mus musculus* and *rattus norvegicus* with occasional deviations of single amino acids. Therefore, the species type of the antigen is not expected to influence the result of nanobody binding. This is also supported by the fact that both nanobodies detected a single protein in immunoblots regardless of the species type as shown in Figure 20.

Besides these observations, it is a remarkable fact that the nanobodies are at all working in Western blots detecting the antigen after denaturing SDS-PAGE as demonstrated in section 3.4.4. Although nanobodies detecting linear epitopes have been reported before, the detection of unfolded proteins is generally rather untypical for those probes [51,79,84]. A possible explanation could be the incomplete denaturation or partial refolding of SNAP-25 and syntaxin 1A during SDS-PAGE. Alternatively, the nanobodies might indeed bind to linear or unstructured epitopes, which do not require the antigen to acquire a specific conformation.

To narrow down the region of nanobody binding to the antigen, I generated truncated forms covering the antigen sequence piece by piece. As shown in Figure 23, individual domains of the antigen seem to be in fact sufficient to mediate nanobody binding. The epitope nanobody S25-Nb10 was found to localize in the N-terminal domain of SNAP-25 which constitutes one of the two SNARE domains of that protein. Generally, those domains are composed of an alpha-helical structure, which form intermolecular bundles resulting in a stable helical bundle [162]. As a single SNARE domain is not expected to acquire a tertiary structure, the epitope mapping shown in Figure 23 suggests that both nanobodies might indeed detect a linear epitope or a helical secondary structure.

If by future NMR analyses the epitope of the nanobody S25-Nb10 can be confirmed to reside within the SNARE domain, the nanobody could be an interesting tool to investigate the SNARE complexes. By intracellular expression of the nanobodies in neurons, the SNARE complex formation could be

impaired due to sequestering of SNAP-25. Alternatively also the ratio of free SNAP-25 compared to pre-assembled complexes or clusters could be determined if the nanobody is found to only bind free SNAP-25. This might be a valuable approach to investigate the dynamics of synaptic vesicle cycling and synaptic physiology in more details. A first indication that S25-Nb10 cannot detect SNAP-25 engaged in a SNARE complex can be inferred from Figure 30 where both nanobodies were imaged in dual channel STED microscopy.

Due to the interaction of SNAP-25 and syntaxin 1A on the plasma membrane to nucleate a SNARE complex for vesicle fusion, both proteins are expected in direct proximity [179,180]. The low colocalization of SNAP-25 and syntaxin 1A observed in Figure 30 might thus be caused by steric hindrance or conformational change in the SNARE bundle which masks the epitope. Similarly, antibodies often localize an epitope within the SNARE domain (see section 3.5) and therefore might likewise be impaired in binding their antigen in a complex. So far, SNAP-25 and syntaxin 1A have been only reported to localize in adjacent domains but not in the same SNARE complex as it would be expected [166].

Despite the apparent binding specificity for the SNARE domain of SNAP-25 and syntaxin 1A, the nanobodies merely detect other closely related SNAP or syntaxin proteins (see section 3.4.4 and Figure 21). The high specificity of S25-Nb10 was expected as SNAP-25 shares only little homology with other SNAP proteins (see Figure 21 and Figure 31). On the contrary, currently 16 different syntaxin proteins are known in human, most of which show high degree of similarity [181]. I tested three syntaxin variants that show the highest level of sequence conservation to syntaxin 1A, indicated by the green box in Figure 31. Still the stx-Nb6 shows specificity for syntaxin 1A with little cross-reactivity to syntaxin 3 but no reactivity for the phylogenetically close protein syntaxin 1B.

Taking into account that the nanobody might detect a linear part of the protein this narrows down the potential position for the epitope drastically. In practice, an amino acid sequence found in both syntaxin 1A and syntaxin 3 but not in syntaxin 1B could be a likely position for the nanobody to bind. An exemplary region is located in between the amino acid residues 53-59, where syntaxin 1A possesses higher sequence similarity to syntaxin 3 than to syntaxin 1B. Interestingly, this region is also part of the truncation construct showing nanobody binding in Figure 23. Hence, recombinant expression of this peptide to use for dot blot or blocking assays could pinpoint the epitope to a short peptide. If that peptide shows binding to the nanobody, it may also be used as a ligand for NMR to gain structural information on the interaction between stx-Nb6 and syntaxin 1A.

In further experiments, the specificity of stx-Nb6 for syntaxin 1A can be used to quantify the ratio between cellular levels of endogenous syntaxin 1A and 1B. Despite the high degree of sequence conservation in between those molecules, syntaxin 1A and 1B have a different impact on synaptic physiology and neuronal survival [182,183]. The nanobody could thus be used as a tool to selectively detect endogenous levels of syntaxin 1A as many commercially available antibodies cannot distinguish between those two syntaxin variants (see Figure 21 and Figure 31).

Yet my primary focus lies on the application of nanobodies as a versatile tool for super-resolution microscopy in fixed samples. High affinity and high specificity were therefore considered to be the main criteria to define my nanobodies, regardless of the epitope position. After identification of S25-Nb10 and stx-Nb6 as the final candidates, I therefore focused on their implementation in IF experiments.

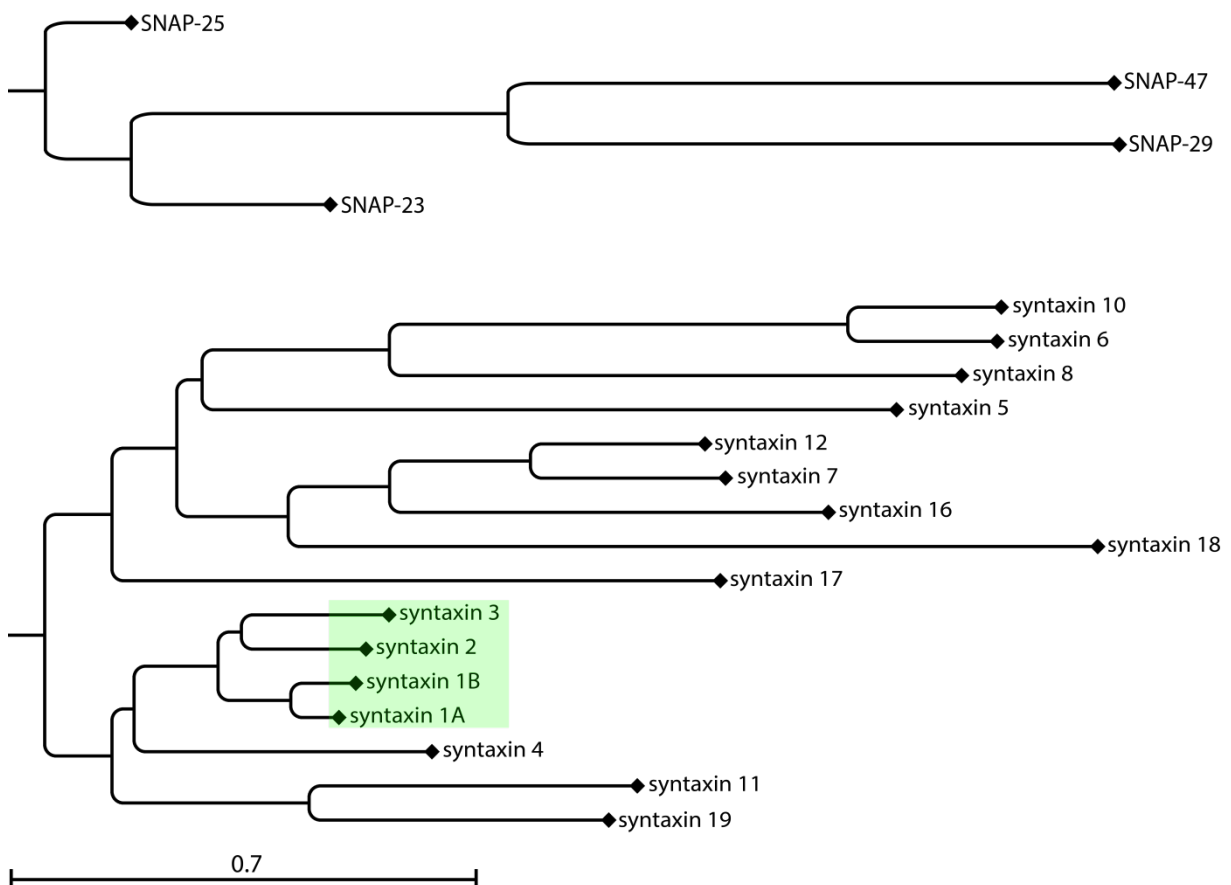


Figure 31: Phylogenetic alignment of the SNAP and syntaxin protein family. During this study, I focused on SNAP-25 and syntaxin 1A as two major SNARE proteins present in neuronal synapses. The highlighted syntaxin variants were used to analyze the specificity of nanobodies directed against syntaxin 1A. Alignment was created with CLC sequence viewer 7.

4.5 Labeling of Nanobodies

Before using my nanobodies for immunostaining, they were conjugated with a fluorophore to allow direct detection of the target antigen and to avoid creation of artifacts due to secondary antibodies (see section 1.5). As a default fluorophore atto647N was used, which is known for its tendency to unspecifically bind to membranes but shows a high quantum yield compared to other fluorophores in the far-red range [159].

I carefully performed control experiments using unspecific nanobodies conjugated to atto647N at the same concentration to confirm the negligible level of background fluorescence caused by the dye moiety. Atto647N is known to be a preferred dye for STED microscopy and maleimide-functionalized fluorophores can efficiently be coupled to the protein. Other functionalized dyes used for coupling reactions and listed in Table 20 showed lower (Alexa dyes) or even very poor (Abberior dyes) DOL values upon conjugation (data not shown). The labeling efficiency directly influences the quality of subsequent immunostainings. Whereas an excess of dye can be removed by size-exclusion chromatography (see Figure 18) unreacted nanobody molecules cannot easily be removed after the labeling reaction. Contaminations of unconjugated nanobody in an immunostaining should be avoided as they will block binding sites of the antigen, which subsequently elude the observation by fluorescence microscopy.

The method used for labeling also drastically influences the DOL and specifications of the conjugated nanobody. As already indicated in previous studies, using the enzyme sortase A results in labeling of only a minor fraction of the nanobody sample associated with the problems stated in section 3.4.2 [65]. In contrast, labeling with NHS-activated fluorophores is commonly used for the conjugation nanobodies [81,91]. These dye moieties are attached unspecifically to exposed lysine residues of the molecule. If a lysine residue takes part in the epitope detection, the affinity probe might lose its binding capability if a fluorophore gets attached to this residue [110]. By adding a poly-lysine tag to the C-terminus of the nanobody, this effect can be alleviated, but not completely resolved [112].

Attaching multiple fluorophores to a single molecule might also cause self-quenching of the dye resulting in a major loss of fluorescence [184]. Furthermore, I observed that conjugating multiple hydrophobic fluorophores to the relatively small nanobody is prone to cause precipitation of the molecule if stored over longer time. In addition to the hydrophobicity brought in by the dye moiety, the solubility of the protein is reduced as the conjugation reaction happens at charged lysine residues, which contribute to the solubility.

Consequently, I decided to use a method combining site specificity and high labeling efficiency for conjugating the nanobodies to a fluorophore. By adding an additional cysteine to the C-terminus of the nanobody during recombinant expression, a specific reaction site for maleimide activated

fluorophores was created. A short linker sequence separated the extra cysteine from the major part of the nanobody to prevent interference with the intramolecular formed disulfide bridges. If those purified nanobodies were reduced before labeling (see section 2.2.18), routinely a DOL of >90 % was obtained, while using only minimal to moderate excess of dye, depending on the manufacturer.

Another major advantage of this labeling approach is the defined stoichiometric ratio of fluorophores per nanobody (DOL values reach almost 100 %), which allows direct quantitative analysis of the antigen. Nowadays, several research groups are aiming to quantify biological compounds directly using modern microscopy techniques [108,185,186].

If the fluorescence signal of the labeled nanobody is normalized by measuring individual molecules, this calibration may be used to estimate the absolute number of antigen in an IF experiment. However, this approach requires a very sensitive camera for detection of individual fluorophores. I performed a quantitative analysis of GFP molecules using nanobodies conjugated to a single atto647N molecule, similar to the approach described by Mi and coworkers [187].

In addition to a blinking behavior of the dye, the analysis of the detected fluorescence signal turned out to be challenging: The possibly emitted fluorescence of a single fluorophore is not given by a discrete value but is described by a Gaussian distribution. Hence, the fluorescent signal is blurred out if more than five molecules in direct proximity are detected simultaneously. In such a case, the exact number of molecules cannot be determined anymore without an error, however an estimation of the copy number is still possible. The analysis is further assuming a linear correlation between the fluorescent intensity and the number of fluorophores. Although the fluorescence signal generally correlates with its concentration, the linearity is lost at very high fluorophore concentrations [188].

Finally, for complex biological samples, a high detection density is required not to miss any epitopes, which might be challenging even for small affinity probes such as nanobodies. In my experiments I addressed all aspects mentioned above individually generating a reliable fit to count individual GFP molecules (data not shown). This underlines the capability of nanobodies to be used in quantitative microscopy approaches. Even if they cannot reveal an exact protein copy number in IF experiments, nanobodies represent molecular organization substantially better than a conventional staining using primary and secondary antibodies.

4.6 Comparison of Nanobodies to Classical Affinity Probes

The limited possibility to use antibodies as a tool for protein quantification is only one difference to nanobodies. As pointed out in section 1.5 and supported by my findings in section 3.5, antibodies are impaired by their size from penetration deep into complex biological samples as demonstrated in section 3.5.3. Consequently, they might not detect all available target epitopes yielding an inhomogeneous staining and thus not necessarily reflecting the actual protein distribution in the sample [72] as shown in section 3.5.5.

Typically, biological samples are chemically fixed prior to immunostainings using aldehydes such as PFA or glutaraldehyde. However, the fixation is often not completed as the aldehydes may take up to several days to achieve complete immobilization of the molecules in the sample [189,190].

Moreover, the crosslinking induced by the aldehydes can be reversed if the fixation was performed only shortly and the sample is left in an aqueous solution. Therefore divalent probes such as antibodies might cluster together insufficiently immobilized antigens upon binding. This effect is even enhanced by the use of secondary antibodies for detection as the sample is commonly not fixed again after application of the primary antibody. Divalent polyclonal antibodies such as secondaries can bind multiple primary antibodies, which might thus increase the clustering effects.

Figure 28 shows the difference in phenotype when using primary and secondary antibodies or directly conjugated nanobodies to detect endogenous proteins. My data suggest that using antibodies not only results in the tendency to observe more bright spots, but might result in omitting antigens in between these spots. As a consequence, the IF image does not necessarily represent the biological distribution of the antigen. In contrast, nanobodies used in IF experiments generally showed a more smooth antigen distribution as shown in section 3.5.

These effects can merely be seen in confocal microscopy, but they become a major problem in super-resolution microscopy [91,105]. At a diffraction-limited resolution, the size of antibody clusters is expected to be well below the maximum attainable resolution of 200 nm resulting in a similar staining pattern compared to nanobodies [91,105]. If using current super-resolution techniques, the technically possible resolution is compromised by the size of the antibody as illustrated in Figure 32. Modern microscopes for STED and STORM can achieve resolutions in the low nanometer range, whereas the size of a single antibody molecule already ranges around 15 nm [12,27,111].

In addition to the resulting fluorophore delocalization, the molecular clustering and inhomogeneous fluorescent labeling of the secondary antibody are prone to distort the phenotype of antigen organization (see section 1.5). In contrast, a monovalent small affinity probe is able to efficiently decorate the target antigen resulting in a better resolved staining resembling the antigen distribution in super-resolution (represented by blurred red circles in Figure 32A). Although Figure 32 is a simplified 2D-projection, it illustrates the problem for one exemplary protein. In a complex biological sample, not only special dimensions of the depicted proteins but also the densely packed molecular environment needs to be considered as depicted in section 1.6.

In such an environment, the epitopes of the target antigen might be masked by other proteins and thus are not accessible for antibodies. The flexible CDR3 loop of nanobodies (see section 1.4.4) in combination with the small size of the probe can be beneficial in such a case.

However, the missing of epitopes might also happen to nanobodies if the antigen is engaged in a multimeric complex as it might be the case for S25-Nb10 where the epitope is located within the SNARE domain (see Figure 23). This would also impair nanobodies from accessing the epitope in assembled SNARE complexes, which could be an explanation for the low degree of colocalization observed in Figure 30.

Despite the increase in resolution achieved by using directly conjugated affinity probes, this detection system is to some extent rather inflexible. If an alternative fluorescent label is desired, the molecule needs to be labeled *de novo* with the dye. In contrast, the label in an antibody staining can easily be exchanged by using an alternative secondary antibody providing a flexible platform for fluorescent labeling. However the conjugation of nanobodies to functionalized dyes can be performed with reasonable effort following standard protocols. The conjugation to recombinant tags or enzymes is even facilitated as they can directly be fused to the nanobody on DNA level. Along these lines, nanobodies might be useful tools to replace secondary antibodies to compensate for potential artifacts introduced while performing conventional antibody stainings.

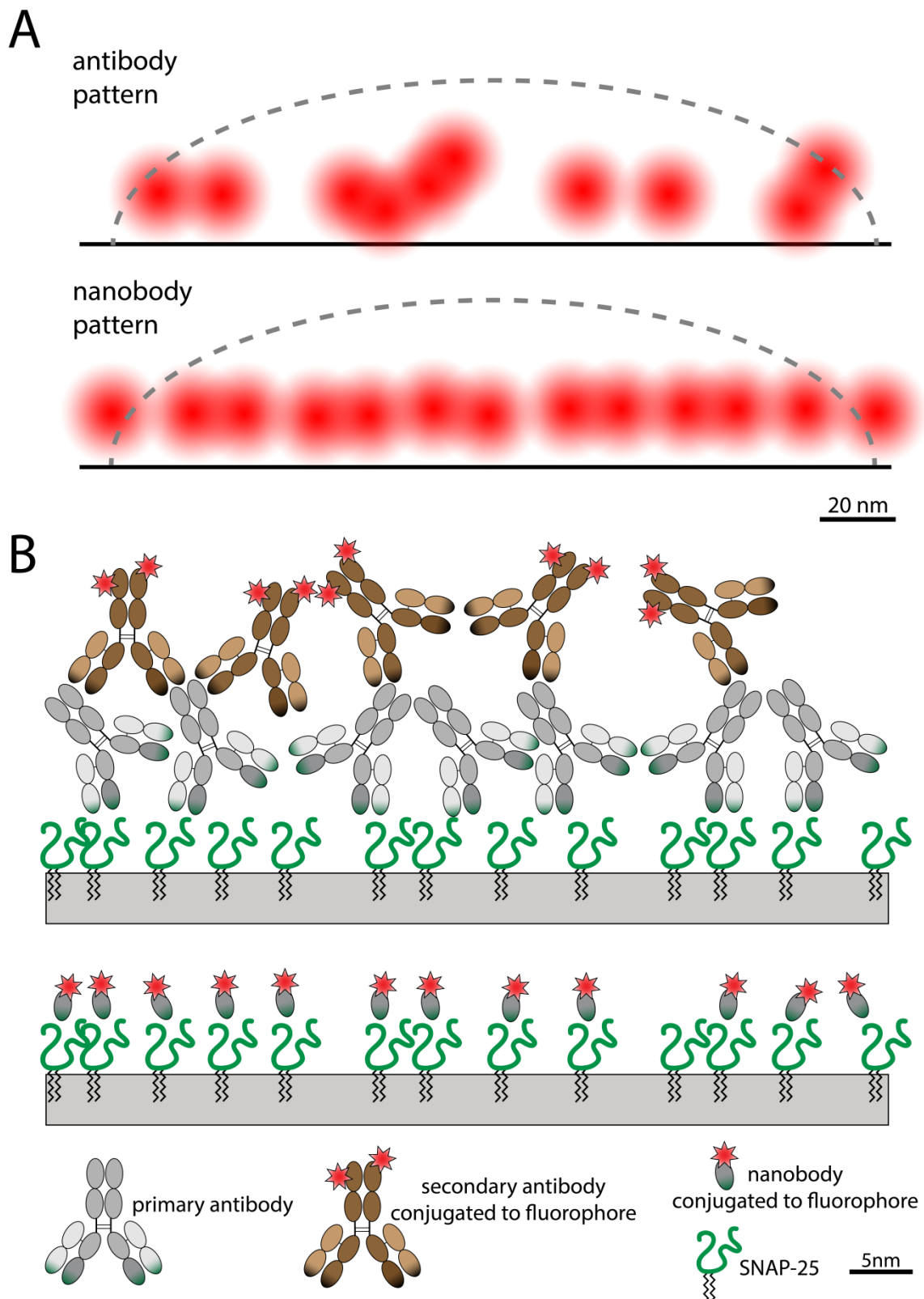


Figure 32: Schematic illustration of antibody and nanobody binding to a target antigen. **A:** Exemplary representation of fluorescence signals detected by microscopy. With super-resolution techniques, individual fluorophores (blurred red circles) can be localized indicating the arrangement of the target antigen. Notably, when using confocal microscopy, the diffraction limit would cause the fluorescent signals to overlap impeding conclusions on molecular organization (represented by the dashed grey line). **B:** A potential molecular arrangement of affinity probes resulting in a fluorescence pattern observed in **A**. Although the detected fluorescence pattern resulting from antibody or nanobody staining is different, the molecular organization of the antigen (SNAP-25) is still identical. The fluorescence signal resulting from the nanobody resembles the molecular organization of the antigen with higher accuracy thus increasing the resolution.

The scalability of nanobody production further broadens the possible applications as experiments are typically not limited by the amount of affinity probe available. Hybridoma cell lines for the production of monoclonal antibodies are cost-intensive and might eventually die or stop the secretion of functional antibodies [107]. Although polyclonal antibodies are more easy to produce than monoclonal antibodies, they often show high batch variability in binding to their antigen resulting in several researches recommending to substitute them [107,191].

Those antibody characteristics often associated with artifacts in IF experiments are not observed when using nanobodies as affinity probes. Their small size and monovalent nature facilitate the efficient decoration of cellular epitopes thus providing a higher level of detail than conventional affinity probes. If introducing the fluorescent label in a quantitative manner, the microscopy image can even be assumed to directly reflect the actual distribution of the antigen. However, the labeling of nanobodies requires careful optimization as mentioned above. If only one dye molecule is attached per nanobody, the absolute fluorescence signal is essentially lower than observed with secondary antibodies, which are known to amplify the signal.

On the other hand, the high detection rate of the nanobody somewhat compensates for this effect as the number of fluorescent molecules is higher compared to conventional antibodies. If the antigen is present in plethora, using nanobodies might be even more reliable as the higher fluorescence of antibodies is counteracted by their poor penetration capability (see section 3.5.4). During the studies, I primarily used one antibody clone for each SNAP-25 and syntaxin 1A for direct comparison with my nanobodies. Although it might be interesting to analyze also the performance of other antibodies, I chose the clones 71.1 and 78.2 as two very established antibodies in the field [128,165,192]. As the aforementioned observations are due to general properties of antibodies, also alternative clones are likely to yield the same result.

I observed significant differences in the fluorescence signal revealed by antibodies or nanobodies in both cell lines and primary neuron cultures. The accumulation of overexpressed syntaxin 1A in the ER and Golgi if expressed without cofactors has been reported before [193]. This explains the phenotype in the EGFP-channel showing high concentration of syntaxin 1A in the perinuclear region as depicted in section 3.5.2. Similarly, SNAP-25 was found in higher concentrations at the periphery of the nucleus.

After expression, SNAP-25 is palmitoylated to be anchored into cellular membranes. Enzymes of the DHHC family that mediate the palmitoylation of SNAP-25 were reported to predominantly be located at the Golgi apparatus, which resembles the structure and location of high SNAP-25-EGFP signal in COS-7 cells [194]. The high copy numbers of the overexpressed protein presumably saturate the capacity of the cellular palmitoylation machinery and cause the protein to accumulate. In both cases,

the antigen is localized in a protein-dense region, where the nanobodies represent the EGFP signal significantly better compared to conventional antibodies.

A similar phenotype could also be observed when staining PC-12 cells with either antibodies or nanobodies, shown in section 3.5.4. As those cells originate from the neural crest, they endogenously express both SNAP-25 and syntaxin 1A, albeit in lower amount than in an overexpressing system [192]. This suggests that at the level of endogenous protein expression, the conventional antibodies used in this experiment cannot reliably detect the entirety of present antigens and their organization. This is a crucial point particular for the detection of the SNARE proteins SNAP-25 and syntaxin 1A in neuronal synapses as they play a major role in synaptic vesicle fusion and neurotransmitter release [126]. It is therefore of major interest to analyze the organization of those proteins in the highest level of detail possible, which can only partially be done with conventional antibodies.

4.7 Organization of Synaptic Proteins Revealed by Nanobodies

Using the nanobodies S25-Nb10 and stx-Nb6 to image primary cultured hippocampal neurons in super-resolution, I observed a phenotype deviating from classical observation with antibodies. Both target proteins were reported to form clusters all over the neuronal membrane if observed with super-resolution microscopy [135,167]. Those assemblies are considered to form clusters of defined sizes due to lateral interaction of the SNARE domains [195,196].

The homophilic interaction between the molecules might compensate the loss in entropy when proteins are clustered in one place. It has been debated that the clusters serve as platform to recruit SNARE proteins for its complex formation or to participate in maintaining membrane integrity [165]. Still, no obvious physiological relevance of the reported clusters was found so far and the role of SNARE cluster formation is still under investigation.

Notably, so far all major microscopic investigation on SNARE protein assembly exclusively either used overexpressing proteins tagged with EGFP or primary and secondary antibodies for the detection of endogenous SNARE proteins [134,195,197]. Many observations on syntaxin clustering were made in PC-12 cells, which are known to resemble the proteome machinery for synaptic vesicle fusion like in neurons without readily forming synapses.

When I used my nanobodies to investigate the distribution and organization of SNAP-25 and syntaxin 1A under more native conditions, I found both protein clusters to be less evident compared to antibody stainings (see section 3.5.5). Averaging the fluorescence signal of several hundred synapses, I could show an average distribution of the SNARE proteins using either of the two affinity probes as shown in Figure 29. Upon using nanobodies in IF microscopy, the overall distribution of the proteins was found to be substantially more uniformly distributed than observed with antibodies [167].

As the nanobody phenotype differed so drastically from the conventionally observed pattern, I carefully performed control experiments to exclude false positive or unspecific binding of the probe. The commonly used GFP nanobody was coupled to the same fluorophore (atto647N) and used under the same conditions as the S25-Nb10 and stx-Nb6 to stain primary cultured neurons [198]. The nanobody did not show any background signal to the neuron indicating that the atto647N moiety does not cause any unspecific binding despite its hydrophobic nature.

Furthermore, the enrichment of SNAP-25 and syntaxin 1A in synapses detected with my nanobodies is well in line with the literature and supports the specificity of my probes. The generic detection in the neurites is very likely to reflect proteins, which are transported along the cytoskeleton as they need to reach the synapse after synthesis in the cell body. Moreover, both specificity and affinity of the nanobodies have been tested in various experiments before (see section 3.4.4).

Therefore I consider the phenotype revealed by my nanobodies to resemble the distribution of the SNARE proteins SNAP-25 and syntaxin 1A in a reasonable and even more native manner.

The question remains which impact these findings have on the model of SNARE protein organization in the synapse. First, my results do not directly contradict the existence of SNAP-25 and syntaxin 1A clusters, which might still be organized in microdomains as suggested before [166]. The very high average copy number of both proteins per synapse (around 26,600 copies of SNAP-25 and 20,100 copies of syntaxin 1A) also raises the possibility that even nanobodies cannot detect all antigens in the dense protein environment [128]. Notably, some proteins might be extracted due to the permeabilization protocol commonly applied in IF stainings. As discussed above, the accessibility of the epitope for a specific probe has a major influence on antigen detection. Proteins engaged in a closely bundled SNARE complex thus might elude detection from both antibodies and nanobodies.

In either case SNAP-25 and syntaxin 1A do not seem to be localized in an all-or-nothing pattern, which is suggested by antibody staining. Together with my previous observations, these findings prompt that the observed SNARE cluster formation is at least partially based on antibody artifacts.

Another interesting question would be whether SNAP-25 and syntaxin 1A, which are known to form a SNARE bundle upon vesicle fusion also interact while residing in the plasma membrane. Generally, both proteins have not been found to colocalize in super-resolution microscopy [135]. More recently SNAP-25 and syntaxin 1A were suggested to preassemble into microdomains used for subsequent vesicle fusion events [166]. Although this study by Pertsinidis *et al.* claims a colocalization of SNAP-25 and syntaxin 1A revealed by super-resolution microscopy, it actually shows only very poor data supporting the colocalization.

Notably, this study was based on results using antibodies as affinity probes to detect the proteins. As discussed above, nanobodies could have a great impact on the investigation of SNAP-25 and syntaxin 1A colocalization in dual-channel super-resolution microscopy. Thus my nanobodies might be valuable tools to reveal possible interaction between those molecules at nanoscale which has not been done so far in microscopy. The nanobodies could be further used in several experimental approaches such as EM or Expansion Microscopy to investigate the synaptic anatomy and plasticity.

4.8 Future Applications for Selected Nanobodies

The key role of SNAP-25 and syntaxin 1A in synaptic physiology was the major motivation to generate nanobodies to study those two proteins. To confirm and pursue my findings in neurons, the nanobodies could be used in several alternative approaches. To achieve nanometer resolution without encountering photobleaching, small quantum dots ($\varnothing \approx 7$ nm) were already successfully coupled to nanobodies [199]. Similar to organic fluorophores, quantum dots show a defined emission spectrum while surpassing the brightness of conventional dyes up to 20-fold [200]. The blinking behavior and photostability of quantum dots furthermore allows precise localization in super-resolution microscopy even in 3D [201].

Combining quantum dots with my nanobodies could be an elegant way to increase the fluorescence signal and to investigate cluster assembly in synapses at nanoscale resolution. The conjugation of mono-functionalized quantum dots to the nanobodies can be performed analogously to fluorescent labeling using chemically functionalized molecules (see section 2.2.18). The valency of the quantum dots is an important parameter as multivalent conjugation would result in signal bias similar to the case of divalent antibodies as discussed in section 4.6.

As an alternative, the nanobodies may also be conjugated to colloidal gold for use in electron microscopy. EM was one of the first methods to depict the ultrastructure of synapses and is still widely used for sub-diffraction imaging [114,115]. However, the use of antibodies in immune-EM is often challenging due to harsh sample preparation conditions [202]. Fixation with glutaraldehyde links the molecules in the sample to a proteinaceous network impairing the accessibility for antibodies [72,203]. The small size of nanobodies after coupling it to colloidal gold particles could bypass this problems resulting in a higher detection rate of the antigens revealing a more detailed structure. In initial trials, I already successfully coupled the GFP nanobody to mono-functionalized colloidal gold particles for future use in EM experiments. By chemically conjugating the nanobodies stx-Nb6 and S25-Nb10 to colloidal gold particles, a tool to improve visualization of synaptic structures in EM could be developed.

The nanobodies against SNAP-25 and syntaxin 1A can as well be applied in other correlative and molecular imaging techniques. The nanoSIMS technology combining super-resolution microscopy and mass spectrometry (see section 1.2.3) could benefit from using small probes for detection. Chemical labels for affinity probes have been developed, which allow detection in both nanoSIMS and STED microscopy [28,204]. Coupling those labels to nanobodies would unify the benefit of small affinity probes with high-resolution imaging at the molecular level. Although establishing the nanoSIMS technology is a time and cost-intensive procedure, the implementation of this technology may be an important milestone towards atomic mapping of complex biological samples.

Also other recently developed techniques such as expansion microscopy may benefit from the use of small probes such as nanobodies. As described in section 1.2.3, this technology achieves super-resolution by physical expansion of the fluorophores in space after labeling. The distance between the fluorophore and the epitope plays an important role in this method as it will also be increased according to the expansion factor. Due to their spatial organization and their tendency to form clusters, antibodies delocalize the fluorophore from the epitope [34]. In contrast, nanobodies could be used to direct the fluorophore to the antigen with nanometer precision, thus directly increasing the resolution in expansion microscopy.

Apart from descriptive microscopy approaches, nanobodies are also commonly used as reporters and regulators in live-cell experiments [80]. Monitoring the synaptic activity upon intracellular expression and binding of my nanobodies would be an interesting field of application. After binding of GFP-tagged nanobodies to the SNARE proteins, the cellular faith and organization of these molecules could be studied *in vivo*. Recently, a new nanobody has been reported, which specifically blocks the activity of a vesicular glutamate transporter, which was not possible before [205]. A similar approach could be used to block synaptic activity by intracellular expression of my nanobodies. If the epitope of these probes is confirmed to localize within the SNARE-domain, they may impair SNARE-mediated fusion events thus interfering with synaptic function.

All in all, the development of novel nanobodies specifically binding SNAP-25 and syntaxin 1A opens a wide field of application in neurobiology. I am confident that my novel probes will contribute to understand basic mechanisms of synaptic physiology and reveal new insights on subcellular protein organization.

4.9 Summary and Conclusion

I demonstrated that small affinity probes such as nanobodies have a great potential for various biological and biochemical applications such as IF microscopy and ELISA, respectively. They show several advantages in comparison to conventional antibodies including a reduction in size, enhanced tissue penetration, the prevention of clustering effects and the increase in localization precision. Thus I intended to implement the two nanobodies S25-Nb10 and stx-Nb6 described in this project into various applications, including super-resolution imaging. As I showed, the resolution in biology and thus the density of information does not only depend on the microscopy setup but also on the affinity probe used.

Notably, in immunocytochemistry and particular in fluorescence microscopy approaches, antibodies are still the dominating type of affinity probe.

On the one hand, antibodies are very well established tools with several hundred targets available, which have constantly been used and developed throughout the last decades.

On the other hand, the selection of novel specific affinity probes is a laborious procedure and requires extensive screening and validation procedures. Therefore, antibodies are still a valuable tool to specifically mark and detect specific proteins in a complex biological sample. However, it should be kept in mind that the (fluorescence) signal detected indicates the position of the fluorophore, which does not necessarily reflect the position of the antigen. Thus it is important to consider how the applied affinity probes function in molecular interaction with their target protein, especially in protein-dense compartments such as the synapse. Researchers are advised to interpret microscopy data very carefully and with respect to potential artifacts created by the detection technique.

A large number of antibodies on the market does not yield reproducible results due to insufficient validation or variation in quality during the production of the probe [107,191]. The use of well-characterized and reliable tools for IF microscopy therefore is of fundamental importance to obtain meaningful results in imaging.

Another important aspect, commonly influencing the imaging result, is the treatment of the sample prior to the staining procedure. For instance, artifacts in IF microscopy caused due to fixation and permeabilization of the sample should be considered and minimized [111]. As each technology has specific requirements for sample treatment and handling, a combination of multiple approaches is possibly required to complete the picture of neuronal organization and function. The implementation of small probes is very likely to take a key role in such future investigations. My two new small and versatile nanobodies for super-resolution microscopy should make a major contribution to understand synaptic and neuronal physiology.

5. References

- 1 Minsky, M. (1988) Memoir on inventing the confocal scanning microscope. *Scanning* **10**, 128–138.
- 2 Abbe, E. (1873) Beiträge zur Theorie des Mikroskops und der mikroskopischen Wahrnehmung. *Arch. f. Mikroskop Anat* **9**, 413–420.
- 3 Abbe, E. (1881) VII.-On the Estimation of Aperture in the Microscope. *J. R. Microsc. Soc.* **1**, 388–423.
- 4 Wilson, M. (2017, July 12) Collecting Light: The Importance of Numerical Aperture in Microscopy.
- 5 Lukosz, W. and Marchand, M. (1963) Optischen Abbildung Unter Überschreitung der Beugungsbedingten Auflösungsgrenze. *Opt. Acta Int. J. Opt.* **10**, 241–255.
- 6 Lu-Walther, H. W., Hou, W., Kielhorn, M., Arai, Y., Nagai, T., Kessels, M. M., Qualmann, B. and Heintzmann, R. (2016) Nonlinear structured illumination using a fluorescent protein activating at the readout wavelength. *PLoS One* **11**, 1–14.
- 7 Xu, K., Babcock, H. P. and Zhuang, X. (2012) Dual-objective STORM reveals three-dimensional filament organization in the actin cytoskeleton. *Nat. Methods* **9**, 185–8.
- 8 Hell, S. W. and Wichmann, J. (1994) Breaking the diffraction resolution limit by stimulated emission: stimulated-emission-depletion fluorescence microscopy. *Opt. Lett.* **19**, 780–2.
- 9 Huang, B., Bates, M. and Zhuang, X. (2009) Super-Resolution Fluorescence Microscopy. *Annu. Rev. Biochem.* **78**, 993–1016.
- 10 Hell, S. W. (2003) Toward fluorescence nanoscopy. *Nat. Biotechnol.* **21**, 1347–1355.
- 11 Willig, K. I., Rizzoli, S. O., Westphal, V., Jahn, R. and Hell, S. W. (2006) STED microscopy reveals that synaptotagmin remains clustered after synaptic vesicle exocytosis. *Nature* **440**, 935–939.
- 12 Vicidomini, G., Moneron, G., Han, K. Y., Westphal, V., Ta, H., Reuss, M., Engelhardt, J., Eggeling, C. and Hell, S. W. (2011) Sharper low-power STED nanoscopy by time gating. *Nat. Methods* **8**, 571–573.
- 13 Moffitt, J. R., Osseforth, C. and Michaelis, J. (2011) Time-gating improves the spatial resolution of STED microscopy. *Opt. Express* **19**, 4242.
- 14 Göttfert, F., Wurm, C. a, Mueller, V., Berning, S., Cordes, V. C., Honigmann, A. and Hell, S. W. (2013) Coaligned dual-channel STED nanoscopy and molecular diffusion analysis at 20 nm resolution. *Biophys. J.* **105**, L01-3.
- 15 Rust, M. J., Bates, M. and Zhuang, X. (2006) imaging by stochastic optical reconstruction microscopy (STORM). *Nat. Methods* **3**, 793–795.
- 16 Betzig, E., Patterson, G. H., Sougrat, R., Lindwasser, O. W., Olenych, S., Bonifacino, J. S., Davidson, M. W., Lippincott-Schwartz, J. and Hess, H. F. (2006) Imaging intracellular fluorescent proteins at nanometer resolution. *Science* **313**, 1642–1645.

- 17 Dempsey, G. T., Vaughan, J. C., Chen, K. H., Bates, M. and Zhuang, X. (2011) Evaluation of fluorophores for optimal performance in localization-based super-resolution imaging. *Nat. Methods* **8**, 1027–36.
- 18 Thompson, R. E., Larson, D. R. and Webb, W. W. (2002) Precise Nanometer Localization Analysis for Individual Fluorescent Probes. *Biophys. J.* **82**, 2775–2783.
- 19 Ruska, E. (1987) The Development of the Electron Microscope and of Electron Microscopy. *Angew. Chemie - Int. Ed.* **26**, 595–706.
- 20 Salapaka, S. and Salapaka, M. (2008) Scanning Probe Microscopy. *IEEE Control Syst. Mag.* **28**, 65–83.
- 21 Ayache, J., Beaunier, L., Boumendil, J., Ehret, G. and Laub, D. (2010) *Sample Preparation Handbook for Transmission Electron Microscopy*, Springer New York, New York, NY.
- 22 Zhong, L., Brown, J. C., Wells, C. and Gerges, N. Z. (2013) Post-embedding Immunogold labeling of synaptic proteins in hippocampal slice cultures. *J. Vis. Exp.* 1–7.
- 23 Zhao, S., Studer, D., Chai, X., Graber, W., Brose, N., Nestel, S., Young, C., Rodriguez, E. P., Saetzler, K. and Frotscher, M. (2012) Structural plasticity of hippocampal mossy fiber synapses as revealed by high-pressure freezing. *J. Comp. Neurol.* **520**, 2340–2351.
- 24 Adrian, M., Dubochet, J., Lepault, J. and McDowell, A. W. Cryo-electron microscopy of viruses. *Nature* **308**, 32–6.
- 25 Griffiths, G. and Lucocq, J. M. (2014) Antibodies for immunolabeling by light and electron microscopy: Not for the faint hearted. *Histochem. Cell Biol.* **142**, 347–360.
- 26 Watanabe, S., Punge, A., Höllopeter, G., Willig, K. I., Hobson, R. J., Davis, M. W., Hell, S. W. and Jorgensen, E. M. (2011) Protein localization in electron micrographs using fluorescence nanoscopy. *Nat. Methods* **8**, 80–4.
- 27 Balzarotti, F., Eilers, Y., Gwosch, K. C., Gynnå, A. H., Westphal, V., Stefani, F. D., Elf, J. and Hell, S. W. (2017) Nanometer resolution imaging and tracking of fluorescent molecules with minimal photon fluxes. *Science (80-.)*. **355**, 606–612.
- 28 Vreja, I. C., Kabatas, S., Saka, S. K., Kröhnert, K., Höschel, C., Opazo, F., Diederichsen, U. and Rizzoli, S. O. (2015) Secondary-Ion Mass Spectrometry of Genetically Encoded Targets. *Angew. Chem. Int. Ed. Engl.* 1–6.
- 29 Behrens, S., Lösekann, T., Pett-Ridge, J., Weber, P. K., Ng, W. O., Stevenson, B. S., Hutcheon, I. D., Relman, D. A. and Spormann, A. M. (2008) Linking microbial phylogeny to metabolic activity at the single-cell level by using enhanced element labeling-catalyzed reporter deposition fluorescence in situ hybridization (EL-FISH) and NanoSIMS. *Appl. Environ. Microbiol.* **74**, 3143–3150.
- 30 Richter, K. N., Rizzoli, S. O., Jähne, S., Vogts, A. and Lovric, J. (2017) Review of combined isotopic and optical nanoscopy. *Neurophotonics* **4**, 20901.
- 31 Chen, F., Tillberg, P. W. and Boyden, E. S. (2015) Expansion microscopy. *Science (80-.)*. **347**, 543–548.
- 32 Chozinski, T. J., Halpern, A. R., Okawa, H., Kim, H.-J., Tremel, G. J., Wong, R. O. L. and Vaughan,

- J. C. (2016) Expansion microscopy with conventional antibodies and fluorescent proteins. *Nat. Methods* **13**, 485–488.
- 33 Truckenbrodt, S., Maidorn, M., Crzan, D., Wildhagen, H., Kabatas, S. and Rizzoli, S. O. (2017) X10 Expansion Microscopy Enables 25 nm Resolution on Conventional Microscopes. *bioRxiv*.
- 34 Chang, J.-B., Chen, F., Yoon, Y.-G., Jung, E. E., Babcock, H., Kang, J. S., Asano, S., Suk, H.-J., Pak, N., Tillberg, P. W., et al. (2017) Iterative expansion microscopy. *Nat. Methods* **14**, 593–599.
- 35 Chalfie, M., Tu, Y., Euskirchen, G., Ward, W. W. and Prasher, D. C. (1994) Green Fluorescent Protein as a Marker for Gene Expression. *Science* (80-.). **263**, 802–805.
- 36 Stagge, F., Mitronova, G. Y., Belov, V. N., Wurm, C. a and Jakobs, S. (2013) SNAP-, CLIP- and Halo-tag labelling of budding yeast cells. *PLoS One* **8**, e78745.
- 37 Opazo, F., Punge, A., Bückers, J., Hoopmann, P., Kastrop, L., Hell, S. W. and Rizzoli, S. O. (2010) Limited Intermixing of Synaptic Vesicle Components upon Vesicle Recycling. *Traffic* **11**, 800–812.
- 38 Jinek, M., Chylinski, K., Fonfara, I., Hauer, M., Doudna, J. A. and Charpentier, E. (2012) A Programmable Dual-RNA – Guided DNA Endonuclease in Adaptive Bacterial Immunity. *Science* **337**, 816–822.
- 39 Dawson, R. M. (2005) Characterization of the binding of cholera toxin to ganglioside G M1 immobilized onto microtitre plates. *J. Appl. Toxicol.* **25**, 30–38.
- 40 Cooper, J. A. (1987) Effects of cytochalasins and phalloidin on actin. *J. Cell Biol.* **105**, 1473–1478.
- 41 Evan Ingley and Hemmings, B. A. (1994) Pleckstrin Homology (PH) Domains in Signal Transduction. *J. Cell. Biochem.* **56**, 436–443.
- 42 Balla, T. and Várnai, P. (2009) Visualization of Cellular Phosphoinositide Pools with GFP-fused Protein-Domains. *Curr Protoc Cell Biol.*
- 43 Janeway, C. A., Travers, P., Walport, M. and Shlomchik, M. J. (2011) *Janeway’s Immunobiology* (8th ed.), Garland Science; 8 edition.
- 44 G. Köhler, C. M. (1975) Continuous cultures of fused cells secreting antibody of predefined specificity. *Nature* **256**, 495–497.
- 45 Hudson, P. J. and Souriau, C. (2003) Engineered antibodies. *Nat. Med.* **9**, 129–134.
- 46 Holliger, P. and Hudson, P. J. (2005) Engineered antibody fragments and the rise of single domains. *Nat. Biotechnol.* **23**, 1126–1136.
- 47 Coleman, L. and Mahler, S. M. (2003) Purification of Fab fragments from a monoclonal antibody papain digest by Gradiflow electrophoresis. *Protein Expr. Purif.* **32**, 246–251.
- 48 Huston, J. S., Levinson, D., Mudgett-Hunter, M., Tai, M. S., Novotný, J., Margolies, M. N., Ridge, R. J., Brucoleri, R. E., Haber, E. and Crea, R. (1988) Protein engineering of antibody binding sites: recovery of specific activity in an anti-digoxin single-chain Fv analogue produced in *Escherichia coli*. *Proc. Natl. Acad. Sci. U. S. A.* **85**, 5879–5883.

- 49 Monnier, P., Vigouroux, R. and Tassew, N. (2013) In Vivo Applications of Single Chain Fv (Variable Domain) (scFv) Fragments. *Antibodies* **2**, 193–208.
- 50 Hamers-Casterman, C., Atarhouch, S., Muyldermans, S., Robinson, G., Hamers, C., Bajyana Songa, E., Bendahman, N. and Hamers, R. (1993) Naturally occurring antibodies devoid of light chains. *Nature* **363**, 446–448.
- 51 Muyldermans, S. (2013) Nanobodies: Natural Single-Domain Antibodies. *Annu. Rev. Biochem.* **82**, 775–97.
- 52 Škrlec, K., Štrukelj, B. and Berlec, A. (2015) Non-immunoglobulin scaffolds: a focus on their targets. *Trends Biotechnol.* **33**, 408–418.
- 53 Löfblom, J., Feldwisch, J., Tolmachev, V., Carlsson, J., Ståhl, S. and Frejd, F. Y. (2010) Affibody molecules: Engineered proteins for therapeutic, diagnostic and biotechnological applications. *FEBS Lett., Federation of European Biochemical Societies* **584**, 2670–2680.
- 54 Gebauer, M. and Skerra, A. (2009) Engineered protein scaffolds as next-generation antibody therapeutics. *Curr. Opin. Chem. Biol.* **13**, 245–255.
- 55 Desmet, J., Verstraete, K., Bloch, Y., Lorent, E., Wen, Y., Devreese, B., Vandenbroucke, K., Loverix, S., Hettmann, T., Deroo, S., et al. (2014) Structural basis of IL-23 antagonism by an Alphabody protein scaffold. *Nat. Commun., Nature Publishing Group* **5**, 5237.
- 56 Desmet, J. and Lasters, I. (2010, December 2) Non-natural proteinaceous scaffold made of three non-covalently associated peptides.
- 57 Lakhin, V., Tarantul, V. Z. and Gening, L. V. (2013) Aptamers: problems, solutions and prospects. *Acta Naturae* **5**, 34–43.
- 58 Opazo, F., Levy, M., Byrom, M., Schäfer, C., Geisler, C., Groemer, T. W., Ellington, A. D. and Rizzoli, S. O. (2012) Aptamers as potential tools for super-resolution microscopy. *Nat. Methods, Nature Publishing Group* **9**, 938–9.
- 59 Krehenbrink, M., Chami, M., Guilvout, I., Alzari, P. M., Pécorari, F. and Pugsley, A. P. (2008) Artificial Binding Proteins (Affitins) as Probes for Conformational Changes in Secretin PulD. *J. Mol. Biol., Elsevier Ltd* **383**, 1058–1068.
- 60 Bennett, V. and Stenbuck, P. (1979) Identification and partial purification of ankyrin, the high affinity membrane attachment site for human erythrocyte spectrin. *Chem, J Biol* 2533–2541.
- 61 Varadamsetty, G., Tremmel, D., Hansen, S., Parmeggiani, F. and Plückthun, A. (2012) Designed armadillo repeat proteins: Library generation, characterization and selection of peptide binders with high specificity. *J. Mol. Biol., Elsevier Ltd* **424**, 68–87.
- 62 Smith, G. (1985) Filamentous fusion phage: novel expression vectors that display cloned antigens on the virion surface. *Science (80-)*. **508**, 4–6.
- 63 Boder, E. T. and Wittrup, K. D. (1997) Yeast surface display for screening combinatorial polypeptide libraries. *Nat. Biotechnol.* **15**, 553–557.
- 64 Plückthun, A. (2012) Ribosome display: a perspective. *Methods Mol. Biol., Springer, New York, NY* **805**, 3–28.

- 65 Maidorn, M. (2014) Design of new affinity probes for super resolution microscopy. Master's Thesis, Georg-August Universität Göttingen.
- 66 Vincke, C. and Muyldermans, S. (2012) Introduction to Heavy Chain Antibodies and Derived Nanobodies. *Methods Mol Biol* (Saerens, D., and Muyldermans, S., eds.), Humana Press, Totowa, NJ **911**, 15–26.
- 67 Pardon, E., Laeremans, T., Triest, S., Rasmussen, S. G. F., Wohlkönig, A., Ruf, A., Muyldermans, S., Hol, W. G. J., Kobilka, B. K. and Steyaert, J. (2014) A general protocol for the generation of Nanobodies for structural biology. *Nat. Protoc.* **9**, 674–93.
- 68 Baral, T. N., MacKenzie, R. and Arbabi Ghahroudi, M. (2013) Single-domain antibodies and their utility. *Curr. Protoc. Immunol.*
- 69 (2016) Ablynx 2016 Annual report, Gent, Belgium, Belgium.
- 70 Weber, M., Bujak, E., Putelli, A., Villa, A., Matasci, M., Gualandi, L., Hemmerle, T., Wulhfard, S. and Neri, D. (2014) A highly functional synthetic phage display library containing over 40 billion human antibody clones. *PLoS One* **9**.
- 71 Yan, J., Li, G., Hu, Y., Ou, W. and Wan, Y. (2014) Construction of a synthetic phage-displayed Nanobody library with CDR3 regions randomized by trinucleotide cassettes for diagnostic applications. *J. Transl. Med.* **12**.
- 72 Maidorn, M., Rizzoli, S. O. and Opazo, F. (2016) Tools and limitations to study the molecular composition of synapses by fluorescence microscopy. *Biochem. J.* **473**, 3385–3399.
- 73 Nizak, C., Martin-Lluesma, S., Moutel, S., Roux, A., Kreis, T. E., Goud, B. and Perez, F. (2003) Recombinant antibodies against subcellular fractions used to track endogenous Golgi protein dynamics in vivo. *Traffic* **4**, 739–53.
- 74 Dmitriev, O. Y., Lutsenko, S. and Muyldermans, S. (2016) Nanobodies as Probes for Protein Dynamics in Vitro and in Cells. *J. Biol. Chem.* **291**, 3767–3775.
- 75 Vu, K. B., Ghahroudi, M. A., Wyns, L. and Muyldermans, S. Comparison of llama VH sequences from conventional and heavy chain antibodies. *Mol. Immunol.* **34**, 1121–31.
- 76 van Der Linden, R. H., Frenken, L. G., de Geus, B., Harmsen, M. M., Ruuls, R. C., Stok, W., de Ron, L., Wilson, S., Davis, P. and Verrips, C. T. (1999) Comparison of physical chemical properties of llama VHH antibody fragments and mouse monoclonal antibodies. *Biochim. Biophys. Acta* **1431**, 37–46.
- 77 Pérez, J. M. J., Renisio, J. G., Prompers, J. J., Van Platerink, C. J., Cambillau, C., Darbon, H. and Frenken, L. G. J. (2001) Thermal unfolding of a llama antibody fragment: A two-state reversible process. *Biochemistry* **40**, 74–83.
- 78 Arbabi Ghahroudi, M., Desmyter, a, Wyns, L., Hamers, R. and Muyldermans, S. (1997) Selection and identification of single domain antibody fragments from camel heavy-chain antibodies. *FEBS Lett., Federation of European Biochemical Societies* **414**, 521–526.
- 79 Williams, T., El-Turk, F., Buell, A. K., O'Day, E. M., Aprile, F. a, Esbjörner, E. K., Vendruscolo, M., Cremades, N., Pardon, E., Wyns, L., et al. (2013) Nanobodies raised against monomeric α -synuclein distinguish between fibrils at different maturation stages. *J. Mol. Biol., Elsevier Ltd* **425**, 2397–411.

- 80 Rothbauer, U., Zolghadr, K., Tillib, S., Nowak, D., Schermelleh, L., Gahl, A., Backmann, N., Conrath, K., Muyldermans, S. and Cardoso, M. C. (2006) Targeting and tracing antigens in live cells with fluorescent nanobodies **3**, 887–889.
- 81 Fridy, P. C., Li, Y., Keegan, S., Thompson, M. K., Nudelman, I., Scheid, J. F., Oeffinger, M., Nussenzweig, M. C., Fenyö, D., Chait, B. T., et al. (2014) A robust pipeline for rapid production of versatile nanobody repertoires. *Nat. Methods* **11**, 1253–1260.
- 82 De Genst, E., Silence, K., Decanniere, K., Conrath, K., Loris, R., Kinne, J., Muyldermans, S. and Wyns, L. (2006) Molecular basis for the preferential cleft recognition by dromedary heavy-chain antibodies. *Proc. Natl. Acad. Sci.* **103**, 4586–4591.
- 83 Stijlemans, B., Conrath, K., Cortez-Retamozo, V., Van Xong, H., Wyns, L., Senter, P., Revets, H., De Baetselier, P., Muyldermans, S. and Magez, S. (2004) Efficient targeting of conserved cryptic epitopes of infectious agents by single domain antibodies: African trypanosomes as paradigm. *J. Biol. Chem.* **279**, 1256–1261.
- 84 Braun, M. B., Traenkle, B., Koch, P. A., Emele, F., Weiss, F., Poetz, O., Stehle, T. and Rothbauer, U. (2016) Peptides in headlock – a novel high-affinity and versatile peptide-binding nanobody for proteomics and microscopy. *Sci. Rep.*, Nature Publishing Group 1–10.
- 85 Olichon, A., Marco, A. De, Vincke, C. and Muyldermans, S. (2012) Single Domain Antibodies. *Methods Mol Biol* (Saerens, D., and Muyldermans, S., eds.), Humana Press, Totowa, NJ **911**, 65–78.
- 86 de Marco, A. (2009) Strategies for successful recombinant expression of disulfide bond-dependent proteins in *Escherichia coli*. *Microb. Cell Fact.* **8**, 26.
- 87 Kim, Y., Ho, S. O., Gassman, N. R., Korlann, Y., Landorf, E. V., Collart, F. R. and Weiss, S. (2008) Efficient site-specific labeling of proteins via cysteines. *Bioconjug. Chem.* **19**, 786–91.
- 88 Massa, S., Xavier, C., De Vos, J., Caveliers, V., Lahoutte, T., Muyldermans, S. and Devoogdt, N. (2014) Site-specific labeling of cysteine-tagged camelid single-domain antibody-fragments for use in molecular imaging. *Bioconjug. Chem.* **25**, 979–88.
- 89 Yardehnavi, N., Behdani, M., Pooshang Bagheri, K., Mahmoodzadeh, A., Khanahmad, H., Shahbazzadeh, D., Habibi-Anbouhi, M., Ghassabeh, G. H. and Muyldermans, S. (2014) A camelid antibody candidate for development of a therapeutic agent against *Hemiscorpius lepturus* envenomation. *FASEB J.* **28**.
- 90 Jähnichen, S., Blanchetot, C., Maussang, D., Gonzalez-Pajuelo, M., Chow, K. Y., Bosch, L., De Vrieze, S., Serruys, B., Ulrichts, H., Vandeveld, W., et al. (2010) CXCR4 nanobodies (VHH-based single variable domains) potently inhibit chemotaxis and HIV-1 replication and mobilize stem cells. *Proc. Natl. Acad. Sci. U. S. A.* **107**, 20565–70.
- 91 Ries, J., Kaplan, C., Platonova, E., Eghlidi, H. and Ewers, H. (2012) A simple, versatile method for GFP-based super-resolution microscopy via nanobodies. *Nat. Methods* **9**, 582–4.
- 92 Chakravarty, R., Goel, S. and Cai, W. (2014) Nanobody: the “magic bullet” for molecular imaging? *Theranostics* **4**, 386–98.
- 93 Hassanzadeh-Ghassabeh, G., Devoogdt, N., De Pauw, P., Vincke, C. and Muyldermans, S. (2013) Nanobodies and their potential applications. *Nanomedicine* **8**, 1013–1026.

- 94 Schmidthals, K., Helma, J., Zolghadr, K., Rothbauer, U. and Leonhardt, H. (2010) Novel antibody derivatives for proteome and high-content analysis. *Anal. Bioanal. Chem.* **397**, 3203–8.
- 95 Chen, S., Bagley, J., Marasco, W. A. and Al, C. E. T. (1994) Intracellular Antibodies as a New Class of Therapeutic Molecules for Gene Therapy **601**, 595–601.
- 96 Melak, M., Plessner, M. and Grosse, R. (2017) Actin visualization at a glance. *J. Cell Sci.* **130**, 1688–1688.
- 97 Chen, S., Bagley, J., Marasco, W. A. and Al, C. E. T. (1994) Intracellular Antibodies as a New Class of Therapeutic Molecules for Gene Therapy **601**, 595–601.
- 98 Harmsen, M. M. and De Haard, H. J. (2007) Properties, production, and applications of camelid single-domain antibody fragments. *Appl. Microbiol. Biotechnol.*, Springer-Verlag **77**, 13–22.
- 99 Chames, P., Van Regenmortel, M., Weiss, E. and Baty, D. (2009) Therapeutic antibodies: Successes, limitations and hopes for the future. *Br. J. Pharmacol.* **157**, 220–233.
- 100 Vercruysse, T., Pardon, E., Vanstreels, E., Steyaert, J. and Daelemans, D. (2010) An intrabody based on a llama single-domain antibody targeting the N-terminal α -helical multimerization domain of HIV-1 Rev prevents viral production. *J. Biol. Chem.* **285**, 21768–21780.
- 101 Ibañez, L. I., De Filette, M., Hultberg, A., Verrips, T., Temperton, N., Weiss, R. A., Vandeveld, W., Schepens, B., Vanlandschoot, P. and Saelens, X. (2011) Nanobodies with in vitro neutralizing activity protect mice against H5N1 influenza virus infection. *J. Infect. Dis.* **203**, 1063–1072.
- 102 Cortez-Retamozo, V., Backmann, N., Senter, P. D., Wernery, U., De Baetselier, P., Muyldermans, S. and Revets, H. (2004) Efficient Cancer Therapy with a Nanobody-Based Conjugate. *Cancer Res.* **64**, 2853–2857.
- 103 Siontorou, C. G. (2013) Nanobodies as novel agents for disease diagnosis and therapy. *Int. J. Nanomedicine* **8**, 4215–4227.
- 104 Van Audenhove, I. and Gettemans, J. (2016) Nanobodies as Versatile Tools to Understand, Diagnose, Visualize and Treat Cancer. *EBioMedicine*, The Authors **8**, 40–48.
- 105 Mikhaylova, M., Cloin, B. M. C., Finan, K., van den Berg, R., Teeuw, J., Kijanka, M. M., Sokolowski, M., Katrukha, E. a., Maidorn, M., Opazo, F., et al. (2015) Resolving bundled microtubules using anti-tubulin nanobodies. *Nat. Commun.*, Nature Publishing Group **6**, 7933.
- 106 Perruchini, C., Pecorari, F., Bourgeois, J.-P., Duyckaerts, C., Rougeon, F. F. and Lafaye, P. (2009, November) Llama VHH antibody fragments against GFAP: better diffusion in fixed tissues than classical monoclonal antibodies. *Acta Neuropathol.*
- 107 Bradbury, A. and Plückthun, A. (2015) Standardized antibodies used in research. *Nat. Comment* **518**, 27–29.
- 108 Durisic, N., Cuervo, L. L. and Lakadamyali, M. (2014) Quantitative super-resolution microscopy: Pitfalls and strategies for image analysis. *Curr. Opin. Chem. Biol.*, Elsevier Ltd **20**, 22–28.

- 109 Marx, V. (2013) Finding the right antibody for the job. *Nat. Methods*, Nature Publishing Group **10**, 703–707.
- 110 Pleiner, T., Bates, M., Trakhanov, S., Lee, C. T., Schliep, J. E., Chug, H., Böhning, M., Stark, H., Urlaub, H. and Görlich, D. (2015) Nanobodies: Site-specific labeling for super-resolution imaging, rapid epitope-mapping and native protein complex isolation. *Elife* **4**, 1–21.
- 111 Fornasiero, E. F. and Opazo, F. (2015) Super-resolution imaging for cell biologists: Concepts, applications, current challenges and developments. *Bioessays* **37**, 436–51.
- 112 Platonova, E., Winterflood, C. M., Junemann, A., Albrecht, D., Faix, J. and Ewers, H. (2015) Single-molecule microscopy of molecules tagged with GFP or mRFP derivatives in mammalian cells using nanobody binders. *Methods*, Elsevier Inc.
- 113 Foster, M. and Sherrington, C. (1897) *A textbook of physiology, part three: The central nervous system*. MacMillan Co Ltd, London.
- 114 Palay, S. L. and Palade, G. E. (1955) The fine structure of neurons. *J. Biophys. Biochem. Cytol.* **1**, 69–88.
- 115 Palade, G. E. and Palay, S. L. (1954) Electron microscopical observations of interneuronal and neuromuscular synapses. *Anat. Rec.* **118**.
- 116 Harris, K. M. and Weinberg, R. J. (2012) Ultrastructure of synapses in the mammalian brain. *Cold Spring Harb. Perspect. Biol.* **4**, 7.
- 117 Völgyi, K., Gulyássi, P., Háden, K., Kis, V., Badics, K., Kékesi, K. A., Simor, A., Györfy, B., Tóth, E. A., Lubec, G., et al. (2015) Synaptic mitochondria: A brain mitochondria cluster with a specific proteome. *J. Proteomics*, Elsevier B.V. **120**, 142–157.
- 118 Erni, R., Rossell, M. D., Kisielowski, C. and Dahmen, U. (2009) Atomic-resolution imaging with a sub-50-pm electron probe. *Phys. Rev. Lett.* **102**, 1–4.
- 119 Roth, J., Benday, M. and Orci, L. (1978) Ultrastructural localization on intracellular antigens by the use of protein A-gold complex. *J. Histochem. Cytochem.* **26**, 1074–1081.
- 120 Berning, S., Willig, K. I., Steffens, H., Dibaj, P. and Hell, S. W. (2012) Nanoscopy in a living mouse brain. *Science* **335**, 551.
- 121 Oyler, G. A., Higgins, G. A., Hart, R. A., Battenberg, E., Billingsley, M., Bloom, F. E. and Wilson, M. C. (1989) The identification of a novel synaptosomal-associated protein, SNAP-25, differentially expressed by neuronal subpopulations. *J. Cell Biol.* **109**, 3039–3052.
- 122 Bennett, M. K., Calakos, N. and Scheller, R. H. (1992) Syntaxin: a synaptic protein implicated in docking of synaptic vesicles at presynaptic active zones. *Science* **257**, 255–259.
- 123 Pocklington, a J., Armstrong, J. D. and Grant, S. G. N. (2006) Organization of brain complexity-synapse proteome form and function. *Brief. Funct. Genomic. Proteomic.* **5**, 66–73.
- 124 Opazo, F. and Rizzoli, S. O. (2010) The fate of synaptic vesicle components upon fusion. *Commun. Integr. Biol.* **3**, 427–9.
- 125 Malsam, J. and Söllner, T. H. (2011) Organization of SNAREs within the Golgi stack. *Cold Spring Harb. Perspect. Biol.* **3**, 1–17.

- 126 Rizzoli, S. O. (2014) Synaptic vesicle recycling: Steps and principles. *EMBO J.* **33**, 788–822.
- 127 Südhof, T. C. (2004) The Synaptic Vesicle Cycle. *Annu. Rev. Neurosci.* **27**, 509–47.
- 128 Wilhelm, B. G., Mandad, S., Truckenbrodt, S., Krohnert, K., Schafer, C., Rammner, B., Koo, S. J., Classen, G. A., Krauss, M., Haucke, V., et al. (2014) Composition of isolated synaptic boutons reveals the amounts of vesicle trafficking proteins. *Science* (80-.). **344**, 1023–1028.
- 129 Takamori, S., Holt, M., Stenius, K., Lemke, E. A., Grønborg, M., Riedel, D., Urlaub, H., Schenck, S., Brügger, B., Ringler, P., et al. (2006) Molecular Anatomy of a Trafficking Organelle. *Cell* **127**, 831–846.
- 130 Saka, S. and Rizzoli, S. O. (2012) Super-resolution imaging prompts re-thinking of cell biology mechanisms. *BioEssays* **34**, 386–395.
- 131 Denker, A., Bethani, I., Kröhnert, K., Körber, C., Horstmann, H., Wilhelm, B. G., Barysch, S. V, Kuner, T., Neher, E. and Rizzoli, S. O. (2011) A small pool of vesicles maintains synaptic activity in vivo. *Proc. Natl. Acad. Sci. U. S. A.* **108**, 17177–82.
- 132 Dani, A., Huang, B., Bergan, J. and Dulac, C. (2010) Neuron - Superresolution Imaging of Chemical Synapses in the Brain **68**, 843–856.
- 133 Südhof, T. C. (2006) Synaptic Vesicles: An Organelle Comes of Age. *Cell* **127**, 671–673.
- 134 Lang, T., Bruns, D., Wenzel, D., Riedel, D., Holroyd, P., Thiele, C. and Jahn, R. (2001) SNAREs are concentrated in cholesterol-dependent clusters that define docking and fusion sites for exocytosis. *EMBO J.* **20**, 2202–13.
- 135 Lang, T. and Rizzoli, S. O. (2010) Membrane Protein Clusters at Nanoscale Resolution: More Than Pretty Pictures. *Physiology* **25**, 116–124.
- 136 Ikeda, K. and Bekkers, J. M. (2009) Counting the number of releasable synaptic vesicles in a presynaptic terminal. *Proc. Natl. Acad. Sci. U. S. A.* **106**, 2945–2950.
- 137 Südhof, T. C. (2004) the Synaptic Vesicle Cycle Neurotransmitter Release and the Synaptic Vesicle Cycle. *Annu. Rev. Neurosci.* **27**, 509–47.
- 138 Rizzoli, S. O. and Betz, W. J. (2005) Synaptic vesicle pools. *Nat. Rev. Neurosci.* **6**, 57–69.
- 139 Denker, A. and Rizzoli, S. O. (2010) Synaptic vesicle pools: An update. *Front. Synaptic Neurosci.* **2**, 1–12.
- 140 Barysch, S. V, Aggarwal, S., Jahn, R. and Rizzoli, S. O. (2009) Sorting in early endosomes reveals connections to docking- and fusion-associated factors. *Proc. Natl. Acad. Sci. U. S. A.* **106**, 9697–9702.
- 141 Kaech, S. and Banker, G. (2007) Culturing hippocampal neurons. *Nat. Protoc.* **1**, 2406–2415.
- 142 Thomas, P. and Smart, T. G. (2005) HEK293 cell line: A vehicle for the expression of recombinant proteins. *J. Pharmacol. Toxicol. Methods* **51**, 187–200.
- 143 Lang, T., Wacker, I., Steyer, J., Kaether, C., Wunderlich, I., Soldati, T., Gerdes, H. H. and Almers, W. (1997) Ca¹⁺-triggered peptide secretion in single cells imaged with green fluorescent protein and evanescent-wave microscopy. *Neuron* **18**, 857–863.

- 144 Ta, H., Keller, J., Haltmeier, M., Saka, S. K., Schmieid, J., Opazo, F., Tinnefeld, P., Munk, A. and Hell, S. W. (2015) Mapping molecules in scanning far-field fluorescence nanoscopy. *Nat. Commun.* **6**, 7977.
- 145 Saka, S. K., Vogts, A., Kröhnert, K., Hillion, F., Rizzoli, S. O. and Wessels, J. T. (2014) Correlated optical and isotopic nanoscopy. *Nat. Commun.* **5**, 3664.
- 146 Scheich, C., Kümmel, D., Soumailakakis, D., Heinemann, U. and Büssow, K. (2007) Vectors for co-expression of an unrestricted number of proteins. *Nucleic Acids Res.* **35**.
- 147 Gibson, D. G., Young, L., Chuang, R., Venter, J. C., Iii, C. A. H., Smith, H. O. and America, N. (2009) Enzymatic assembly of DNA molecules up to several hundred kilobases **6**, 12–16.
- 148 Schägger, H. and von Jagow, G. (1987) Tricine-sodium dodecyl sulfate-polyacrylamide gel electrophoresis for the separation of proteins in the range from 1 to 100 kDa. *Anal. Biochem.* **166**, 368–79.
- 149 Promega. (1996) *Protocols and Applications Guide* 3rd ed., Promega Corporation; 3rd edition (1996).
- 150 Janeway, C. (2001) *Immunobiology 5 : the immune system in health and disease*, Garland Pub.
- 151 Smith, G. P. (1985) Filamentous fusion phage: novel expression vectors that display cloned antigens on the virion surface. *Science* **228**, 1315–7.
- 152 Tiede, C., Tang, A. a S., Deacon, S. E., Mandal, U., Nettleship, J. E., Owen, R. L., George, S. E., Harrison, D. J., Owens, R. J., Tomlinson, D. C., et al. (2014) Adhiron: a stable and versatile peptide display scaffold for molecular recognition applications. *Protein Eng. Des. Sel.* **27**, 145–55.
- 153 Qi, H., Lu, H., Qiu, H.-J., Petrenko, V. and Liu, A. (2012) Phagemid vectors for phage display: properties, characteristics and construction. *J. Mol. Biol., Elsevier Ltd* **417**, 129–43.
- 154 Lee, C. M. Y., Iorno, N., Sierro, F. and Christ, D. (2007) Selection of human antibody fragments by phage display. *Nat. Protoc.* **2**, 3001–8.
- 155 Maass, D. R., Sepulveda, J., Pernthaner, A. and Shoemaker, C. B. (2007) Alpaca (Lama pacos) as a convenient source of recombinant camelid heavy chain antibodies (VHHs). *J. Immunol. Methods* **324**, 13–25.
- 156 Theile, C. S., Witte, M. D., Blom, A. E. M., Kundrat, L., Ploegh, H. L. and Guimaraes, C. P. (2013) Site-specific N-terminal labeling of proteins using sortase-mediated reactions. *Nat. Protoc., Nature Publishing Group* **8**, 1800–7.
- 157 Rondot, S., Koch, J., Breitling, F. and Dübel, S. (2001) A helper phage to improve single-chain antibody presentation in phage display 75–78.
- 158 Piotukh, K., Geltinger, B., Heinrich, N., Gerth, F., Beyermann, M., Freund, C. and Schwarzer, D. (2011) Directed evolution of sortase A mutants with altered substrate selectivity profiles. *J. Am. Chem. Soc.* **133**, 17536–9.
- 159 Hughes, L. D., Rawle, R. J., Boxer, S. G., Alexa, C., Bodipy-tmr, C., Invitrogen, P., Nhs-ester, O. R. A., Nhs-ester, A., Se, A. and Alexa, M. (2014) Choose Your Label Wisely : Water-Soluble Fluorophores Often Interact with Lipid Bilayers **9**.

- 160 Fan, J., Yang, X., Lu, J., Chen, L. and Xu, P. (2007) Role of Habc domain in membrane trafficking and targeting of syntaxin 1A. *Biochem. Biophys. Res. Commun.* **359**, 245–250.
- 161 McEwen, J. M. and Kaplan, J. M. (2008) UNC-18 Promotes Both the Anterograde Trafficking and Synaptic Function of Syntaxin. *Mol. Biol. Cell* **19**, 3836–3846.
- 162 Jahn, R. and Scheller, R. H. (2006) SNAREs--engines for membrane fusion. *Nat. Rev. Mol. Cell Biol.* **7**, 631–43.
- 163 Bethani, I., Lang, T., Geumann, U., Sieber, J. J., Jahn, R. and Rizzoli, S. O. (2007) The specificity of SNARE pairing in biological membranes is mediated by both proof-reading and spatial segregation. *EMBO J.* **26**, 3981–3992.
- 164 Greene, L. A., Tischlert, A. S. and Kuffler, S. W. (1976) Establishment of a noradrenergic clonal line of rat adrenal pheochromocytoma cells which respond to nerve growth factor. *Cell Biol.* **73**, 2424–2428.
- 165 Milovanovic, D. and Jahn, R. (2015) Organization and dynamics of SNARE proteins in the presynaptic membrane. *Front. Physiol.* **6**, 89.
- 166 Pertsinidis, A., Mukherjee, K., Sharma, M., Pang, Z. P., Park, S. R., Zhang, Y., Brunger, A. T., Sudhof, T. C. and Chu, S. (2013) Ultrahigh-resolution imaging reveals formation of neuronal SNARE/Munc18 complexes in situ. *Proc. Natl. Acad. Sci.* **110**, E2812–E2820.
- 167 Ullrich, A., Böhme, M. A., Schöneberg, J., Depner, H., Sigrist, S. J. and Noé, F. (2015) Dynamical Organization of Syntaxin-1A at the Presynaptic Active Zone. *PLOS Comput. Biol.* **11**, e1004407.
- 168 Moutel, S., Bery, N., Bernard, V., Keller, L., Lemesre, E., De Marco, A., Ligat, L., Rain, J. C., Favre, G., Olichon, A., et al. (2016) NaLi-H1: A universal synthetic library of humanized nanobodies providing highly functional antibodies and intrabodies. *Elife* **5**, 1–31.
- 169 Miyazaki, N., Kiyose, N., Akazawa, Y., Takashima, M., Hagihara, Y., Inoue, N., Matsuda, T., Ogawa, R., Inoue, S. and Ito, Y. (2015) Isolation and characterization of antigen-specific alpaca VHH antibodies by biopanning followed by high throughput sequencing.
- 170 Griffin, H., Elston, R., Jackson, D., Ansell, K., Coleman, M., Winter, G. and Doorbar, J. (2006) Inhibition of papillomavirus protein function in cervical cancer cells by intrabody targeting. *J. Mol. Biol.* **355**, 360–78.
- 171 Schmidt, T. G. M., Batz, L., Bonet, L., Carl, U., Holzapfel, G., Kiem, K., Matulewicz, K., Niermeier, D., Schuchardt, I. and Stanar, K. (2013) Development of the Twin-Strep-tag® and its application for purification of recombinant proteins from cell culture supernatants. *Protein Expr. Purif., Elsevier Inc.* **92**, 54–61.
- 172 Rickman, C. and Duncan, R. R. (2010) Munc18/syntaxin interaction kinetics control secretory vesicle dynamics. *J. Biol. Chem.* **285**, 3965–3972.
- 173 Tian, J. H., Das, S. and Sheng, Z. H. (2003) Ca²⁺-dependent phosphorylation of syntaxin-1A by the death-associated protein (DAP) kinase regulates its interaction with Munc18. *J. Biol. Chem.* **278**, 26265–26274.
- 174 Lau, C. G., Takayasu, Y., Rodenas-Ruano, A., Paternain, A. V., Lerma, J., Bennett, M. V and Zukin, R. S. (2010) SNAP-25 is a target of protein kinase C phosphorylation critical to NMDA receptor trafficking. *J Neurosci* **30**, 242–254.

- 175 Katayama, N., Yamamori, S., Fukaya, M., Kobayashi, S., Watanabe, M., Takahashi, M. and Manabe, T. (2017) SNAP-25 phosphorylation at Ser187 regulates synaptic facilitation and short-term plasticity in an age-dependent manner. *Sci. Rep.*, Springer US **7**, 7996.
- 176 Puchtler, H. and Meloan, S. N. (1985) On the chemistry of formaldehyde fixation and its effects on immunohistochemical reactions. *Histochemistry* **82**, 201–4.
- 177 Rosas-Arellano, A., Villalobos-González, J. B., Palma-Tirado, L., Beltrán, F. A., Cárabez-Trejo, A., Missirlis, F. and Castro, M. A. (2016) A simple solution for antibody signal enhancement in immunofluorescence and triple immunogold assays. *Histochem. Cell Biol.*, Springer Berlin Heidelberg **146**, 421–430.
- 178 Shin, J., Lou, X., Kweon, D.-H. and Shin, Y.-K. (2014) Multiple conformations of a single SNAREpin between two nanodisc membranes reveal diverse pre-fusion states. *Biochem J.* **459**, 95–102.
- 179 Fasshauer, D. and Margittai, M. (2004) A Transient N-terminal Interaction of SNAP-25 and Syntaxin Nucleates SNARE Assembly. *J. Biol. Chem.* **279**, 7613–7621.
- 180 Sørensen, J. B., Wiederhold, K., Müller, E. M., Milosevic, I., Nagy, G., de Groot, B. L., Grubmüller, H. and Fasshauer, D. (2006) Sequential N- to C-terminal SNARE complex assembly drives priming and fusion of secretory vesicles. *EMBO J.* **25**, 955–66.
- 181 Teng, F. Y., Wang, Y. and Tang, B. L. (2001) The syntaxins. *Genome Biol.* **2**, REVIEWS3012.
- 182 Kofuji, T., Fujiwara, T., Sanada, M., Mishima, T. and Akagawa, K. (2014) HPC-1/syntaxin 1A and syntaxin 1B play distinct roles in neuronal survival. *J. Neurochem.* **130**, 514–525.
- 183 Mishima, T., Fujiwara, T., Sanada, M., Kofuji, T., Kanai-Azuma, M. and Akagawa, K. (2014) Syntaxin 1B, but not syntaxin 1A, is necessary for the regulation of synaptic vesicle exocytosis and of the readily releasable pool at central synapses. *PLoS One* **9**.
- 184 Zhegalova, N. G., He, S., Zhou, H., Kim, D. M. and Berezin, M. Y. (2014) Minimization of self-quenching fluorescence on dyes conjugated to biomolecules with multiple labeling sites via asymmetrically charged NIR fluorophores **9**, 355–362.
- 185 Jolien Suzanne Verdaasdonk, Lawrimore, J. and Bloom, K. (2014) Determining absolute protein numbers by quantitative fluorescence microscopy. *Methods Cell Biol.* **123**, 347–365.
- 186 Coffman, V. C. and Wu, J.-Q. (2013) Counting protein molecules using quantitative fluorescence microscopy. *Trends Biochem. Sci.* **37**, 499–506.
- 187 Mi, L., Goryaynov, A., Lindquist, A., Rexach, M. and Yang, W. (2015) Quantifying nucleoporin stoichiometry inside single nuclear pore complexes in vivo. *Sci. Rep.* **5 VN-re**, 9372.
- 188 Entwistle, A. and Noble, M. (1992) The quantification of fluorescent emission from biological samples using analysis of polarization. *J. Microsc.* **165**, 347–365.
- 189 Thavarajah, R., Mudimbaimannar, V., Rao, U., Ranganathan, K. and Elizabeth, J. (2012) Chemical and physical basics of routine formaldehyde fixation. *J. Oral Maxillofac. Pathol.* **16**, 400.
- 190 Stradleigha, T. W. and Ishida, A. T. (2015) Fixation Strategies For Retinal Immunohistochemistry 181–202.

- 191 Baker, M. (2015) Blame it on the antibodies. *Nature* **521**, 274–276.
- 192 Halemani, N. D., Bethani, I., Rizzoli, S. O. and Lang, T. (2010) Structure and Dynamics of a Two-Helix SNARE Complex in Live Cells. *Traffic* **11**, 394–404.
- 193 Rowe, J., Corradi, N., Malosio, M. L., Taverna, E., Halban, P., Meldolesi, J. and Rosa, P. (1999) Blockade of membrane transport and disassembly of the Golgi complex by expression of syntaxin 1A in neurosecretion-incompetent cells: prevention by rbSEC1. *J. Cell Sci.* **112**, 1865–77.
- 194 Greaves, J., Gorleku, O. A., Salaun, C. and Chamberlain, L. H. (2010) Palmitoylation of the SNAP25 protein family: Specificity and regulation by DHHC palmitoyl transferases. *J. Biol. Chem.* **285**, 24629–24638.
- 195 Sieber, J., Willig, K. and Lang, T. (2007) Anatomy and Dynamics of a Supramolecular Membrane Protein Cluster. *Science* **317**, 1072–76.
- 196 Milovanovic, D., Platen, M., Junius, M., Diederichsen, U., Schaap, I. A. T. T., Honigmann, A., Jahn, R. and Van Den Bogaart, G. (2016) Calcium promotes the formation of syntaxin 1 mesoscale domains through phosphatidylinositol 4,5-bisphosphate. *J. Biol. Chem.* **291**, 7868–7876.
- 197 Barg, S., Knowles, M. K., Chen, X., Midorikawa, M. and Almers, W. (2010) Syntaxin clusters assemble reversibly at sites of secretory granules in live cells. *Proc. Natl. Acad. Sci. U. S. A.* **107**, 20804–9.
- 198 Kirchofer, A., Helma, J., Schmidthals, K., Frauer, C., Cui, S., Karcher, A., Pellis, M., Muyldermans, S., Casas-Delucchi, C. S., Cardoso, M. C., et al. (2010) Modulation of protein properties in living cells using nanobodies. *Nat. Struct. Mol. Biol.* **17**, 133–8.
- 199 Wang, Y., Cai, E., Rosenkranz, T., Ge, P., Teng, K. W., Lim, S. J., Smith, A. M., Chung, H. J., Sachs, F., Green, W. N., et al. (2014) Small quantum dots conjugated to nanobodies as immunofluorescence probes for nanometric microscopy. *Bioconjug. Chem.* **25**, 2205–2211.
- 200 Gao, X., Yang, L., Petros, J. A., Marshall, F. F., Simons, J. W. and Nie, S. (2005) In vivo molecular and cellular imaging with quantum dots. *Curr. Opin. Biotechnol.* **16**, 63–72.
- 201 Wang, Y., Fruhwirth, G., Cai, E., Ng, T. and Selvin, P. R. (2013) 3D super-resolution imaging with blinking quantum dots *Yong* **13**.
- 202 Miller, S. E. and Howell, D. N. (2014) *Making and Using Antibodies: A Practical Handbook*, Second Edition (Howard, G. C., and Kaser, M. R., eds.) 2nd ed., Boca Ranton.
- 203 Hopwood, D. (1972) Theoretical and practical aspects of glutaraldehyde fixation. *Histochem. J.* **4**, 267–303.
- 204 Opazo, F., Rizzoli, S. O., Diederichsen, U., Kabatas, S., Vreja, I. C., Saka, S. K., Höschel, C., Kröhnert, K., Opazo, F., Rizzoli, S. O., et al. (2015) A contamination-insensitive probe for imaging specific biomolecules by secondary ion mass spectrometry. *Chem. Commun., Royal Society of Chemistry* **51**, 13221–13224.
- 205 Schenck, S., Kunz, L., Sahlender, D., Pardon, E., Geertsma, E. R., Savtchouk, I., Suzuki, T., Neldner, Y., Štefanić, S., Steyaert, J., et al. (2017) Generation and Characterization of Anti-VGLUT Nanobodies Acting as Inhibitors of Transport. *Biochemistry* **56**, 3962–3971.

6. Curriculum Vitae

Scientific Education

Since March 2014:

PhD student with Prof. Dr. Silvio Rizzoli (Neuro- and Sensory Physiology) within the GGNB

Title of thesis:

“Development of Nanobodies to Image Synaptic Proteins in Super-Resolution Microscopy“

October 2012 - March 2014:

Master of Science (final grade ‘very good’), Georg-August-Universität Göttingen

International Max Planck Research School (IMPRS) Molecular Biology

October 2009 - September 2012:

B. Sc. in Biochemistry (final grade 1.2), Free University of Berlin

Research stay from 03/2012 till 06/2012 at Karolinska Institutet, Stockholm, Sweden

August 2008 - July 2009:

Voluntary Social Year (FSJ) including management and training tasks in a local sports club

June 2008

Abitur (final grade 1.3), Gymnasium Alfeld (Leine)

Languages:

German (native)

English (professional)

Latin proficiency certificate

Spanish (basic)

Swedish (basic)

Soft skills & interests:

- Certificate: ‚Social- and leadership competences‘, central facility for languages and key qualifications (ZESS), University of Göttingen
- Licensed and active trainer in athletics / triathlon
- Group leader & guide for international scholarship students invited on behalf of the Pedagogical Exchange Service (PAD) of the Standing Conference of Education Ministers of Germany
- Tutor for Molecular Biology in the X-Lab, Göttingen – Germany’s biggest educational laboratory for undergraduates
- Study advisor for Biochemistry from 2011-2012
- Organization of various events and conferences, including the annual symposium ‘Horizons in Molecular Biology’
- PhD Representative in the IMPRS-Molecular Biology program committee; student representative in the Chemistry Institution Committee (FU Berlin)
- Winner of various Science-Slams: <https://www.youtube.com/watch?v=SyW2041cEBE&t=318>